ABSTRACT

AZEEZ, FADHEL ABBAS. Lithium Bis(Oxalato)Borate-Based Electrolyte for Lithium-Ion Cells. (Under the direction of Prof. Peter S. Fedkiw.)

Compact, light weight rechargeable batteries offering high-energy densities have become necessary in the 21st century especially for applications such as portable electronics devices, hybrid electric vehicles, and load leveling in electric power generation/distribution. Among rechargeable batteries, lithium-based systems seem able to fill these needs.

The state-of-art electrolyte for Li-ion batteries of $LiPF_6$ dissolved in organic-carbonate solvents has disadvantages in low- and high-temperature environments. At high temperature, the thermal instability of $LiPF_6$ is believed to be the main cause for poor performance of lithium-ion batteries. At low temperature, the high viscosity of ethylene carbonate, which is a major component in the solvent mixture, restricts use to above -20 ^{o}C. These factors limit the operation of lithium-ion batteries to be between -20 and 60 ^{o}C.

In an attempt to improve the performance, enhance the safety, and lower the cost of lithium-ion cells, we use a stable salt at high temperature, lithium bis(oxalato)borate (LiBOB), and dissolve it in mixtures of γ-butyrolactone (GBL), ethyl acetate (EA), and ethylene carbonate (EC), with and without fumed silica (FS) nano particulates as a gelling agent. Conductivity, cycling studies of cathode half-cells, rheology, and FTIR measurements are performed for LiBOB in such mixtures as a function of salt concentration, solvent composition, temperature, and FS content and type.

We find that LiBOB in a mixture of GBL:EA:EC yields a technologically acceptable conductivity, and LiBOB in GBL:EA:EC is a potential candidate for Li-ion cells. For example, LiBOB based-electrolyte with a salt concentration of 0.7M LiBOB in a GBL: EA: EC (wt) composition of 1:1:0 has a conductivity ~ 6.0 and 11.1 mS/cm at -3 at 25 ^{o}C,

respectively, and at 1 M LiBOB in solvent composition of 1:1:0.1, the conductivity is ~10.8 and 20.0 mS/cm at 25 and 60 ^{o}C, respectively. These conductivities are higher than that of the state-of-art electrolyte, which is 9.5 mS/cm at 25 ^{o}C.

The product of conductivity with viscosity, which an indication for ion disassociation is essentially independent of temperature. Altough LiBOB in GBL:EA:EC (1:1:1) has the highest product value, it's conductivity is the lowest. This indicates that our system is viscosity dominated.

Adding FS to a LiBOB-based electrolyte yields a mixture with an elastic modulus independent of frequency and larger than the viscous modulus in a dynamic rheology experiment, which indicates formation of a 3-D gel structure. Fumed silica enhanced the mechanical properties of the electrolyte without sacrificing its conductivity. The surface chemistry of FS (native silanol vs octyl-modified) has no effect on conductivity but a significant effect on rheological properties of the mixture. Using a gel electrolyte is anticipated to enhance the safety of lithium-ion batteries by eliminating leakage problems associated with a liquid electrolyte.

Cathode half-cells using a LiBOB-based electrolyte give good performance, and in the case of $LiMn_2O_4$ half-cells, the performance is better than that using state-of-art electrolyte. It is expected that $LiMn_2O_4$ cathodes will lower the cost of lithium-ion batteries based on material cost. The performance of $LiFePO_4$ and $LiCoO_2$ half-cells using the gel electrolyte is comparable to half-cells using state-of-art electrolyte. In addition, a Celgard^{TM} separator can be eliminated by using gel electrolyte, which should lower the cost of lithium-ion batteries. Our results show that using 1M LiBOB in GBL:EA:EC + 20% R805 can

prevent contact between the cathode and the anode without Celgard and give a better performance than cells using the separator.

Results obtained in this dissertation support further study of LiBOB-based gel electrolyte as a potential replacement for the state-of-art electrolyte for use in lithium-ion batteries.

Lithium Bis(Oxalato)Borate-Based Electrolyte For Lithium-Ion Cells

by
Fadhel A Kh A Azeez

A dissertation submitted to the Graduate Faculty of
North Carolina State University
in partial fulfillment of the
requirements for the Degree of
Doctor of Philosophy

Chemical & Biomolecular Engineering

Raleigh, North Carolina

2009

APPROVED BY:

_____	_____
Prof. Peter S. Fedkiw Chairman of the Advisory Committee	Prof. Saad A. Khan
_____	_____
Prof. Orlin D. Velev	Prof. Xiangwu Zhang

BIOGRAPHY

Fadhel Azeez was born November 13, 1977 in Kuwait. In the fall of 1996, he attended Kuwait University, Kuwait, where he spent four and half years completing a Bachelor of Science degree in Chemical Engineering. He worked from January 2001 to August 2003 as a process engineer in Equate (Kuwait), a petrochemical complex producing ethylene glycol, polyethylene, and polypropylene and jointly owned by Kuwait government and Dow Chemical.

In the fall of 2003, he enrolled at North Carolina State University as a graduate student in the Department of Chemical & Biomolecular Engineering, and joined the electrochemical engineering group under the guidance of Prof. Peter S. Fedkiw. He obtained his Master of Science degree in Chemical Engineering in 2005 and joined the PhD program under the guidance of Prof. Fedkiw in 2006.

ACKNOWLEDGEMENTS

I would sincerely like to thank:

My family for their eternal love, long distance support and encouragement, particularly my mother without whom none of this would have been possible.

My wife, for her support, love, and trust, which always helped me face and go through the difficult moments.

My academic advisor, Prof. Peter Fedkiw, for his time and energy in developing this project and my engineering career.

My committee members, Prof. Saad A. Khan, and Prof. Orlin D. Velev, and Prof. Xiangwu Zhang, for their interest and advice.

My electrochemical engineering group members for their morale and technical support. Their friendship and high-spirit made the office and laboratory pleasant places to be.

Dr. Simon Leppi for assistance with the FTIR work which was conducted at the Laser Imaging and Vibrational Spectroscopy Facility located at NCSU in the Department of Chemistry.

All my friends for their cheer and encouragement. The good time we shared together made my extra-curricular life enjoyable and pleasant.

TABLE OF CONTENTS

LIST OF TABLES

LIST OF FIGURES

CHAPTER 1: INTRODUCTION

1. 1. Motivation for this research

The growth in portable electronics devices such as cellular phones and laptop computers during the past two decades has created great interest in compact, light-weight batteries offering high energy densities that show good rechargeability and reliability. In addition, strengthened environmental regulation and a more rational use of available energy resources prompt the development of advanced batteries for electric vehicles.

Currently, the state-of-art electrolyte for the lithium-ion battery, which is the best battery presently available for a variety of applications, is composed of lithium hexafluorophosphate ($LiPF_6$) dissolved in a mixture of ethylene carbonate (EC) and linear esters such as dimethyl carbonate (DMC), diethyl carbonate (DEC), and ethyl methyl carbonate (EMC). Lithium hexafluorophosphate is the common salt in commercial lithium-ion batteries because it has many advantages such as good conductivity in solution, good mobility, and the ability to passivate the positive electrode's aluminum (Al) current collector. Ethylene carbonate is a major solvent in commercial lithium-ion batteries because of its high-dielectric constant and ability to form a good solid electrolyte interface (SEI) on the graphitic anode in lithium-ion batteries. However, current lithium-ion batteries operate only up to 60 ^{o}C due to the low thermal stability of $LiPF_6$[1-5] and its susceptibility to hydrolysis. In addition, the low-temperature performance of current lithium-ion batteries is limited to -20^{o}C and is affected by high melting point of EC[6-8]. Improving the high- and low-temperature performance of lithium-ion batteries electrolyte will have a significant impact on batteries

and their applications. In order to improve the high- and low-temperature performances of lithium-ion batteries, researchers have been trying to replace $LiPF_6$ and reduce or eliminate EC from the electrolyte system.

To improve the possibility of using lithium-ion batteries in hybrid electric vehicle (HEV), issues like high cost and safety of currently used lithium-ion batteries need to be addressed. The high cost of current lithium-ion batteries stems, in part, from using expensive cathodes such as $LiCoO_2$. Cheap cathodes such as $LiFePO_4$ and $LiMn_2O_4$ are not being used with $LiPF_6$ because of detrimental effects of HF, which is a side product from the reaction between H_2O and $LiPF_6$, on these cathodes. By not using $LiPF_6$ as the salt, we can eliminate these effects and use other cathodes to lower the cost of lithium-ion batteries. The second issue of improving the lithium-ion battery performance, which is related to safety, can be enhanced by eliminating the leakage problem of liquid electrolyte by adding fumed silica nano particulates to the mixture and convert the liquid to a gel electrolyte.

Efforts have been devoted to develop alternative lithium salts to replace $LiPF_6$, including lithium perchlorate ($LiClO_4$), lithium arsenate ($LiAsF_6$), lithium tetrafluoroborate ($LiBF_4$), lithium triflate ($LiCF_3SO_3$), and lithium bis(trifluoromethane sulfonyl)imide ($LiN(SO_2CF_3)_2$). However, each salt has its own challenges that prevent it from being used in commercial Li-ion batteries. [9-14]

Recently, lithium bis(oxalato)borate (LiBOB), which was independently disclosed by Lischka *et al.* in Germany and Angell *et al.* in the USA [15, 16], has attracted attention as a promising candidate for Li-ion batteries [17-20]. The LiBOB salt has many advantages such as high thermal stability (up to 302 ^oC), ability to passivate aluminum, and ability to form a

solid electrolyte interface (SEI) on graphite even in the absence of EC[21, 22], which is a major solvent component due to its ability to form the SEI. Almost all the studies done with LiBOB in the past six years use mainly carbonate solvents. Although LiBOB has many advantages, it also has disadvantages when used with linear carbonate solvents, which are used in state-of-art electrolytes as co-solvents to lower the viscosity of the electrolyte. The problems of using LiBOB with linear carbonate solvents comes from LiBOB essentially being insoluble in these solvents [23] and, consequently, the formulation of the solvents is restricted to be EC- or PC-rich. However, high-EC or -PC content in an electrolyte formulation tends to increase its viscosity, which renders the electrolyte with poor low-temperature performance and rate capability. For low-temperature application, one needs to find a proper solvent mixture that is tailored for LiBOB to give high conductivity and good salt solubility. Since it is reported that esters (such as ethyl acetate (EA)…) can improve the low-temperature performance of Li-ion batteries [24-25], we decided to use esters instead of linear carbonate solvents in our system. Our hypothesis is that LiBOB in GBL:EA:EC has the potential to improve the performance (by eliminating problems caused by HF), lower the cost (by using cheaper salt and cathodes), and enhance the safety of lithium-ion batteries (by eliminating leakage problem associated with liquid electrolyte).

1.2. Objectives of this study

1.2.1. Liquid electrolyte

The first objective of this study is to determine if LiBOB-based electrolytes can be used in practical lithium-ion batteries, as determined by cycling performance of cells using

these electrolytes. In this work, we study the cycling performance of cells using LiBOB-based electrolyte as a function of LiBOB salt concentration and solvent composition. For these studies, half cells are made using three types of metal-oxide cathode: lithium cobalt oxide, lithium manganese oxide, and lithium iron phosphate. The cycling performance of cathode half-cells using all three cathode materials and anode half-cells using graphite with LiBOB in GBL+EA+EC are evaluated and compared with cells using state-of-art electrolyte ($LiPF_6$ in EC:EMC).

1.2.2. Gel electrolyte

The second objective of this study is to evaluate the cycling performance of cells using LiBOB-based gel electrolyte. A first step in our efforts to achieve this objective is to examine the ability of a LiBOB-containing liquid electrolyte to form a gel electrolyte. Two types of fumed silica are chosen: R805 and A200 (Evonik [26-27]). The R805 fumed silica contains octyl surface group at 48% coverage and silanol surface group at 52% coverage, and the A200 fumed silica contains only native silanol on the surface. These two silica types are chosen to examine the effect of surface chemistry of fumed silica on conductivity and rheology of the gel electrolytes. In this study, conductivity and rheological properties of the gel electrolytes as a function of salt concentration, solvent composition, fumed-silica content, fumed-silica type and temperature are evaluated and compared to those of liquid electrolyte.

From these results, an understanding for the effects of solvent composition, salt concentration, temperature, fumed silica content and type is gained. That understanding can enable us to determine the best solvent composition, salt concentration and fumed silica

percentage in the electrolyte to produce a mixture that yields good cycleability, mechanical strength, and conductivity.

In order to determine if the gel electrolyte can be used in lithium-ion cells, the performance of cathode and anode half-cells using the gel electrolyte is evaluated. Three types of cathodes: lithium cobalt oxide, lithium manganese oxide, and lithium iron phosphate are used in this study. The cycleability of all these cells is be evaluated and compared with those of LiBOB-based liquid electrolyte.

1.3. Our approach

To enable an electrolyte capable of working in a wide temperature range, our strategy was to choose a salt (other than $LiPF_6$) that satisfies the requirements given in section 3.1.2 and gives better high-temperature performance than the currently used $LiPF_6$. Suitable solvents must be used with the chosen salt to improve the low-temperature performance of lithium-ion batteries. We have chosen LiBOB as the salt for this study, and mixtures of γ-butyrolactone (GBL), ethyl acetate (EA) and ethylene carbonate (EC) as the solvents.

The solvent γ-butyrolactone (GBL) is chosen because it has a reasonably high-dielectric constant (~39), a relatively moderate viscosity (~1.73 cP at 25 ^{o}C), a similar structure to EC, and good solubility for LiBOB[28-30]. In addition, it was reported that GBL can improve the low-temperature performance of a LiBOB based electrolyte system[31-32]. The solvent EA is chosen because it has a low-melting point (~ -84 ^{o}C), which increases the liquid range of the electrolyte. In addition, the low viscosity (~ 0.45 cP at 25 ^{o}C) of ethyl acetate (EA) improves the conductivity of the electrolyte. Ethyl acetate (EA) also

has the ability to improve the low-temperature performance for lithium-ion cells by improving solution transport properties[33-34].

To achieve our objectives, electrochemical impedance spectroscopy (EIS) is used to measure the conductivity of the LiBOB-based electrolyte as a function of salt concentration, solvent composition, fumed-silica content, fumed-silica type and temperature. A rheometer is used to study the rheological properties of our gel electrolytes as a function of salt concentration, solvent composition, fumed-silica type and fumed-silica content. An Arbin battery cycler controlled by Arbin ABTS software is used to measure cycleability for the cathode and anode half-cells. In these cells, three types of cathodes are used: lithium cobalt oxide, lithium manganese oxide, and lithium iron phosphate. Finally, IR spectroscopy is used to study the effect of surface chemistry of fumed silica on rheological properties. The full plan to achieve our goals is schematically illustrated in scheme 1.1, which shows our approach to formulate and characterize LiBOB-based liquid and gel electrolytes for use in lithium-ion and lithium cells.

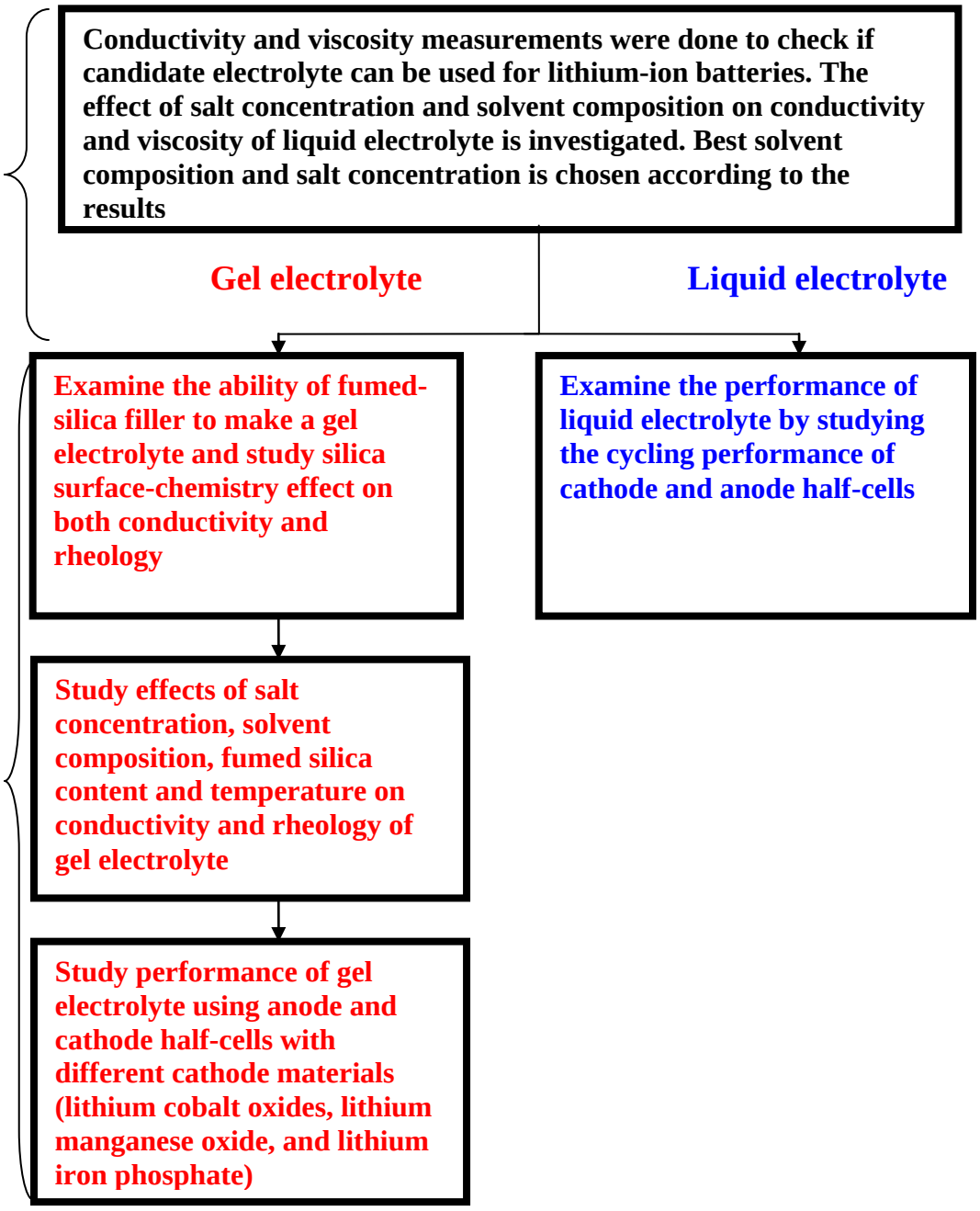

Scheme 1.1. Work plan.

1.4. Outline of thesis

An overview about lithium-ion batteries and electrolytes for Li-ion batteries are presented in Chapters 2 and 3, followed by an experimental section detailing the material preparation and characterization in Chapter 4. Submitted (or prepared for submission) manuscripts to peer-reviewed journals are presented in the following four chapters. Chapter 5 reports the effect of salt concentration, solvent composition, and temperature on the conductivity and viscosity of the LiBOB-based liquid electrolyte. Chapter 6 reports the effect of salt type and concentration, solvent composition, fumed silica type and content on rheological properties of LiBOB-based electrolyte. Chapter 7 reports the effect of salt concentration, solvent composition, fumed silica type and content, temperature, and cathode type on conductivity of LiBOB-based gel electrolyte and on cycling performance of cells using LiBOB-based electrolyte and state of art electrolyte. Chapter 8 reports performance of half cells using LiBOB-based electrolyte without using Celgard separator and compare its performance with a cell using Celgard separator. In Chapter 9, conclusions from the experimental results and recommendations for future work are presented. Experimental results are presented in Appendix A, which illustrates the effect of salt concentration, solvent compositions, fumed-silica content, fumed-silica type, temperature, and cathode type on conductivity, rheology, and cell performance of LiBOB-based electrolyte for lithium-ion batteries.

1.5. References

1. S. E. Sloop, J. K. Pugh, S. Wang, J. B. Kerr, K. Kinoshita, Electrochem. Solid-State Lett. 4 ,(2001), A42.

2. S. E. Sloop, J. B. Kerr, and K. Kinoshita, J. Power Sources 119-121, (2003), 330.

3. B. Ravdel, K. M. Abraham, R. Gitzendanner, J. DiCarlo, B. L. Lucht, and C. Campion, J. Power Sources 119-121, (2003), 805.

4. C. L. Campion, W. Li, W. B. Euler, B. L. Lucht, B. Ravdel, J. F. DiCarlo, R. Gitzendanner, and K. M. Abraham, Electrochem. Solid-State Lett. 7, (2004), A194.

5. K. Tasaki, K. Kanda, S. Nakamura, and M. Ue, J. Electrochem. Soc. 150, (2003), A1628.

6. A. Ohta, H. Koshina, H. Okuno, and H. Murai, J. Power Sources 54, (1995), 6.

7. Y. Ein-Eli, S. R. Thomas, R. Chadha, T. J. Blakely, and V. R. Koch, J. Electrochem. Soc. 144, (1997), 823.

8. S. P. Ding, K. Xu, and T. R. Jow, J. Electrochem. Soc. 147, (2000), 1688.

9. R. Jasinski, and S. Carroll, J. Electrochem. Soc. 117, (1970), 218.

10. A. Webber, J. Electrochem. Soc. 138, (1991), 2586.

11. S. S. Zhang, K. Xu, and T. R. Jow, J. Solid State Electrochem. 7, (2003), 147.

12. F. Croce, A. D'Aprano, C. Nanjundiah, V. R. Koch, C. Walker, and M. Salomon, J. Electrochem. Soc. 143,(1996), 154.

13. M. Ue, J. Electrochem. Soc 141, (1994), 3336.

14. L. J. Krause, W. Lamanna, J. Summerfield, M. Engle, G. Korba, R. Loch, and R. Atanasoski, J. Power Sources 68, (1997), 320.

15. U. Lischka, U. Wietelmann, and M. Wegner, German Pat. DE 19829030 C1 (1999) doi:10.1149/1.1701584.

16. W. Xu and C. A. Angell, Electrochem. Solid-State Lett., 4, (2001), E1.

17. S.S. Zhang, J Power Sources 162, (2006).1379.

18. K. Xu, S.S. Zhang, U. Lee, J.L. Allen, and T.R. Jow, J Power Sources 146, (2005), 79.

19. W. Xu and C.A. Angell, Solid State Ionics 147, (2002), 295

20. Yu BT, Qiu WH, Li FS and Xu GX, Electrochem Solid-State Lett 9, (2006), A1.

21. K. Xu, S. Zhang, B. A. Poese, and T. R. Jow, Electrochem. Solid-State Lett., 5, (2002), A259.

22. Gnanaraj JS, Levi MD, Gofer Y, Aurbach D and Schmidt M, J. Electrochem Soc 150: (2003), A445.

23. K. Xu, J. Electrochem Soc, 155 (2008), A733.

24. A. Chagnes, B. Carre, P. Willmann, R. Dedryvere, D. Gonbeau, and D. Lemordant, J. Electrochem. Soc., 150, (2003), A1255.

25. M. C. Smart, B. V. Ratnakumar, and S. Surampudi, J. Electrochem. Soc., 149, (2002), A361.

26. G. Michael and H. Ferch, Basic Characteristics of Aerosil, Degussa Technical Bulletin Pigment No. 11, (1998).

27. M. Ettlinger, Highly Dispersed Metallic Oxides Produced by the AEROSIL® Process, Degussa Technical Bulletin Pigments No. 56, Akron, OH (2002).

28. M. Salomon, and E. Plichta, J. Electrochim. Acta 30, (1985), 113.

29. A. Chagnes. B. Carre, P. Willmann, and D. Lemordant, J. Power Sources 109, (2002), 203.

30. T. Fukushima, Y. Matsuda, H. Hashimoto, and R. Arakawa, J. Power Sources 110, (2002), 34.

31. N. Takami, T. Ohsaki, H. Hasebe, and M. Yamamoto, J. Electrochem. Soc. 149, (2002), A9.

32. T.R. Jow, K. Xu, M.S. Ding, S.S. Zhang, J.L. Allen, and K. Amine, J. Electrochem. Soc 151, (2004), A1702.

33. K. Sawai, snd T. Ohzuku, J. Electrochem. Soc. 150, (2003), A674.

34. S. Herreyre, O. Huchet, S. Barusseau, F. Perton, J. M. Bodet, and Ph. Biensan, J. Power Sources 97/98, (2001), 576.

CHAPTER 2: AN OVERVIEW ON LITHIUM-ION BATTERIES

2.1. Introduction

The growth in portable electronics devices such as cellular phones and laptop computers during the past two decades has created huge interest in compact, light weight batteries offering high energy densities that show good re-chargeability and reliability. In addition, strengthened environmental regulation and a more rational use of available energy resources prompt the development of advanced batteries for electric vehicles.

In portable devices, initially the rechargeable Ni-Cd battery took the biggest market share. However, the environmental concerns of Cd and the low capacity of Ni-Cd cells stimulated the development of Ni-MH batteries, which use hydrogen storage alloys as anodes. The Ni-MH battery started production around 1990 and the demand for the Ni-MH battery keeps increasing. However, both the Ni-Cd and Ni-MH batteries have low cell voltages (~1.35 V) and heavy reactants/products. On the other hand, lithium batteries provide cell voltages as high as 4 V, and following the announcement of Sony Inc. in 1990, rechargeable lithium batteries have captured the market share. The higher voltage of lithium cells and low molecular weight of lithium lead to a higher volumetric and gravimetric energy density. The energy densities of the various secondary battery systems are compared in Figure 2.1 [1], which clearly shows that the lithium batteries are smaller and lighter compared to other rechargeable system. In what follows, some basic overview about batteries is given after that the reaming of this chapter is focusing on lithium and lithium-ion batteries.

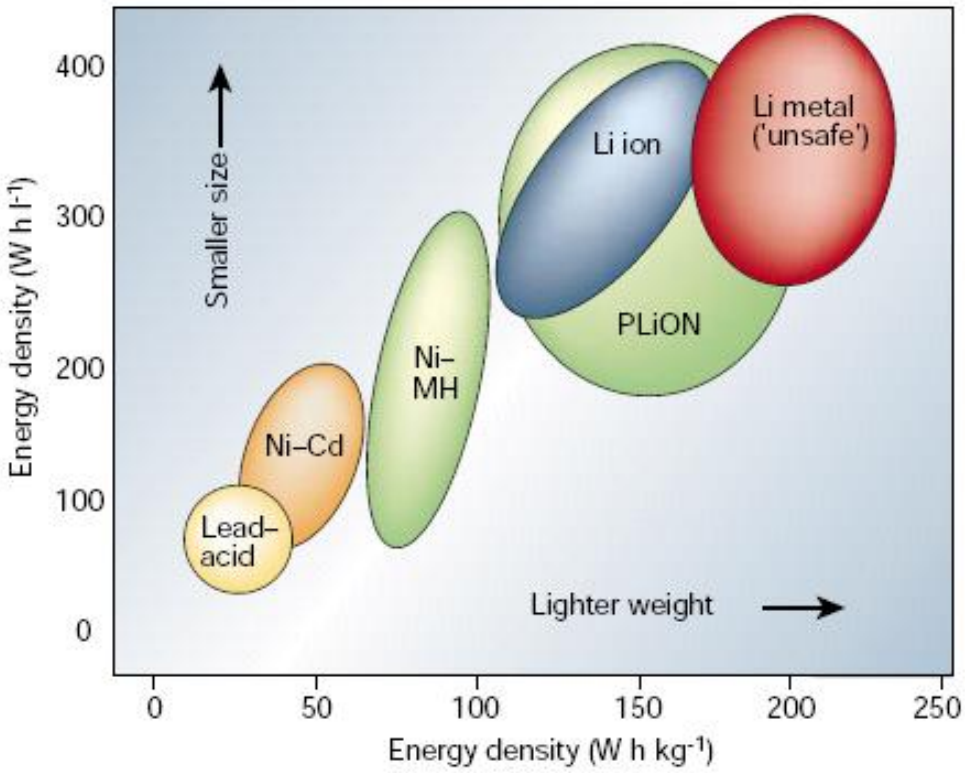

Figure 2.1. Comparison of the gravimetric and volumetric energy densities of rechargeable lithium batteries with those of other systems [1]

2.2. What is a battery?

A battery is an electrochemical device that converts chemical energy into electricity, by use of a galvanic cell. A galvanic cell is a fairly simple device consisting of two electrodes and an electrolyte solution. Batteries consist of one or more galvanic cells. Batteries can be classified to two types according to their ability of recharging:

1. Primary batteries
2. Secondary batteries

2.2.1. Primary battery

A primary battery is a battery that is designed to be used only once; it can not be recharged again. The amount of energy it can deliver is limited to that obtainable from the reactants that were placed in it at the time of manufacture.

2.2.2. Secondary battery

A secondary battery (rechargeable battery) can be recharged and used again after being fully discharged. Its electrode reactions can proceed in either direction. During charging, electrical work is done on the cell to provide the free energy needed to force the reaction in the non-spontaneous direction. It is usually designed to have a lifetime of between 100 and 1000 recharge cycles, depending on the electrode materials. Secondary batteries are, generally, more cost effective over time than primary batteries, since the battery can be recharged and reused.

2.2.3. How does a battery work?

Figure 2.2 shows a simple galvanic cell. Two electrodes are placed in an electrolyte solution. External wires connect the electrodes to an electrical load. During the discharge, an anode, where the oxidation is occurring, release electrons. These electrons flow to the cathode where they get accepted by the reduction reaction. In the same time there is a flow of anions and cations to the anode and cathode, respectively. When the anode is fully oxidized or the cathode is fully reduced, the chemical reaction will stop and the battery is considered

to be discharged. Recharging a battery is usually a matter of externally applying a voltage (i.e., energy source) across the plates to reverse the chemical process.

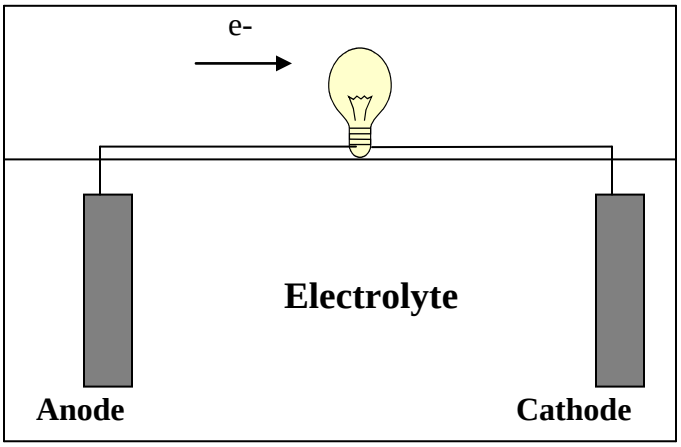

Figure 2.2. Galvanic cell during discharge process

The voltage and current that a galvanic cell produces are directly related to the types of materials used in the electrodes and electrolyte. The length of time the cell can produce that voltage and current is related to the amount of active material in the cell and the cell's design. Every metal or metal compound has an electromotive force, which is the property of the metal to gain or lose electrons in relation to another material. Compounds with a positive electromotive force will make good cathodes and those with a negative electromotive force will make good anodes. The larger the difference between the electromotive forces of the anode and cathode, the greater the amount of energy that can be produced by the cell. Table 2.1 shows the electromotive force of some common battery components. Over the years, battery scientists have experimented with many different combinations of material and have

generally tried to balance the potential energy output of a battery with the cost of manufacturing. Other factors, such as battery weight, shelf life, and environmental impact, also enter into a battery's design.

2.2.4. Galvanic cells vs. batteries

A battery is one or more galvanic cells connected in series or in parallel. A battery composed of two 1.5 V galvanic cells connected in series, for example, will produce 3 V. A typical 9 V battery is simply six 1.5 V cells connected in series. Such a series battery, however, will produce a current that is the equivalent to just one of the galvanic cells. A battery composed of two 1.5 V galvanic cells connected in parallel, on the other hand, will still produce a voltage of 1.5 V, but the current provided can be double the current that just one cell would create. Such a battery can provide current twice as long as a single cell. Many galvanic cells can be thus connected to create a battery with almost any current at any voltage level.

2.3. Battery performance

Battery performance is evaluated by a number of different parameters. In order to evaluate the performance of a battery, a basic understanding of these parameters is necessary. A brief overview of some of the important parameters for batteries is given in this section.

Table 2.1. The electromotive series for some battery components

Anode Materials from worst (most positive) to best (most negative)	**Cathode Materials from best (most positive) to worst (most negative)**
Gold	Ferrate
Platinum	Iron oxide
Mercury	Cuprous oxide
Palladium	Iodate
Silver	Cupric oxide
Copper	Mercuric oxide
Hydrogen	Cobaltic oxide
Lead	Manganese oxide
Tin	Lead oxide
Nickel	Silver oxide
Iron	Oxygen
Chromium	Nickel oxyhydroxide
Zinc	Nickel dioxide
Aluminum	Silver peroxide
Magnesium	Permanganate
Lithium	Bromate

2.3.1. Voltage

Voltage is the potential difference in charge between two points in an electrical field. There are many type of voltage definitions used for describing a battery's voltage. These definitions are theoretical voltage, open circuit voltage, actual or closed circuit voltage, and nominal voltage. Theoretical voltage depends on of the electrodes materials, electrolyte, and temperature. Open-circuit voltage is the voltage measured under no load conditions. Actual voltage or closed circuit voltage (CCV) is the voltage measured under load and it will depend on the current, the state of charge, and on the cell's history. The actual voltage will be lower than open-circuit voltage due to Ohmic (internal resistance) and polarization (activation and concentration) losses. Figure 2.3 [2] shows the typical effect of cell polarization on voltage as a function of the operating current. Nominal voltage is the generally accepted typical operating voltage for a battery.

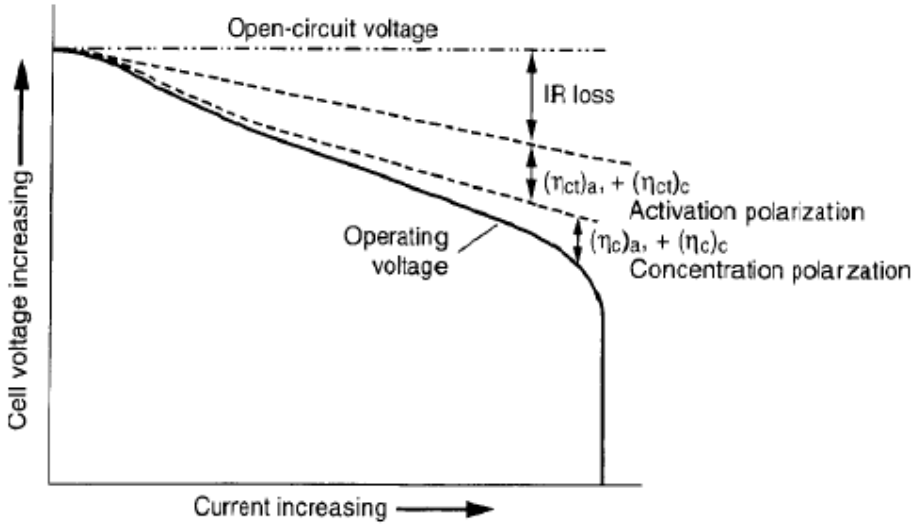

Figure 2.3. Cell polarization as a function of operating current [2]

2.3.2. Capacity

The capacity of a battery is the electrical charge (typically in units of Ah) that can be drawn from the battery. When the battery is discharged with a constant current, its capacity is given by the relation

$$C_{Ah} = I.\Delta t \quad /\boldsymbol{Ah} \tag{1}$$

A more general definition would be

$$C_{Ah} = \int_0^t I(t).dt \quad /\boldsymbol{Ah} \tag{2}$$

Capacity can be influenced by many parameters such as discharge current, voltage limit, temperature, state of charge, and history of the battery. Figure 2.4. [2] shows that cell capacity will be dramatically affected by discharge rate. Higher discharge currents result in a loss of cell capacity.

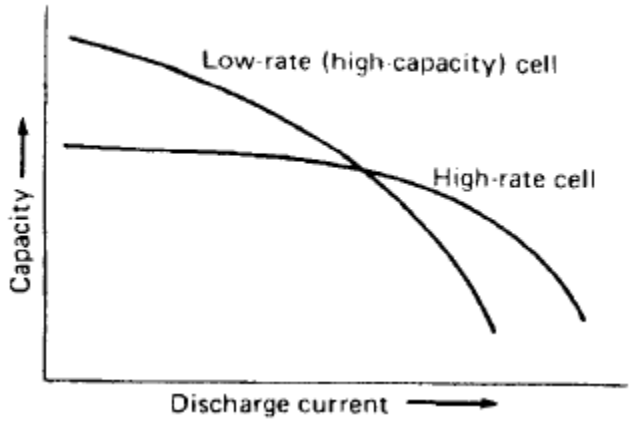

Figure 2.4. Comparison of cells of high- and low-rate services [2]

Cells are often designed for high discharge rates, but there is generally a sacrifice in capacity. The additional loss in voltage at higher currents (Figure 2.3) causes even greater losses in specific energy. Charge and discharge rates are generally rated by values denoted as C rates. A C rate of C/10, for example, signifies a discharge rate that expends the entire cell capacity in ten hours. Thus, the discharge rate (C/10) is numerically equal to 1/10 the cell capacity (Ah).

Capacity can be used to represent the quantity of electricity involved in electrochemical reaction based only on the active materials and in that case it will be called theoretical specific capacity (Ah/kg). However, if the capacity used to represent the quantity of electricity involved in electrochemical reaction based on both the active and inactive materials (electrolyte, separator, casing, and seals) it will be called actual specific capacity.

2.3.3. Self discharge

Charged batteries will slowly lose their charge over time, even if they are not connected to a device. Moisture in the air and the slight conductivity of the battery housing will serve as a path for electrons to travel to the cathode from the anode, discharging the battery. The rate at which a battery loses power in this way is called the self-discharge rate.

2.3.4. Energy content

Energy content is the energy (E) in Wh that can be drawn from a battery and it is represented by the product

$$E = \int_{t}^{t} U(t).I(t).dt \qquad \textbf{/Wh} \qquad \textbf{(3)}$$

With U=cell voltage (V); I=discharge current (A); t=discharge period (hours).

2.3.5. Specific Energy and Energy Density

For system comparison it has been become common practice to relate the energy content of a given battery either to its weight or to its volume. The weight-related energy in Wh/kg is the specific energy.

The volume-related energy density is given in units of Wh/L. The energy density is of special interest for batteries designed to power portable priority than its weight.

Given the above discussion of important battery characteristics, comparisons can now be made among the various battery systems. Table 2.2 [3] compares characteristics of some rechargeable battery technologies.

Table 2.2. Technical comparison for some rechargeable batteries [3]

	Normal Voltage (V)	*Specific Energy (Wh/kg)*	*Energy Density (Wh/L)*	*Specific Power (W/kg)*	*Power Density (W/L)*	*Cycle Life*	*Self Discharge (%/mon)*
Li Ion[1]	3.6	115	260	200-250	400-500	500-1000	5-10
Li Metal[2]	3	100-200	150-350	>200	>350	200-1000	~1
Lead Acid	2	35	70	~200	~400	250-500	4-8
Ni-Cd	1.2	40-60	60-100	140-200	220-360	300-700	10-20
NiMH	1.2	60	220	130	475	300-600	30
Zn/Air	1.2	150	200	150	190	~200	~5

1) $LiCoO_2$ used as a cathode
2) V_2O_5 used as a cathode

The values provided in the table are based upon typical cell designs, but will vary depending on the specific anode, cathode, and electrolyte. In general, lithium cells have considerably higher voltages and specific energies than other common cells and equivalent or superior performance in the other categories as well. Because of their high performance coupled with low weight and minimal volume, they are ideally suited for applications in portable devices (communications, laptops, etc) and electric vehicles.

Performance characteristics are not the only issues when comparing existing batteries or evaluating new ones. Safety is also important, particularly for domestic applications. Batteries with liquid electrolytes present the danger of leakage, and precautions must be taken by using a sturdy battery case (most often driving up both cost and weight of the battery), particularly for cells containing corrosive electrolytes. Charging is another important factor in comparing various rechargeable batteries. Just as capacity can be lost with too high a discharge rate, it can also be lost with too high a charging rate. Charging too quickly results in a build up of heat, possibly damaging the cell and reducing the capacity. Overcharging can also damage some cells. If the voltage limit on lithium-ion cells is exceeded (for example 4.2 V in the case of $LiCoO_2$), the cathode and electrolyte could decompose, the pressure could rise, and in Li-ion cells, metallic lithium could plate on the carbon surface.

2.4. History of lithium-based batteries

Lithium has the lightest weight, highest voltage, and greatest energy density of all metals. The theoretical specific capacity of lithium is 3860 mAh/g and the redox potential for

lithium is -3.01 V versus standard hydrogen electrode. These features have attracted battery investigators. Research into lithium batteries started in 1950s when it was discovered that metallic lithium was stable in a number of nonaqueous electrolytes such as fused salts, liquid SO_2, or organic electrolytes such as $LiClO_4$ in propylene carbonate. This stability was due to the formation of a passivation layer that prevents the direct chemical reaction between metallic lithium and the electrolyte but still allows for ionic transport. The first published interest in lithium batteries started with the work of Harris in 1958 [4]. The work eventually led to the development and commercialization of a variety of primary lithium cells during the 1970s.

The higher energy densities associated with lithium batteries motivated huge interest to develop lithium insertion compounds as cathodes for rechargeable lithium batteries. Studies of fast-ion conduction in solids showed that alkali metal ion could move quickly in an electronically conducting lattice containing transition metal atoms in a mixed-valence state. This led to the development of room temperature rechargeable lithium cells using lithium insertion compounds as positive electrode. In the mid 1970s, Exxon announced its intentions to commercialize the system Li/TiS_2[5]. Since then, large numbers of rechargeable systems with different cathode materials using either transition metal chalcogenides (TiS_2, MoS_2, $NbSe_3$) or transition metal oxides (V_2O_5,V_6O_{13}, MnO2), different metallic lithium or lithium alloy based anodes and electrolytes have been investigated and developed, as illustrated in Table 2.3[6]. The rechargeable Li/MnO_2 "Molicel" AA size cell ,which was manufactured by Moli Energ. Ltd. (British Columbia, Canada) in the late 80s, was probably the most sophisticated product. Apart from a few small size secondary coin cell products,

these chemistries did not generally survive into the 1990s. Cells with AA and larger size have proved difficult to make safe and there are incidents of fires in equipment powered by secondary Li/MoS_2 cells which led to a product recall[7]. A big achievement in the rechargeable lithium battery systems was in June 1990 when Sony Energytec Inc. commercialized a lithium-ion battery including a $LiCoO_2$ cathode and a non graphitic carbon anode. This battery was much safer than Li metal anode batteries.

Table 2.3. Sequence development of components and systems for rechargeable lithium batteries (LE for liquid electrolytes and PE for polymer electrolytes) [6]

Year	Development of components			Systems
	anode	cathode	electrolyte	
1970's	lithium metal (Li) lithium alloys	transition metal sulfides (TiS_2, MoS_2)	liquid organic electrolytes	Li/LE/TiS_2
		transition metal oxides (V_2O_5, V_6O_{13})	solid inorganic electrolytes (Li_3N)	
		liquid cathodes (SO_2)		Li/SO_2
1980's				
	Li-intercalation ($LiWO_2$)		polymer electrolytes	
		selenides ($NbSe_3$)		Li/LE/MoS_2 Li/LE/$NbSe_3$
		discharged cathodes ($LiCoO_2$, $LiNiO_2$)		Li/LE/$LiCoO_2$
	Li-carbon (LiC_{12}) (coke)		plasticized polymer electrolytes	Li/PE/V_2O_5, V_6O_{13}
		manganese oxide (Li_xMnO_2)		Li/LE/MnO_2
1990's				C/LE/$LiCoO_2$
	Li-carbon (LiC_6) (graphite)	manganese spinels ($LiMn_2O_4$)		C/LE/$LiMn_2O_4$

2.4.1. Problems with metallic lithium anode

Although metallic lithium anodes offer a greater energy capacity (3860 mAg/h) than lithiated carbon (372 mAg/h), difficulties stem from using metallic lithium as anode inhibit its development. The problem of using metallic lithium is its reactivity with the electrolyte and changes to its surface morphology after repetitive charge/discharge cycling. For example, when lithium is electroplated during recharge onto a metallic lithium electrode, it forms a mossy, and in some cases dendritic, deposit with a larger surface area than the original metal. While the thermal stability of lithium metal foil in many organic electrolytes is good, with minimal exothermic reactions occurring up to temperature near the melting point of lithium (181°C), the large surface area of dendrites increases lithium reactivity, thereby lowering the thermal stability of the system. This makes cells become increasingly sensitive to abuse as they are cycled. In addition, the fine metallic lithium can easily penetrate into the separator which can cause an internal short circuit, resulting in heat generation and ignition.

Another problem is the failure of attaining 100% lithium cycling efficiency. This occurs because lithium is not thermodynamically stable in the organic electrolytes and the surface of lithium is covered with a film of reaction products between the lithium and electrolyte. Every time the lithium is stripped and replaced during discharge and charge, a new lithium surface is exposed and then passivated with a new film, which mean more lithium is consumed. Because of the mossy deposit, some lithium becomes electrochemically unreactive on repeated cycling. In order to obtain a reasonable cycle life, a 3 to 5 fold excess of lithium is required. The failure to control the surface area of the lithium anode remains a

problem, limiting the commercialization of lithium anode cells with liquid organic electrolytes.

The reactions of lithium electrode with electrolyte were studied extensively and this included a number of strategies to modify the reactivity of the lithium solution interface and thus improve its utility and safety. The best strategy was to eliminate metallic lithium anode and replace it with lithiated carbon. In early 1990 Sony Energy Tec. commercialized the first lithium-ion battery. The theoretical specific capacity of the lithiated graphite LiC_6 is only 372 mAh/g, much lower than that of metallic lithium (3860 mAh/g). In spite of the lower energy density, the current rechargeable lithium battery (lithium-ion battery) technology uses a lithiated carbonaceous anode [8-10] since it offers a significant advantage in terms of safety and cycle life.

2.5. Lithium-ion batteries

In early 1990, a breakthrough was announced by Sony Energy Tech.: an anode based on lithium intercalated carbon or graphite for rechargeable lithium battery. These cells, which contain lithium insertion compounds as both cathodes and anodes, are called lithium-ion cells or rocking chair cells since the lithium ion shuttles or rocks between the cathode and anode hosts during the charge/discharge process as illustrated in Figure 2.5.[11]

During charge, the positive material (cathode) is oxidized and the negative material (anode) is reduced. In this process, lithium ions move from cathode to anode through the electrolyte and electrons flow through the external circuit from the cathode to the anode. The reverse reaction occurs during the discharge process.

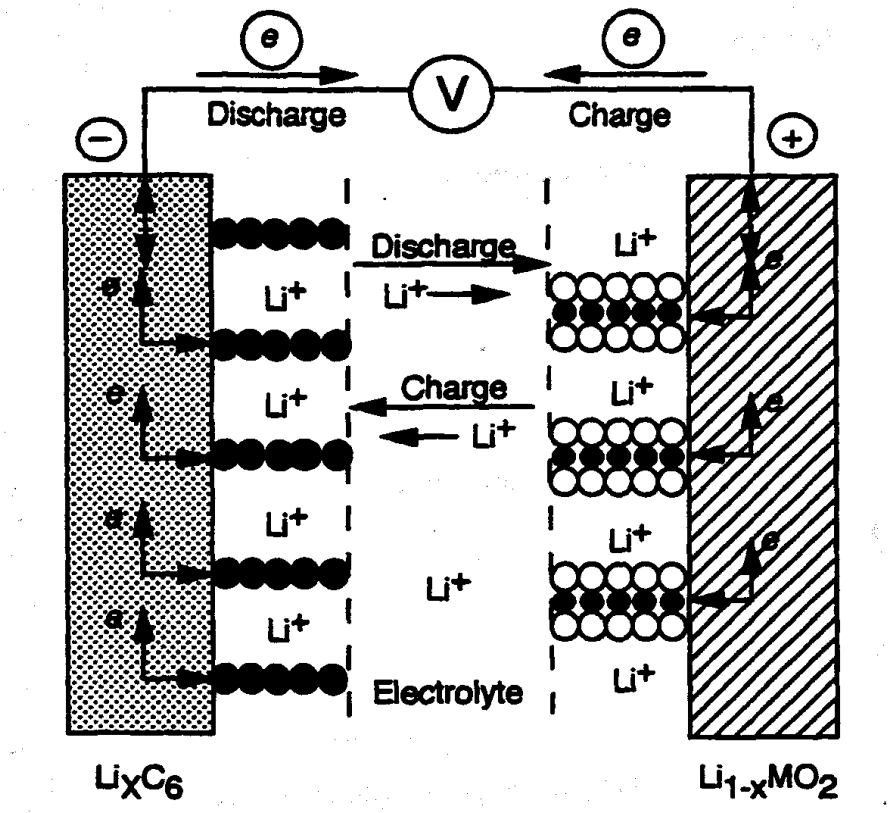

Figure 2.5. Lithium-ion battery operation [11]

Lithium-ion batteries typically consist of (i) a graphite negative electrode (anode) on a copper current collector, (ii) a lithium metal oxide positive electrode (cathode) typically a metal oxide with a layered structure, such as lithium cobalt oxide ($LiCoO_2$), or a material with a tunneled structure, such as lithium manganese oxide ($LiMn_2O_4$), on a current collector of aluminum foil, (iii) a microporous separator between the electrodes, and (iv) a liquid electrolyte that consists of a lithium salt dissolved in an organic solvent. Typical electrolytes are composed of $LiPF_6$ salt dissolved in organic-carbonate solvent. The separator does not

support ion conductivity itself, but instead allows lithium ions in the electrolyte to move between the electrodes and diffuse into the porous structure of the electrodes.

The lithium-ion battery is currently replacing all other battery types in the market, particularly in the field of electronics, computers, and communications. In recent years, the application of lithium-ion batteries for more power demanding applications such as power tools, stationary, and transportation has started.

In lithium-ion cells, the anode and cathode insertion hosts should have low and high voltages, respectively, versus metallic lithium in order to maximize the cell voltage while satisfying the other required criteria. Accordingly, among the various known lithium insertion compounds, $LiCoO_2$, $LiNiO_2$ and $LiMnO_4$ oxides having a high electrode potential of 4V versus metallic lithium have become attractive cathodes for lithium-ion cells. On the other hand, graphite and coke having a lower electrode potential of <1 V versus metallic lithium and being lightweight have become attractive anodes, as illustrated in Figure 2.6 [11]. The first batteries to be marketed, and the majority of those currently available, use $LiCoO_2$ as the positive electrode material since $LiCoO_2$ offers good electrical performance, is easily prepared, has good safety properties, and is relatively insensitive to process variation and moisture. More recently lower cost or higher performance materials, such as $LiMn_2O_4$ or lithium nickel cobalt oxide ($LiNi_{1-x}\ Co_xO_2$), have been introduced, permitting development of cells and batteries with improved performance. The batteries that were first commercialized employed cells with coke negative electrode materials. As improved graphite became available, the industry shifted to graphitic carbons as negative electrode materials as they offer higher specific energy with improved cycle life and rate capability.

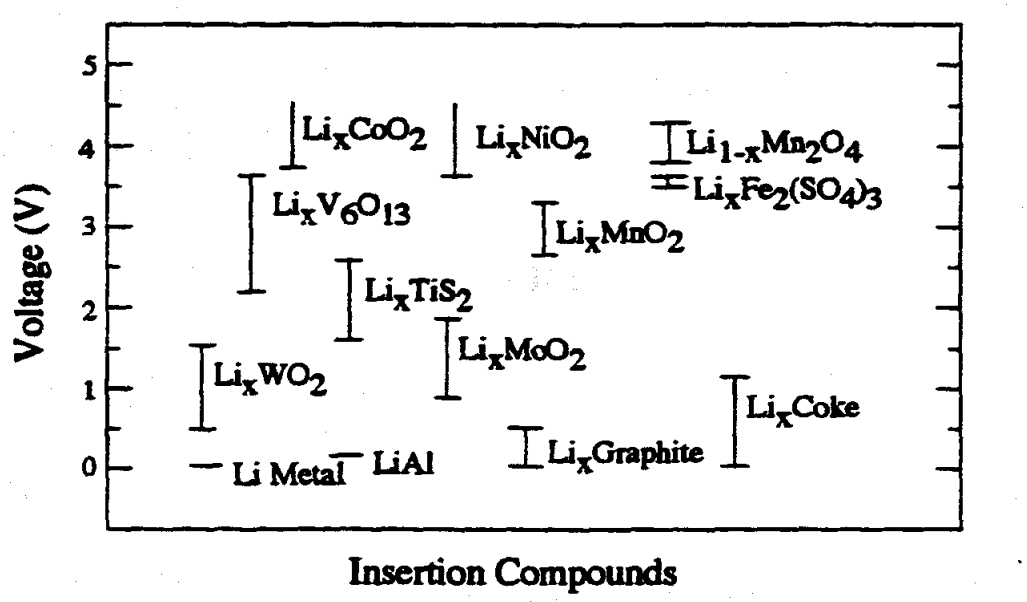

Figure 2.6. Electrochemical potential ranges of some lithium insertion compounds in reference to metallic lithium [11]

2.6. Features and benefits of lithium-ion cells

Rechargeable lithium-ion batteries offer significant advantages compared to Ni-Cd and Ni-MH cells. Lithium-ion batteries are lighter, about half the weight of Ni-Cd batteries, 30-50% smaller in volume, yet have a life span and energy density nearly twice that of Ni-Cd batteries. Lithium-ion batteries also do not suffer from many of the problems of Ni-Cd batteries. For example, Ni-Cd batteries show a self-discharge of 20-30% over a month, compared to the 5% of a Li-ion battery. Lithium-ion batteries recharge more quickly, with an 80% charge in an hour, and full charge within 2.5 hours. Lithium-ion cells also do not present environmental hazards (i.e., those with lithium manganese oxide and lithium iron phosphate cathodes), especially compared with Ni-Cd batteries, because they contain no lead,

cadmium or mercury. Most importantly, Li ion batteries have no memory effect; memory effect refers to a change in crystalline formation from the desirable small size to a large size which leads to capacity loss, which happens because of earlier incomplete charge/recharge cycles. For Ni-Cd batteries, memory effect is a serious issue. Lithium-ion batteries store three times the voltage of competing cells, so that a single 3.7 V Li ion battery can replace three Ni-Cd or Ni-MH cells. By weight, Li-ion batteries provide roughly twice the energy density (~150 Wh/Kg) of Ni-Cd cells. Consequently, to provide the same output as a Ni-Cd or Ni-MH battery, a Li-ion battery will weigh about half as much, an important factor in portable equipment. By volume, Li-ion cells provide about 25% and 40% more energy (~400 Wh/L) than Ni-MH or Ni-Cd cells, respectively. The greater energy in a small volume is an important factor in some of the most critical applications for batteries: laptop computers and cellular phones. In addition, Li-ion batteries have a wide temperature operating range. The lithium-ion cell can be charged between 0 and 45°C and discharged between -20 and 65°C. Also Li-ion cells can typically be discharged at rates up to 1.5C continuously. High capacity, higher drain multi-cell packs are achieved by connecting multiple cells in parallel. Finally, lithium-ion batteries offer long cycle life (greater than 1000 cycles). These features are summarized in Table 2.4 with circa 2000 state of art. [12]

The most significant challenges to the broader application of lithium-ion technologies are related to stability at high temperature, safety, and low-temperature performance. While batteries may be exposed to temperature as high as 70 °C for short periods, the rate of degradation of current lithium-ion batteries is significant above 65 °C. At high temperatures lithium-ion batteries lose their capacity permanently.

Table 2.4. General performance characteristics of lithium-ion batteries [12]

Characteristic	Performance range
Operational cell voltage	4.2 to 2.5 V
Specific energy	100 to 158 Wh/kg
Energy density	245 to 430 Wh/L
Continuous rate capability	Typical: 1C High rate: 5C
Pulse rate capability	Up to 25C
Cycle life at 100% DOD	Typically 3000
Cycle life at 20 to 40% DOD	Over 20000
Calendar life	Over 5 years
Self discharge rate	2 to 10%/month
Operable temperature range	−40°C to 65°C
Memory effect	None
Power density	*2000 to 3000 W/L*
Specific power	700 to 1300 W/Kg

2.7. Future trend of Li-ion batteries

With the explosive growth in portable electronics and development of electric vehicles (EV) and hybrid-electric vehicles (HEV), the battery industry is expected to grow as well. Battery technology, however, has not kept pace with the growth in technology of the fields that require their use. The continued development of portable electronics and the future success of EV and HEV require advancement of light-weight, high energy, reliable power sources. This is where Lithium-ion batteries can play a major role [13].

Lithium-ion batteries sales growth was magnificent in the past few years, as shown in Figure 2.7.

The global Li-ion battery sales reached 0.86 billion pieces in 2002 with a total revenue of $2.818 billion marking a growth rate of 49.10%. The major driving force was its application in mobile phone market, which was responsible for 60% of Li-ion battery sales.

In 2003 Li-ion battery sales reached to 1.255 billion pieces, with total sales revenue of $3.634 billion representing an increase of 28.96%. In 2005, Li-ion battery sales reached two billion pieces, which increased to 2.5 billion in 2006. It is expected that global sales of Li-ion battery will be over three billion pieces in 2010[14]. Li-ion battery is expected to continue its growth in sales in next few years especially with expansion in the use of Li-ion batteries in hybrid applications as expected by Dr. Menahem Anderman[14]. Dr. Menahem Anderman, the president of Advanced Automotive Batteries, projects that the automotive lithium-ion market could reach $1.6 billion in 2015 pushed largely by a dramatic expansion in the use of Li-ion batteries in hybrid applications[15].

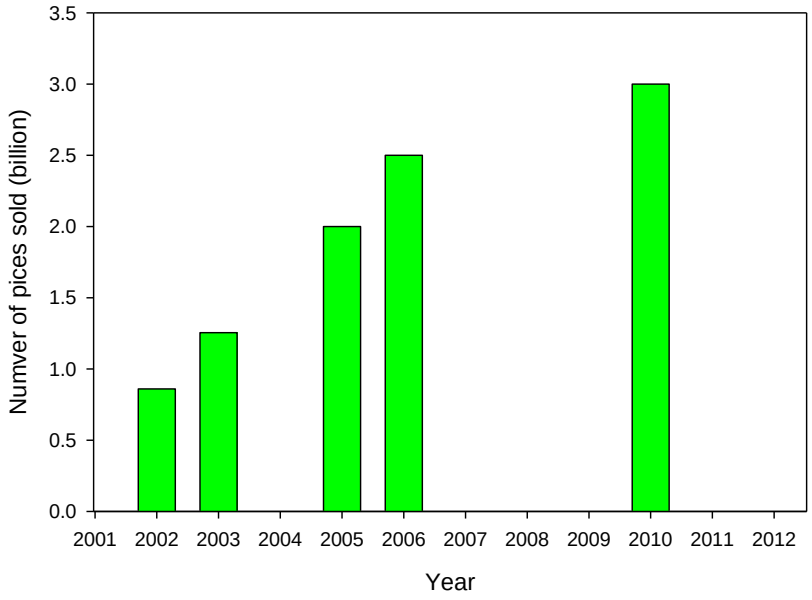

Figure 2.7. Li-ion batteries market

2.8. Design principles

From a materials design point of view, the cathode and anode insertion compounds should satisfy several important criteria such as:

1. The cathode insertion compound should have a high Li chemical potential ($\mu_{Li(c)}$) to maximize the cell voltage. This implies that the transition metal ion M^{n+} in $Li_xM_yX_z$ should have a high oxidation state.
2. The anode insertion compound should have a low Li chemical potential ($\mu_{Li(a)}$) to maximize the cell voltage. This implies that the transition metal ion M^{n+} in $Li_xM_yX_z$ should have a low oxidation state.
3. The insertion compound $Li_xM_yX_z$ should allow a large degree *x* of lithium insertion/extraction, to maximize the cell capacity. This depends on the number of available lithium sites and the accessibility of multiple valences for M in the insertion host. A combination of high capacity and cell voltage can maximize the energy density, which is given by product of the capacity and voltage.
4. The lithium insertion/extraction process should be reversible with no or minimal changes in the host structure over the entire range *x* of Li insertion/extraction in order to provide a good cycle life for the cell. This implies that the insertion compound $Li_xM_yX_z$ should have good structural stability without breaking any M-X bonds.
5. The insertion compound should have good electronic conductivity σ_e and good lithium-ion conductivity σ_{Li} to minimize polarization losses during the

discharge/charge process and thereby to support a high current density and power density. Factors like crystal structure; geometry and interconnection of the lithium sites; nature and electronic configuration of the Mn^{+} ion control if the insertion compound have good electronic and lithium-ion conductivities.

6. The insertion compound should be chemically stable without undergoing any reaction with the electrolyte over the entire range, *x*, of lithium insertion/extraction.
7. The redox energy of the cathode and anode in the entire range, *x*, of lithium insertion/extraction should lie within the band gap of the electrolyte, as shown in Figure 2.8 [11], to prevent unwanted oxidation or reduction of the electrolyte.
8. From a commercial point of view, the insertion compound should be inexpensive, environmentally benign, and lightweight.

In addition to these requirements of insertion electrode materials, several other criteria are important in designing a good lithium-ion cell that can offer high performance with long cycle life. The electrolyte should have high lithium ion conductivity but should be an electronic insulator in order to avoid internal short circuiting. A high ionic conductivity in the electrolyte is essential to minimize Ohmic (IR) polarization and achieve good rate capability. With a given electrolyte, the IR drop due to electrolyte resistance can be reduced and the rate capability can be improved by having a higher electrode interfacial area and thin separators. The electrolyte should also have good chemical stability and should not undergo any chemical reaction with the electrodes. Additionally, the engineering involved in cell design and fabrication plays a critical role in the overall cell performance. For example, high

electronic conductivity and lithium ion diffusion rate in the electrodes are essential to minimize cell polarization and the electronic conductivity of the electrodes can be improved by adding electronically conducting additives such as carbon. However, the amount of additive should be minimized to avoid any undue sacrifice in gravimetric or volumetric capacity. Finally, cell safety, environmental factors, and raw material fabrication costs are additional important considerations in both materials selection and cell design.

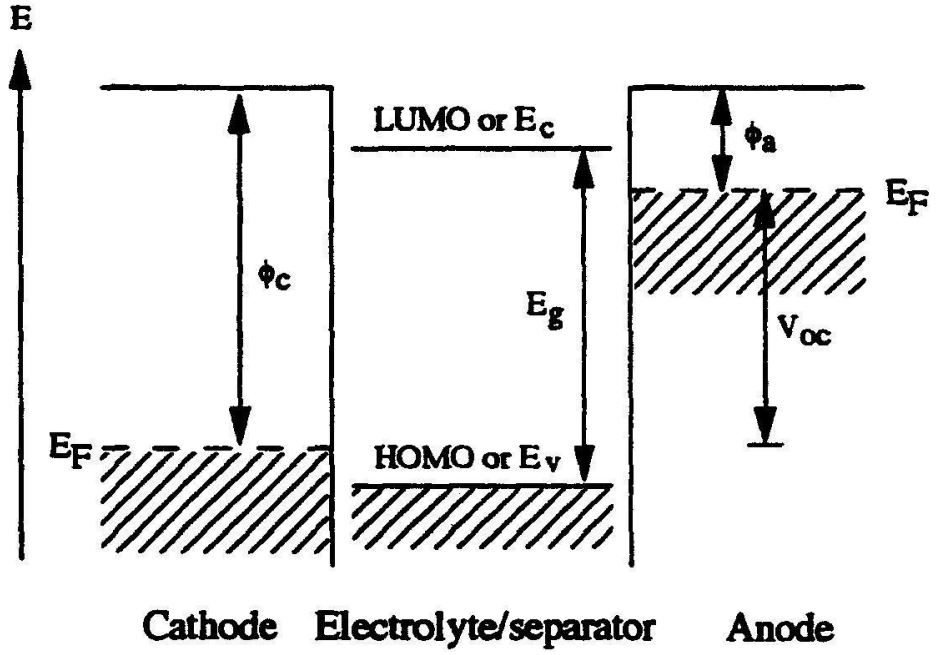

Figure 2.8. Schematic energy diagram of a cell at open circuit [11]

2.9. Lithium-ion battery components and their development

A battery consists of a positive electrode (cathode), negative electrode (anode) and an electrolyte. In addition to these major active components, a separator between the cathode and anode compartments and current collectors attached to the electrodes are also involved. A brief discussion about these components and recent research to improve their performance is discussed in the following sections.

2.9.1. Anode hosts

Carbon is the material which is used for anode in the present generation of lithium-ion cells [16,17]. The light weight and low electrochemical potential near that of metallic lithium (Figure 2.6) have made carbon an attractive anode. It has a theoretical capacity of 372 mAh/g, which corresponds to an insertion of one lithium per 6 carbon atoms (x=1 in Li_xC_6).

One of the drawbacks with the carbon anodes is the occurrence of significant amount of irreversible capacity during the first charge-discharge cycle. During the first electrochemical intercalation of lithium into carbon, some lithium is irreversibly consumed forming a solid electrolyte interface (SEI) and cannot be recovered in the following discharge, resulting in loss of capacity. This SEI depends on the electrolyte solution and the type of carbon material. When the film is sufficiently thick to prevent electron tunneling, the electrolyte reduction is suppressed and the electrode can be cycled reversibly. The capacity on the second and subsequent cycles is about the same, and lithium intercalation during charge and discharge is nearly 100% reversible. In an electrolyte containing propylene carbonate (PC), natural graphite cannot be charged as it leads to gas evolution at around 1V.

However, with electrolytes consisting of other solvents such as ethylene carbonate (EC) and diethyl carbonate (DEC) or electrolytes contain lithium bis(oxalato)borate LiBOB salt [18], the side reactions are suppressed and it can be cycled without much difficulty.

Carbonaceous materials used in Li-ion are roughly divided into three categories: graphite, soft carbon and hard carbon. Their structure is shown in Figure 2.9.[19]

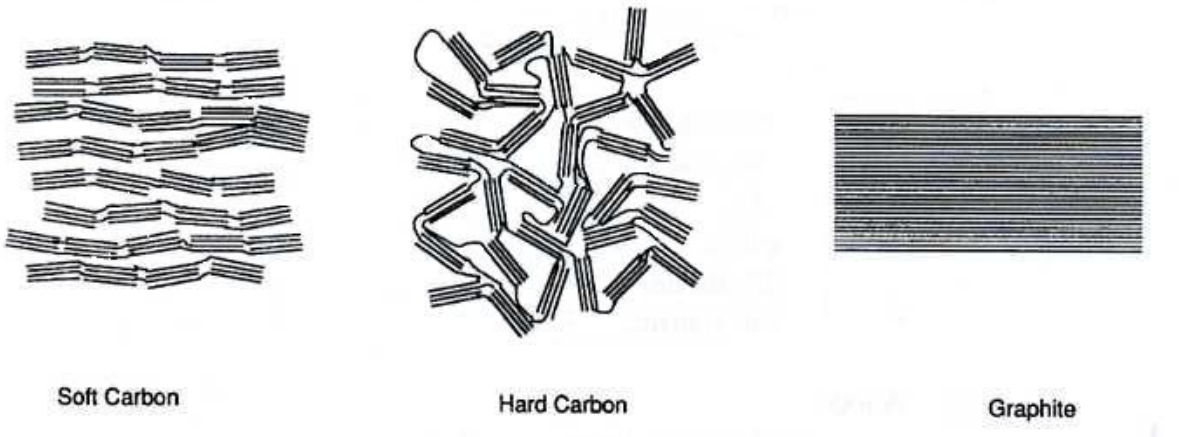

Figure 2.9. Three types of carbon used in lithium-ion batteries [19]

The structure of graphite is quite regular, namely constructed from many stacks of sheet-like layers of carbon. In the layers the carbon atoms are connected with covalent bond. In between the layers, Van der Waals force binds them to each other loosely. When charged, Li ions are doped into the layers to form lithiated carbon as shown in Figure 2.10 [19]. Soft carbon is relatively crystalline (not a perfect crystal such as graphite) and shows preferred orientation like graphite, as shown in Figure. 2.9. Hard carbon, on the other hand, is quite different from the two others. Hard carbon is relatively poorly crystalline and consists of

aggregates of small crystallites randomly oriented and amorphous, in which there are small irregular spaces Figure 2.9. Each crystallite has a layer structure like a broken piece of graphite, which is capable of smoothly storing and releasing Li ion (Figure 2.10.). The distance between neighboring layers is wider than that of graphite. Hard carbon has the advantage of yielding higher capacity, which is thought to be due to the adsorption of lithium on both sides of the single graphene sheets, accommodation of extra lithium into cavities[19], and storage of additional lithium at the edges and surfaces. In addition, hard carbon can be used with PC-based electrolyte unlike graphite. However, hard carbons show a sloping discharge profile unlike graphite, which shows a nearly flat discharge profile as shown in Figure 2.11. [20]

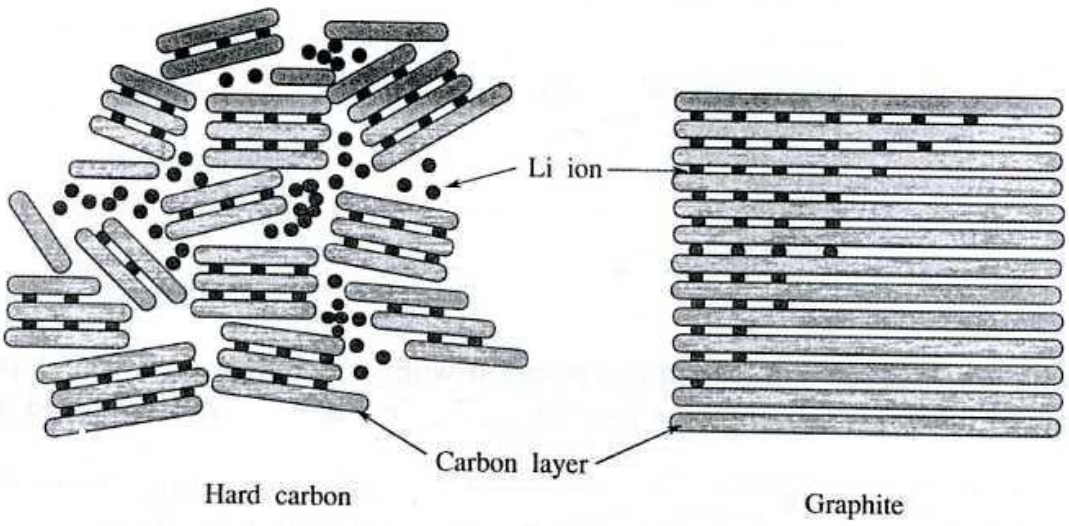

Figure 2.10. Model of lithium-ion intercalation into carbon material [19]

The choice of anode materials whether hard carbon or graphite makes a big difference when designing equipments. It is mostly due to the shape of discharge curve. Customers who want to know the residual energy capacity at any time prefer hard carbon for anode. They can detect the residual energy simply by knowing the open circuit voltage value in the discharge curve of the battery in operation. Therefore, it works as the charge-discharge indicator. On other hand, systems such as cellular phones which operate by a single Li-ion cell with cut-off voltage above 3 V, prefers graphite because hard carbon reaches the cut-off voltage faster. Consequently, the energy capacity above cut-off voltage is less than that with lower cut-off voltage because it has still residual capacity below 3 V. In such a case, graphite with its flat discharge curve has the advantage, as shown in Figure 2.11.

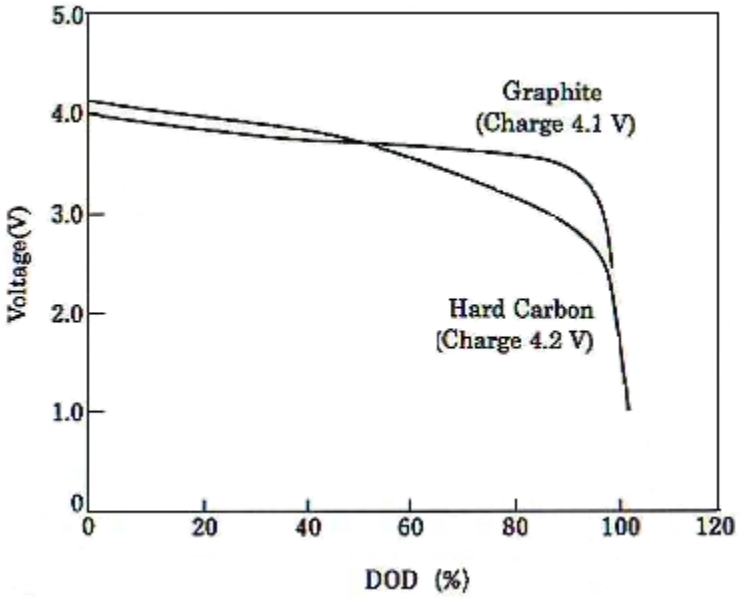

Figure 2.11.Discharge characteristics of lithium-ion with coke and graphite electrodes [19]

With an aim to improve the performance of carbon anodes, structural modifications such as texture control, surface modifications by mild oxidation and coating, and incorporation of other elements such as B, O, S and P have been studied. A few oxides, nitrides, phosphides, and intermetallic compounds have also been investigated as anode hosts. Metal nitrides and phosphides offer lower voltages versus lithium due to the covalent character and stabilization of lower oxidation states. Spinel $Li_4Ti_5O_{12}$ offers 175 mAh/g at around 1.5 V [20], but it is less attractive compared to carbon due to its lower capacity and higher voltage. Tin dioxide (SnO_2) shows a reversible capacity of as high as 600 mAh/g at 0 to 2 V, but it exhibits a highly irreversible capacity loss during the first cycle [21]. Rutile type MoO_2 and WO_2 [22,23], Fe_2O_3 [24], MnP_4 [25] and intermetallic compounds [19] such as Cu_6Sn_5 having the NiAs-type structure have also been investigated. These anodes, including carbon, do not contain lithium and they can be coupled only with cathodes such as $LiCoO_2$ and $LiMn_2O_4$ that already contain lithium. With respect to finding anodes that could be coupled with cathodes free from lithium, some lithiated transition metal nitrides [26] and intermetallic compounds [27] have become appealing. For example, $Li_{7-x}MnN_4$ and $Li_{3-x}FeN_2$ exhibit capacities of around 200 mAh/g with a flat discharge voltage of around 1.2 V. $Li_{2.6-x}Co_{0.4}N$, $Li_{2.6-x}Cu_{0.4}N$, and $Li_{2.7-x}Fe_{0.3}N$ that have structures similar to that of Li_3N exhibits much higher capacities of around 500 mAh/g at 0.2 to 1.3 V due to formation of an amorphous phase during the initial stages. Two lithium per formula unit could be reversibly extracted from Li_2CuSn[27]. However, further work is necessary to assess the full potential of these anodes especially their fast capacity fading due to the large change in volume upon

insertion/extraction. If successful, they have the possibility of being coupled with some of the lithium-free cathodes.

2.9.2. Cathode materials

In lithium-ion batteries, substances should be used as cathode materials which can intercalate/de-intercalate lithium ions at a highly positive potential (compared to the intercalation into the carbon anode) and with only low-kinetic hindrance, i.e., at low over voltage or nearly reversible. The first requirement is fulfilled especially by transition metal oxides and halides and also, to a lesser extent, by sulfides. The second requirement of low-kinetic hindrance for insertion and release of lithium ions is meant as a requirement of high mobility of lithium ions and electrons within the cathode lattice and of unhindered mass transfer across phase boundaries as far as phase transitions happen in the host lattice during insertion and removal of lithium. As the transition metal halides are poorer electronic conductors than oxides, only the latter are used in practice. Candidate cathode materials include layered compounds such as $LiCoO_2$[28-32], $LiNiO_2$[33-36], $LiNi_{1-y}Co_yO_2$, three-dimensional $LiMn_2O_4$ spinel phase, and Olivine structure cathode such us $LiFePO_4$. Although the 4 V cathodes are preferred for lithium-ion cells, cathodes with < 4 V are preferred for polymer lithium batteries, which use metallic lithium anode and solid polymer electrolytes. The instability of polymer electrolytes at higher voltages forces the use of cathodes having about 3V in polymer lithium batteries. As a result, V_6O_{13} has become an attractive cathode for polymer batteries. In addition to voltage, cell capacity is an important factor to achieve high energy density. The preference of high capacity over high voltage is beginning to

dominate in the electronics industry. Although one Li per Co could be extracted in principle, the electrolyte instability and changes in host structure limits the practical utility to 0.5 Li per Co in $Li_{1-x}CoO_2$. Similarly only about 0.4 Li per Mn could be reversibly extracted from $Li_{1-x}Mn_2O_4$. Another 0.5 Li per Mn can be inserted into $Li_{1-x}Mn_2O_4$ in the 3V range, but the 3V region exhibits drastic capacity fading. The sudden voltage change from 4 to 3 V and the poor cycle ability in the 3V region limit the practical capacity of $LiMn_2O_4$ to 0.4 Li per Mn. Thus $LiCoO_2$ and $LiMn_2O_4$ exhibit a practical capacity of about 140 and 120 mAh/g, respectively. $LiCoO_2$ is currently in widespread use as a cathode material in lithium- ion batteries. Due to its high cost, however, other materials such as $LiNiO_2$, $LiMn_2O_4$, $LiFePO_4$ and a large number of doped or substituted materials are being extensively studied as lower cost substitutes with high electrochemical performance. Many studies were conducted to improve $LiCoO_2$ performance. The electrochemical cycling of $LiCoO_2$ at a high cutoff voltage results in a significant deterioration of the stability of the cathode. The capacity loss is related to nonuniform structural change [28,37,38] and an increase in cobalt dissolution into the electrolyte [39]. To improve the electrochemical performance of $LiCoO_2$ above 4.2 V, an innovative approach involved coating the particles with some metal oxides to avoid the unwanted surface reactions and protect the electrode from the bulk [32,40-44]. This method changes the surface properties of the cobalt materials. Recent reports on surface modifications to cathode materials such $LiCoO_2$ and $LiNiO_2$ with Al_2O_3, ZrO_2, MgO, ZnO_2, Ga_2O_3, and SnO_2 have shown that surface coating is an effective way to stabilize the structure of the materials and improve their electrochemical performance.

2.9.3. Electrolyte

The electrolyte in lithium rechargeable batteries falls into one of the following categories: non aqueous liquid electrolyte, a polymer electrolyte, a solid fast ionic conductor, or a combination of one or more of the above.

Due to the low conductivity of solid electrolytes, particularly dry polymers, liquid electrolytes dominate in most electrochemical systems. The battery electrolyte should satisfy the following properties:

1. High ionic conductivity to minimize cell resistance and resistive heating of the device.
2. Good electrochemical stability to withstand the high voltage difference (>4V).
3. High chemical stability to prevent decomposition of electrolyte.
4. Low reactivity toward the components of the battery such as the electrodes, current collectors, and separators
5. Non-toxicity to be accepted environmentally for ease of handling, mass production, and waste treatment.
6. Low melting point to provide good conductivity at low temperatures.
7. High boiling point to avoid explosions resulting from high pressure build-up in the cell.
8. Low cost to compete with existing power sources using aqueous electrolytes.

The solvents should be aprotic to be stable at negative potentials and should have high polarity to dissolve lithium salts and yield high ionic conductivity. The dielectric constant and viscosity of the solvents are the most important properties that determine the ionic

conductance of the electrolyte solution [45]. Some of solvents and their properties are given in Table 2.5 [46]. Alkyl carbonates have widely been used as excellent solvents in lithium batteries. Cyclic esters like propylene carbonate (PC) and ethylene carbonate (EC) have high dielectric constant because of their high polarity, but their viscosity is high due to strong intermolecular forces. These solvents are mixed with low-viscosity solvents like dimethyl carbonate (DMC) or diethyl carbonate (DEC) to compensate for the viscosity.

Lithium hexafluorophosphate ($LiPF_6$) is a common salt for application in rechargeable lithium-ion batteries. In spite of its high-ionic conductivity, $LiPF_6$ electrolyte has distinctive disadvantages such as limited thermal stability and hydrolytic instability. Upon contact with water, $LiPF_6$ decomposes to generate toxic gaseous products, most notably hydrofluoric (HF) [47]. Hydrofluoric reacts with the electrodes and increases the electrode impedance.

To develop new electrolytes with better performance, researchers have focused on replacing alkyl carbonate with other solvents. The *trans*-2,3-butylene carbonate (4,5-dimethyl-1,3-dioxolan-2-one, *t*-BC) was found to be a suitable solvent in which graphite electrodes behave highly reversibly [48]. Chlorinated and fluorinated alkyl carbonate were also found to be very suitable [49,50] for graphite anodes. The major importance of these solvents is their use as a replacement for EC, whose freezing point is too high. There are studies of pyrocarbonate ($ROCO_2CO_2R$) and bicarbonate ($ROCO_2ROCO_2R$) as co-solvents. Their major advantage relates to modification of surface chemistry of both anodes and cathodes and an improvement of the high-temperature performance.

Table 2.5. Structure and properties of some solvents used for lithium battery electrolytes [46]

Solvent name and abbrev.	*Stuctural fomula*	*Melting point* (°C)	*Boiling point* (°C)	*Dielectric constant,* ε
Ethylene carbonate, **EC**	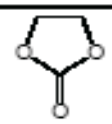	39-40	248	89.6 (40°C)
Propylene carbonate, **PC**	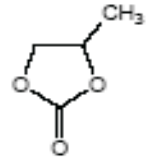	-49	240	64.4
Dimethyl carbonate, **DMC**	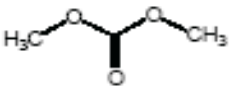	4.6	91	3.12
Diethyl carbonate, **DEC**	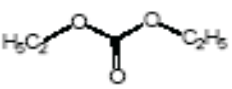	-43	126	2.82
2-Methyl-tetra hydrofuran, **2Me-THF**	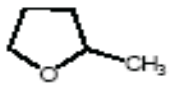	-137	79	6.29
Dimethoxy ethane, **DME**		-58	85	7.20
γ-Butyro lactone, **γ-BL**		-43	204	39.1

In addition to changing the solvents, there were many attempts to introduce new families of salts. Merck KGaA developed the $LiPF_3(CF_2CF_3)_3$(LiFAP) salt [51]. It was proven that this salt is much more stable than $LiPF_6$. Its solution is less acidic and more thermally stable than $LiPF_6$ solutions. Recently, LiBOB was suggested as a stable and non acidic salt [52]. Both Li-C and Li_xMO_y cathodes seem to behave highly reversible in its solution. However, more work is needed to confirm that this salt is a viable alternative to $LiPF_6$.

2.9.4. Separator materials

Lithium-ion cells use a microporous film, which has a thickness between 10 to 30 μm, to electrically isolate the positive and negative electrodes. All commercially available liquid electrolyte cells use microporous polyolefin materials as they provide excellent mechanical properties, chemical stability and acceptable cost. Some of separators used in different lithium batteries are given in Table 2.6. Requirements for lithium-ion separators include:

1. High machine direction strength to permit automated winding.
2. Does not yield or shrink in width.
3. Resistant to puncture by electrode materials.
4. Effective pore size less than 1μm
5. Easily wetted by electrolyte.
6. Compatible and stable in contact with electrolyte and electrode materials.

Microporous polyolefin materials in current use are made of polyethylene, polypropylene or laminate of polyethylene and polypropylene. The low melting point of polyethylene (PE) materials enables their use as a thermal fuse. As the temperature approaches the melting point of polymer, ~135 °C for polyethylene and ~165 °C for polypropylene (PP) porosity is lost, which shut down the ionic path. The following tables[53] summarize the major manufacturers of lithium-ion separators along with their major products (Table 2.7), manufacturing process of typical microporous films (Table 2.8), typical properties of some commercial microporous membranes (Table 2.9), thermal mechanical

analysis (TMA) data for typical Celgard separators (Table 2.10), and safety and performance tests for lithium-ion batteries and the corresponding important separator and its effect on the cell performance and/or safety (Table 2.11). Recently Exxon Mobil and Tenen Chemical Nasu Co. Ltd. announced that they developed a new separator. Exxon claims that the new separator is going to improve Li-ion batteries power and safety performance in hybrid-electric vehicle (HEV) applications. Table 2.12[54] compares the new separator and some other commercial separators.

Table 2.6. Separators used in secondary lithium batteries [53]

Battery system	Type of separator	Composition
Lithium-ion (liquid electrolyte)	microporous	polyolefins (PE, PP, PP/PE/PP)
Lithium-ion gel polymer	microporous	PVdF (polyvinylidene fluoride)
	microporous	polyolefins (PE, PP, PP/PE/PP) coated with PVdF or other gelling agents
Lithium-polymer (e.g. Li-V_6O_{13})	polymer electrolyte	poly(ethylene oxide) with lithium salt

PE= Poly ethylene
PP= Poly propylene

Table 2.7. Major manufacturers of lithium-ion battery separators along with their typical products [53]

Manufacturer	Structure	Composition	Process	Trade name
Asahi Kasai	single layer	PE	wet	HiPore
Celgard LLC	single layer	PP, PE	dry	Celgard
	multilayer	PP/PE/PP	dry	Celgard
	PVdF coated	PVdF, PP, PE, PP/PE/PP	dry	Celgard
Entek Membranes	single layer	PE	wet	Teklon
Mitsui Chemical	single layer	PE	wet	--------
Nitto Denko	single layer	PE	wet	--------
DSM	single layer	PE	wet	Solupur
Tonen	single layer	PE	wet	Setela
Ube Industries	multi layer	PP/PE/PP	dry	U-Pore

Table 2.8. Manufacturing process of typical microporous film. [53]

Process	Mechanism	Raw material	Properties	Typical membranes	Manufacturers
Dry process	drawing	polymer	simple process anisotropic film	PP, PE, PP/PE/PP	Celgard, Ube
Wet process	phase separation	polymer + solvent	isotropic film	PE	Asahi, Tonen
		polymer + solvent + filler	large pore size high porosity	PE	Asahi

Table 2.9. Typical properties of some commercial microporous membranes [53]

Separator/ properties	Celgard 2730	Celgard 2400	Celgard 2320	Celgard 2325	Asahi Hipore	Tonen Setela
Structure	single layer	single layer	trilayer	trilayer	single layer	single layer
Composition	PE	PP	PP/PE/PP	PP/PE/PP	PE	PE
Thickness (um)	20	25	20	25	25	25
Gurley (s) [a]	22	24	20	23	21	26
Ionic resistivity [b] (Ω cm^2)	2.23	2.55	1.36	1.85	2.66	2.56
Porosity (%)	43	40	42	42	40	41
Melt temp. (^{o}C)	135	165	135/165	135/165	138	137

[a] *Gurley is the time in seconds required to pass 10 cc of air through one square inch of product under a pressure of 12.2 inches of water*
[b] *In 1 M $LiPF_6$ EC:EMC (30:70 by volume)*

Table 2.10. TMA data for typical Celgard separators [53]

Test	Celgard 2400	Celgard 2325
shrinkage onset temp. (^{o}C)	121	106
deformation temp. (^{o}C)	156	135, 154
rupture temp. (^{o}C)	183	192

Table 2.11. Safety and performance tests for lithium-ion batteries and the corresponding important separator property and its effect on cell performance and/or safety [53]

Cell property	Separator property	Comments
cell capacity	thickness	cell capacity can be increased by making the separator thinner
cell internal resistance	resistance	separator resistance is a function of thickness, pore size, porosity, and tortuosity
high rate performance	resistance	separator resistance is a function of thickness, pore size, porosity, and tortuosity
fast charging	resistance	low separator resistance will aid in overall faster charging by allowing higher and/or longer constant current charging
high-temp. storage	oxidation resistance	oxidation of separators can lead to poor storage performance and reduce performance life
high-temp. cycling	oxidation resistance	oxidation of separators can lead to poor cycling performance
self-discharge	weak areas, pinholes	soft shorts during cell formation and testing can lead to internal current leakage
long-term cycling	resistance, shrinkage, pore size	high resistance, high shrinkage and very small pore size can lead to poor cycling performance
overcharge	shutdown behavior; high-temp. melt integrity	separator should completely shutdown and then maintain its melt integrity at high temp
external short circuit	shutdown behavior	separator shutdown stops the cells from overheating
hotbox	high-temp. melt integrity	separator should be able to keep the two electrodes apart at high temp
nail crush	shutdown (to stop delayed failure)	in the case of internal shorts, the separator may be the only safety device to stop the cell from overheating
bar crush	shutdown (to stop delayed failure)	in the case of internal shorts, the separator may be the only safety device to stop the cell from overheating

Table 2.12 Properties of prototypes for HEV application, Exxon standard grades, and some commercial Products [54]

Grade	Proto-type	Proto-type	Std.	Celgard 2325	Proto-type	Proto-type	Std.	Celgard 2340
Gauge (um)	25	25	25	25	30	30	30	38
Gurley per gauge (sec/100cc)	180	290	650	575	240	340	740	775
Porosity (%)	47	44	36	41	47	45	37	45
Puncture strength per gauge (gf)	Similar	Even	590		Similar	Improved	680	
Heat shrinkage, MD (%)	Improved	Improved	6		Improved	Improved	5.0	
Heat shrinkage, TD (%)	Even	Even	4.5		Even	Even	4.0	
Tensile Strength, MD (kgf/cm^2)	1050	1250	1500	1900	1100	1200	1500	2100
Tensile Strength, TD (kgf/cm^2)	1150	1350	1300	135	1150	1350	1200	130

2.10. Overcharge/ over discharge

A strict charging regime is necessary to properly and safely charge lithium-ion batteries. Most batteries contain a protective circuit to prevent overcharge and over discharge. This circuit limits the charge voltage to a maximum 4.3 V, and also contains a thermal sensor, which disconnects the cell if the temperature reaches 90 °C. If a cell is inadvertently overcharged, the cell may heat up and vent with a flame. Lithium-ion batteries

permanently lose capacity when they are exposed to elevated temperature greater than 65 °C. The protective circuit also limits the discharge voltage to between 2.7 and 3.0 V per battery. In spite of these preventative measures, over discharge may still occur. If a lithium battery has dwindled to a voltage of less than 1.5 V per battery, recharge should be avoided since copper current collectors may form copper shunts inside the battery, causing a partial or total short circuit. In this case, the battery becomes unstable, charging the battery would cause excessive heat, and safety cannot be assured.

2.10.1. Discharge characteristics

At a constant current discharge rate, the lithium-ion battery maintains a relatively flat voltage discharge profile with a steep decrease in the profile near the end of discharge (for cells with graphite anode). The battery should not be discharge to less than 3.0 V per battery.

2.10.2. Charging characteristics

Operating temperatures for charging are 0 to 45°C. Lithium-ion batteries require a controlled charge regime to properly charge and prevent overcharge. A two-stage charge cycle must be performed to fully charge the battery as illustrated in Figure 2.12 [55]. This is called a CC/CV charge cycle. The first stage of the charge cycle is a constant current charge until the battery voltage reaches 4.1 to 4.2 V. Upon reaching this peak voltage, a constant voltage charge is initiated until the charge current reduces to 3% of the rated current. Upon completing charge, a top off charge may be used to counteract the self-discharge of the battery and protective circuit. This top off charge may be initiated when the open circuit

voltage of the battery reaches less than 4.05 V and terminate upon reaching the full charge voltage of 4.1 to 4.2 V. Depending on the battery, this top off charge may be repeated once every 20 days.

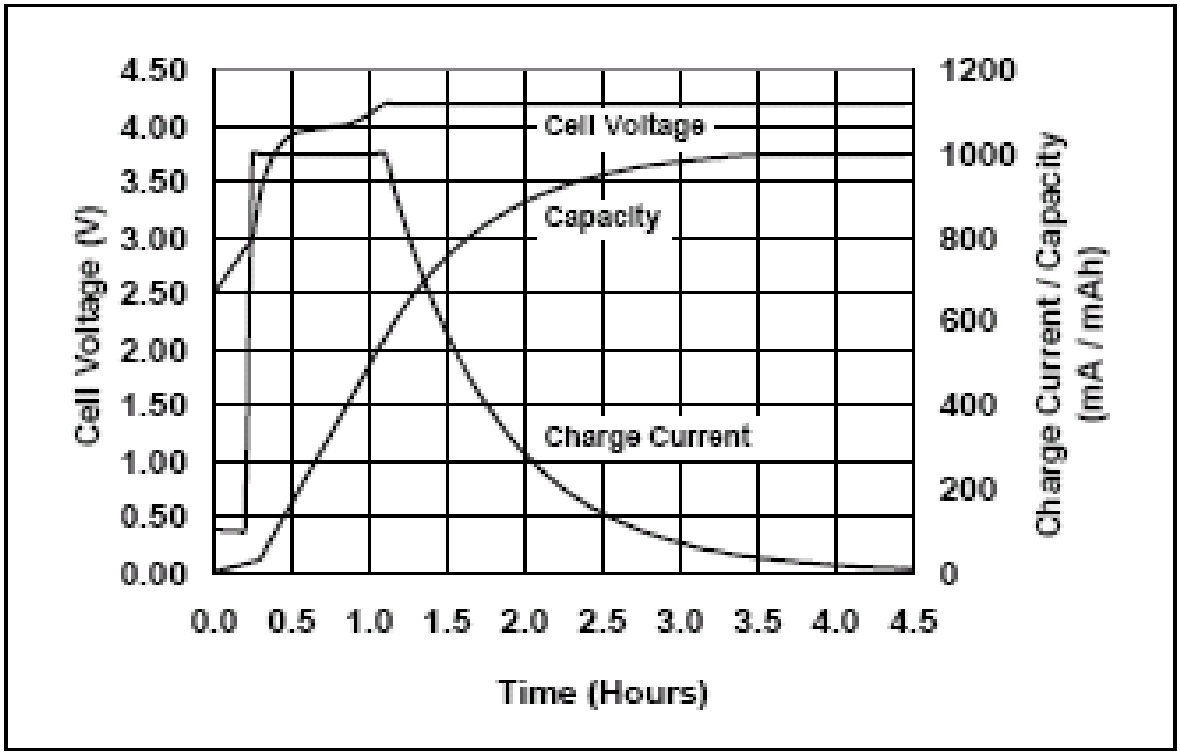

Figure 2.12. Lithium-ion battery charge [55]

2.10.3. Protection circuit

Lithium-ion batteries require a protection circuit that limits each cell's peak voltage during charge and prevents its voltage from dropping too low on discharge. The protection circuit not only limits the maximum charge and discharge current but also monitors the cell temperature. Commercial Li-ion battery packs contain redundant protection devices to ensure

safety under all circumstances. Typically, a field effect transistor opens if the charge voltage of any cell reaches 4.30V, and a fuse activates if the cell temperature approaches 90 °C. In addition, a pressure switch in each cell permanently interrupts the charge current if a safe pressure threshold is exceeded, and internal voltage control circuits cut off the battery at low and high voltage points. The lithium-ion battery is typically discharged to 3 V per cell. The lowest "low-voltage" power cut-off is 2.5 V per cell. During prolonged storage, however, a discharge below this voltage level is possible. Manufacturers recommend a "trickle" charge to gradually raise such a battery back into the "acceptable" voltage window. Not all chargers are designed to apply a charge once a lithium-ion battery has dipped below 2.5 V per cell. Some batteries feature an ultra-low voltage cut-off that permanently disconnects the pack if a cell dips below 1.5 V. This precaution is done to prohibit recharge if a battery has dwelled to 1.5 V. Copper current collector dissolution followed by copper plating will be caused by charging the battery after a deep discharge, which can lead to a short circuit in the cell. Most manufactures do not sell lithium-ion cells by themselves, but make them available in a battery pack, complete with a protection circuit. This precaution is understandable when considering the danger of explosion and fire if the battery is charged and discharged beyond its safe limits. A major concern arises if static electricity or a faulty charger has managed to destroy the battery's protection circuit. Such damage often causes the solid-state switches to fuse to a permanent "on" position without the user's knowledge. A battery with a faulty protection circuit may function normally, but does not provide the required safety. If charged beyond the safe voltage limits with a poorly designed accessory charger, the battery may heat

up, then bulge and, in some cases, vent with flame. Shorting such a battery can also be hazardous.

2.11. Summary

Lithium-ion batteries receive good grades in performance and reliability. From the above discussion, however, we see that there is room for improvement. The Lithium-ion battery has found a strong market position with portable devices demanding small form factors. The future challenge will be to develop a simple oxide cathode without other elements (such as P in $LiFePO_4$ which reduce the energy density of the battery) in which at least one lithium ion per transition metal ion could be reversibly extracted/inserted to give close to 300 mAh/g (for example, $LiCoO_2$ takes 0.5 Li per Co and it gives 140 mAh/g so if it can take 1 Li per Co it will give 280 mAh/g) while keeping the material cost and toxicity low. Such cathodes can double the energy density compared to the present level. There are also possibilities to increase the capacity of anodes perhaps by focusing on amorphous materials and metal nitrides.

2.12. References

1. J.M. Tarascon, and M. Armand, Nature 414, (2001), 359

2. D. Linden. *Handbook of Batteries*, McGraw-Hill, Inc., New York, 1995.

3. M. J. Riezenman. The search for better batteries. *IEEE Spectrum*, 51-56, May 1995.

4. W.S. Harris, Ph.D. Thesis UCRL-8381, University of California, Berkeley (1958)

5. M.S. Whittingham, Science 192 ,4244, (1976),1126

6. K. Brandt, Solid State Ionic's 69 ,(1994), 173

7. Materials for lithium-ion batteries, edited by C. Julien, Zdravko B. Stoynov, page 5, Nato science series, 3. High technology, vol 85.

8. T.Ohzuku, and A.Ueda, J. Electrochem. Soc 144, (1997), 2780

9. P.Novack, K.Miller, K.S.V. Santhanam, and O.Heas, Chem. Rev. 97, (1997), 207.

10. M.Arakawa, and J.Yamaki, J.Power Sources 54, (1995), 250

11. J. Kim ,Master Thesis, University of Texas, Austin p.9

12. David Linden, and Thomas B.Reddy, "Hand Book Of Batteries" 3rd edition 2002

13. S. Megahed and B. Scrosati. The Electrochemical Society Interface, 34 (Winter 1995).

14. http://www.marketavenue.cn/upload/articles/ARTICLES_1269.htm (accessed on 8-18-08)

15. http://www.greencarcongress.com/2008/05/forecast-lithiu.html (accessed on 8-18-08)

16. N.Imanishi, Y. Takeda, and O. Yamamoto, "Lithium-Ion Batteries: Fundamentals and Performance" (M. Wakihara and O. Yamamoto, Eds.), (1998), P. 98, Wiley-VCH, Weinheim

17. M. Winter, and J.O. Besenhard, "Lithium-Ion Batteries: Fundamentals and Performance" (M. Wakihara and O. Yamamoto, Eds.), (1998), P.127, Wiley-VCH, Weinheim.

18. K. Xu, S. Zhang, B.A. Poese, and T.R. Jow, Electrochemical and Solid-Sate Lett. 5, (2002), A259

19. T. Osaka, and M. Datta, Energy Storage System for Electronics, Gordon and Breach scince publishers, (2000)

20. E. Ferg, R.J. Gummow, A.de Kock, and M.M. Thackeray, J.Electrochem. Soc. 141, (1994), L147

21. W.Liu, X. Huang, Z. Wang, H.Li, and L.Chen, J.Electrochem. Soc. 145, (1998), 59.

22. J.J. Auborn, and Y.L. Barberio, J.Electrochem Soc. 134, (1987), 638.

23. K.M. Abraham, D.M. Pasquariellio, and E.B. Willstaedt, J.Electrochem. Soc. 137, (1990), 743

24. S.Morzilli, B.Scrosati, and F.Sgarlatta, Electrochem. Acta 30, (1985), 1271

25. D.C.S. Souza, V.Pralong, A.J.Jacobson, and L.F.Nazar, Science 296, (2002), 2012.

26. J.L.C. Rowsell, V. Pralong, L.F. Nazar, and J.Amer, Chem. Soc. 123, (2001), 8598

27. J.T.Vaughey, K.D. Kepler, R.Benedek, and M.M. Thackeray, Electrochem. Comm. 1, (1999), 517

28. H. Wang, Y. I. Jang, B. Huang, D.R. Sadoway, and Y.-m. Chiang, J.Electrochem. Soc. 146, (1999), 473

29. H.Tukamoto, and A.R. West, J.Electrochem. Soc 144, (1997), 3164.

30. Y.I. Jang, B. Huang, H. Wang, D.R. Sadoway, G. Cedar, Y.-M. Chiang, H.Liu, and H. Tamura, J.Electrochem. Soc 146, (1999), 862.

31. W.S. Yoon, K.-K. Lee, and K.-B. Kim, J.Electrochem. Soc 147, (2000), 2023

32. M.Mladenov, R. Stoyanova, E. Zhecheva, and S.Vassilev, Electrochem. Commun. 3, (2001), 410

33. k.Kubo, M.Fujiwara, S.Yamada, S.Arai, and M.Kanda, J.Power Source 68, (1997), 553

34. C.C. Chang, J.Y. Kim, and P.N. Kumta, J.Electrochem. Soc 149, (2002), A331.

35. J.Cho, G.Kim, and H. S.Lim, J.Electrochem. Soc 146, (1999), 3571.

36. Z.Lu, D.D. MacNeil, and J.R. Dahn, Electrochem. Solid-State Lett. 4, (2001), A200.

37. H. Wang, Y. I. Jang, B. Huang, D.R. Sadoway, and Y.m. Chiang, J.Power Sources 81-82, (1999), 594.

38. J.Cho, C.S.Kim, and S.-I.Yoo, Electrochem. Solid-State Lett. 3, (2000), 362.

39. G.G.Amatucci, J.M.Tarascon, and L.C.Klein, Solid-State Ionics 83, (1996), 167.

40. J.Cho, Y.J.Kim, and B.Park, J.Electrochem. Soc 148, (2001), A1110.

41. Z.Chen, and J.R.Dahn, Electrochem. Solid-State Lett. 5, (2002), A213.

42. J.Cho, T.-J.Kim, Y.J.Kim, and B.Park, Electrochem. Solid-State Lett. 4, (2001), A159

43. T.Miyasaka, U.S. Patent No. 6037095, March 30, 1998.

44. H.-J. Kweon, G.-B. Kim, and D.-G.Park, U.S. Patent No. 6183911, October 29, 1999.

45. Y.Matsuda, H. Nakashima, M.Morita, and Y.Takasu, J. Electrochem. Soc. 128, (1981), 2552.

46. D. Aurbach, "Nonaqueous Electrochemistry", Marcel Dekker, Inc., New York (1999).

47. U.Heider, R.Oesten, and M.Jungnitz, J.Power Sources 81-82, (1999), 119.

48. G.C. Chung, H.J. Kim, S.H.Jun, J.W.Choi, and M.H.Kim, J.Electrochem. Soc. 147, (2000), 4398.

49. X.Z.Shu, R.S.McMillan, J.J.Murray, and J.I.Davidson, J.Electrochem. Soc. 142, (1995), L161

50. M.Inaba, Y.Kawatate, A.Funabiki, S.K.Jeong, T.Abe, and Z.Ogumi, Electrochim. Acta 45,(1999), 99.

51. M.Schmidt, U.Heider, A.Kuehner, R.Oesten, M.Jungnitz, N.Ignat'ev, and P.Sartori, J.Power Sources 97-98, (2001), 557.

52. K.Xu, S.S.Zhang, R.R. Jow, W.Xu, and C.A. Angell, Electrochem. Solid-State Lett. 5, (2002), A26.

53. P. Arora, and Z.M. Zhang, Chem. Rev., 104 (10), (2004), 4419.

54. “Battery Separators for HEV Application: Controlling Its Structure for High Rate Performance”
http://www.exxonmobilchemical.com/Public_Files/PA/WorldwideEnglish/chem_nr_051805_battery.pdf accessed May 2009

55. S. Dearborn, Microchip Technology Inc. “Power Management in Portable Applications: Charging Lithium-Ion/Lithium-Polymer Batteries” 2004.

CHAPTER 3: ELECTROLYTES FOR LITHIUM-ION BATTERIES

3.1. Introduction

Electrolytes are essential in any electrochemical device. The function of electrolyte is to serve as a medium for the transfer of ions between electrodes. There are many types of electrolytes such as solid, liquid, polymer and composite electrolyte but the most used electrolyte in present lithium-ion batteries is a liquid consisting of a lithium salt dissolved in nonaqueous solvents. Also of importance in an electrolyte is the interaction between the electrolyte and electrodes in the battery. The interface between the electrodes and electrolyte usually affects battery performance significantly.

Lithium-ion batteries typically operate at a high voltage (~4.2 V), which requires organic solvents stable to oxidation. A battery electrolyte in general needs to meet requirements such as:

1. High-ionic conductance and electronic insulator to minimize cell resistance and achieve good rate capability and keep self-discharge at minimum.
2. High-thermal and chemical stability
3. Wide potential window, which is defined as the range in voltage between the oxidative and reductive decomposition limits of the electrolyte
4. Low reactivity toward other components in the battery
5. Non-toxic and safe
6. Low melting point (T_m) to help provide conductivity at low temperatures.

7. High boiling point (T_b) to prevent pressure build-up in the cell, which may lead to an explosion.
8. Low cost

The next two sections provide a brief discussion about solvents and salts that are used in lithium-ion battery research.

3.1.1. Solvents

An ideal electrolyte solvent should have the following properties:

1. High-dielectric constant (ε) to dissolve salts well
2. Low viscosity (η)
3. Solvent should remain inert to all cell components
4. Low melting point (T_m)
5. High boiling point (T_b)
6. It should also be safe, nontoxic, and economical
7. The solvents should be aprotic and stable at negative potentials

The most important properties of the solvent for ionic conductance are the viscosity and dielectric constant. Many organic solvents have been investigated, and the majority of them may be classified as alkyl carbonates, esters and ethers. Tables 3.1 and 3.2 list various solvents used in lithium batteries [1], along with their physical properties. As we see from these tables, no single solvent meets all requirements. For example, while all ethers and acyclic esters have low viscosities (η~0.3-0.7 cP), they also have low-dielectric constants (ε~2-7) which make them poor media for salt dissociation. On the other hand, solvents with

high polarity (ε~ 40-90) such as Ethylene carbonate (EC) have high viscosity (η= 1.7-2.0 cP) which limits ion mobility. To overcome this problem mixed solvents are used. For example two solvents may be used, one with a high-dielectric constant and the second with low viscosity. The reason why cyclic esters have a high-dielectric constant is their cyclic structure which helps to maintain a more ordered alignment of the molecule dipoles in contrast to open structure of the linear carbonates, which helps to cancel these dipoles.

Table 3.1. Organic carbonates and esters as electrolyte solvents [1]

Solvent	Structure	M. Wt	T_m/ °C	T_b/ °C	η/cP 25 °C	ε 25 °C	Dipole Moment/debye	T_f/ °C	d/gcm^{-3}, 25 °C
EC		88	36.4	248	1.90, (40 °C)	89.78	4.61	160	1.321
PC		102	-48.8	242	2.53	64.92	4.81	132	1.200
BC		116	-53	240	3.2	53			
γBL		86	-43.5	204	1.73	39	4.23	97	1.199
γVL		100	-31	208	2.0	34	4.29	81	1.057
NMO		101	15	270	2.5	78	4.52	110	1.17
DMC	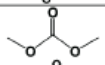	90	4.6	91	0.59 (20 °C)	3.107	0.76	18	1.063
DEC	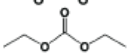	118	-74.3 [a]	126	0.75	2.805	0.96	31	0.969
EMC	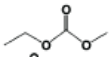	104	-53	110	0.65	2.958	0.89		1.006
EA		88	-84	77	0.45	6.02		-3	0.902
MB	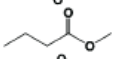	102	-84	102	0.6			11	0.898
EB	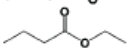	116	-93	120	0.71			19	0.878

a M. S. Ding, K. Xu, S. Zhang, T. R. Jow, J. Electrochem. Soc. 148, (2001) , A299.

Table 3.2. Organic ethers as electrolyte solvents [1]

Solvent	Structure	M. Wt	T_m/ °C	T_b/ °C	η/cP 25 °C	ε 25 °C	Dipole Moment/debye	T_f/ °C	d/gcm^{-3}, 25 °C
DMM	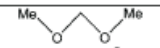	76	-105	41	0.33	2.7	2.41	−17	0.86
DME	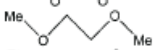	90	-58	84	0.46	7.2	1.15	0	0.86
DEE	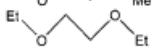	118	-74	121				20	0.84
THF		72	-109	66	0.46	7.4	1.7	-17	0.88
2-Me-THF		86	-137	80	0.47	6.2	1.6	-11	0.85
1,3-DL		74	-95	78	0.59	7.1	1.25	1	1.06
4-Me-1,3-DL		88	-125	85	0.60	6.8	1.43	-2	0.983
2-Me-1,3-DL		88			0.54	4.39			

3.1.2. Salts

Lithium salts are used in lithium-ion batteries as a charge carrier for the current passed in the cell during the electrochemical process. A salt for a lithium-ion battery should meet requirements such as:

1. Good thermal stability
2. High oxidation and low reduction potentials
3. Good solubility and dissociation of the salt in appropriate solvents
4. Chemical stability with the solvents
5. High conductivity in solution
6. Low molecular weight
7. Low cost
8. Ability to passivate the aluminum current collector in lithium-ion batteries
9. Non-toxic

To have a high conductivity, the lithium salt must have good solubility and dissociate in the solvent. The requirement of good solubility eliminates using most simple lithium salts such as LiX (where X for example is Cl^- and F^-), since they do not dissociate well in low-dielectric solvents. Choosing bulky anions with low-negative charge density [2] usually improves its solubility and dissociation, which is why most lithium salts are based on complex anions. The most studied salts include $LiClO_4$ [3-6], $LiAsF_6$ [7-11], $LiPF_6$ [12-13], $LiBF_4$ [14], $LiCF_3SO_3$ [15] and $LiN(SO_2CF_3)_2$ [16]. Some salts used in research and lithium-ion industry are shown in Table 3.3 along with some physical properties [1]. Each salt has advantages and disadvantages, with the later described in the next paragraph.

Table 3.3. Typical salts used in research and industry for lithium-ion cells[1]

Salt	Structure	M. Wt	T_m/ °C	$T_{decomp.}$, / °C in solution	Al-corrosion	σ /mScm^{-1} (1.0 M, 25 ° C)	
						in PC	in EC/DMC
$LiBF_4$		93.9	293 (d)	> 100	N	3.4 [a]	4.9 [c]
$LiPF_6$	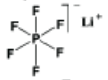	151.9	200 (d)	~ 80 (EC/DMC)	N	5.8 [a]	10.7 [d]
$LiAsF_6$	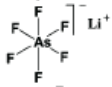	195.9	340	> 100	N	5.7 [a]	11.1 [e]
$LiClO_4$		106.4	236	>100	N	5.6 [a]	8.4 [d]
Li Triflate	$Li^+ CF_3SO_3^-$	155.9	>300	>100	Y	1.7 [a]	
Li Imide	$Li^+ [N(SO_2CF_3)_2]^-$	286.9	234 [b]	>100	Y	5.1 [a]	9.0 [e]
Li Beti	$Li^+ [N(SO_2CF_2CF_3)_2]^-$				N		

a. Ue, M. J. Electrochem. Soc. 1995, 142, 2577.
b. Dominey, L. A.; Koch, V. R.; Blakley, T. Electrochim. Acta 1992, 37, 1551.
c. Hossain, S. Handbook of Batteries, 2nd ed.; Linden, D., Ed.; McGraw-Hill: New York, 1995; Chapter 36.
d. Schmidt, M.; Heider, U.; Kuehner, A.; Oesten, R.; Jungnitz, M.; Ignat'ev, N.; Sartori, P. J. Power Sources 2001, 97/98, 557.
e. Walker, C. W.; Cox, J. D.; Salomon, M. J. Electrochem. Soc. 1996, 143, L80.

Lithium perchlorate (LiClO4) and $LiAsF_6$ cannot be used commercially because of the explosion risks of ClO_4^- [17] and the high toxicity of AsF_6^- [9, 18-19] and its degradation products. The main problem of $LiBF_4$ is its low conductivity. For that reason there is not much interest in using it, although it was observed recently that electrolytes with it have good performance at low temperature [20-23]. The lithium triflate salt ($LiCF_3SO_3$) has two shortcomings. First, it has poor ion conductivity in nonaqueous solvents. The poor ion conductivity is mainly due to two reasons:

1. The low-dissociation constant of $LiCF_3SO_3$ in solvents with a low-dielectric constant [19,24]
2. The moderate ion mobility for $CF_3SO_3^-$ as related to other salts [25].

The second problem with using $LiCF_3SO_3$ is the severe aluminum corrosion that occurs with it [26], which is also a problem with $LiN(SO_2CF_3)_2$ [26]. Among all salts mentioned, $LiPF_6$ is the one used in commercial Li-ion batteries. Discussion about $LiPF_6$ disadvantages in more detail is given in section 2.2.1.

3.2. State-of-art electrolyte

Although that there are many solvents and salts tested in the laboratory [27-29], most commercial lithium-ion battery electrolytes consist of $LiPF_6$ dissolved in alkyl carbonate solvents [30] consisting of EC as one component [31] and a co-solvent mixture that are acyclic alkyl carbonates such as DEC [32], DMC [33], EMC [34], and PMC [35]. Ethylene carbonate is used because its high-dielectric constant leads to improved dissociation of the salt. However, the viscosity of ethylene carbonate is high, so co-solvents with low viscosity are added. Alkyl

carbonate solvents are used because they have a higher anodic stability and higher polarity than ethers and esters. In addition, they have the ability to form a solid electrolyte interface (SEI) on the anode, thereby protecting the electrolyte from further decomposition. The ability to form a good SEI is not available in ethers or esters [27-29, 36-39]. For example, the ethers can co-intercalate into graphite, which causes exfoliation of the graphite [37], and the esters do not form an adhesive passive film. Since the major salt used salt in commercial lithium-ion batteries is $LiPF_6$, more detailed discussion about it is provided below.

3.2.1. $LiPF_6$

Lithium hexafluorophosphate has a combination of well-balanced properties such as high-ionic conductivity, good dissociation, and good ion mobility. However, a major disadvantage is the sensitivity of $LiPF_6$ to residual water in the electrolyte. The $LiPF_6$ reacts with water and forms hydrofluoric acid (HF), which has a detrimental effect on cell performance because HF reacts with the graphite anode and forms a surface film consisting of LiF [40]. The LiF film increases the impedance of the electrolyte/electrode interface due to its poor ionic conductivity. Another disadvantage of the $LiPF_6$ is its thermal instability [26, 41-43] which is believed to be the main cause for the poor performance of lithium-ion batteries at elevated temperature [40, 44-47]. Another disadvantage is that $LiPF_6$ cannot be used in gel electrolytes based on fumed silica (FS) because $LiPF_6$ reacts with Si-OH to form HF which will react with silicon to form SiF_4. Because of these disadvantages, many researchers have focused on finding a new salt to replace $LiPF_6$ [48-57]. Some of these novel salts are summarized in Table 3.4. One new salt that has attained a lot of interest is lithium bis(oxalato)borate (LiBOB)[57-66]. A brief discussion about LiBOB is given in next section.

Table 3.4. Novel lithium salts and their major properties [1]

Salt	Structure	M. Wt	T_d / °C [a]	E_a /V [b] (solvent -electrode)	σ /mScm^{-1} (0.7~1.0 M, 25 ° C/ solvent)
LiMe	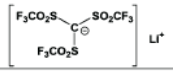	417.9	340	4.4 (THF-GC) 4.0 (EC/DMC-GC)	7.1 (EC/DMC) 12 (EC/MF/DMC)
aromatic Li borates	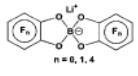	233.4~ 305.4	250 (n=0)	3.6 (PC-SS [c], n=0 [d]) 3.7 (PC-Au, n=1) 4.1 (PC-Au, n=4)	0.6 (PC, n=0) 5.6 (EC/DME, n=0) 0.77 (PC, n=1) 11.07 (DME, n=4)
	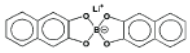	334.1	320	3.75 (PC-Pt)	1.22 (PC) 3.84 (PC/DME) 1.39 (PC/EC)
	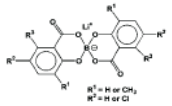	290.0~ 427.7	260 (R^{1-3}=Cl) 290 (R^{1-3}=H) 310 (R^{1-2}=Cl) 320 (R^{1}=CH_3)	4.0 (PC-SS, R^{1-3}=H) 4.4 (PC-Pt, R^{1-3}=Cl) 4.4 (PC-Pt, R^{1-3}=H) 4.3 (PC-Pt, R^{1-2}=Cl) 4.1 (PC-Pt, R^{1}=CH_3)	
		386.1			
	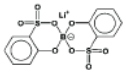	293.9		4.6 (EC/DMC-Pt)	
	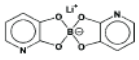	219.9		3.95 (PC/DMC-Pt)	
non-aromatic Li borates		681.9	280	5.4 (DME-Pt) 5.0 (PC-Pt)	11.1 (DME)
	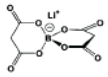	221.9	245		5.6 (DMSO)
	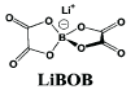 **LiBOB**	193.9	~300 (d)	4.5 (PC-Pt)	3.1 (PC) 9.0 (DME) 7.5 (EC/DMC)
	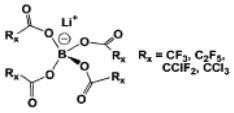	469.9~667.9	100	4.5 (PC-Pt)	8.0 (PC/DMC)
chelated Li phosphates	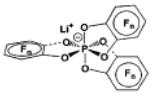	361.9 (n=0) 577.9 (n=4)	150 (n=0)	3.7 (PC-Ni, n=0) 3.95 (EC/DMC-Pt, n=1) 4.3 (EC/DEC-Pt, n=4)	3.89 (EC/THF, n=0) 2.09 (EC/DEC, n=4)
Li FAP	 R_F = perfluorinated alkyl or F	451.9~433.9		5.0 (DME-Pt) 5.0 (EC/DMC-Pt)	8.17 (PC/EC/DMC, R^{1-2} = *i*-C_3F_7, R^{3-6}=F) 8.2 (EC/DMC, R^{1-3} = C_2F_5, R^{4-6}=F)
Li azolate	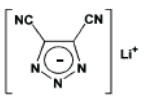	124.9			
Li imidazolide	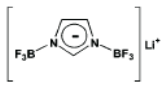	209.9		4.85 (DMC-Pt)	5.06 (EC/EMC)

a Thermal decomposition temperature determined by TGA.
b Anodic stability limit determined by cyclic voltammetry.
c Stainless steel working electrode.
d Number of fluorine substituents on the aromatic ring

3.3. LiBOB

LiBOB (shown below) is a new salt that was independently discovered by Lischka et al. [57] in Germany and Angell et al. [58] in the USA. LiBOB (M.w =194 g/mol)

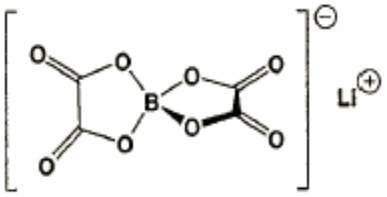

LiBOB

Scheme 3.1. LiBOB structure

Contains four carbonyl oxygen and four ether oxygen. There is only a single negative charge distributed among these atoms which make them very weakly coordinating. Consequently, LiBOB dissociation is high and expected to give a good ionic conductivity. In addition, the electrochemical stability of LiBOB is high (~4.5 V vs. Li^+/Li) [67] and the decomposition temperature for LiBOB is 302 ^oC. LiBOB salt meets the requirements discussed in section 3.1.2 and in addition, it is found that LiBOB has the ability to stabilize the graphite anode for lithium-ion batteries in the presence of PC-rich solvent [60-61] without using EC or any additives, which was not achievable in the past for any lithium salt. The problem of using PC arises from its tendency to severely exfoliate graphitic structure, which results in cell

destruction [28, 68-71]. With LiBOB there is no need to worry about exfoliation which leads to more flexibility in solvent selection. Lithium bis(oxalato)borate has the ability to passivate the Al foil cathode current collector [59-60]. In addition**,** LiBOB salt has better thermal stability and better performance at elevated temperature than $LiPF_6$ [59]. For example, it was shown that Li-ion cells which use graphite as an anode, lithium nickel based mixed oxide cathode, and LiBOB/EC:EMC (1: 1) (wt) electrolyte can be cycled at 60 and 70 ^oC without significant capacity fading [59 -60]. In addition, Jow and coworkers proposed that an electrolyte with wide temperature range is attainable by using LiBOB salt [72]. For these reasons, LiBOB has attracted the attention of recent research [61,-62, 67, 73-78]

3.4. Limitation of the state-of-art electrolyte at low temperature

As mentioned in Chapter 2, the normal operation temperature range for most commercial lithium- ion batteries is -20 to 65 ^oC. The poor performance of state-of-art lithium-ion cells at temperatures below -20 ^oC restricts applications for lithium-ion batteries. The limited range of operation of lithium-ion batteries is attributed to many factors as will be shown in next paragraph.

The poor performance of state-of-art lithium-ion cells at low temperature (-20 to -50 ^oC) arises from the decrease of solution conductivity and Li salt solubility [79-81]. A survey conducted for major manufacturers in 2001 showed that the power rate and energy density of lithium-ion cells at -40 ^oC are only 1.25% and 5%, respectively, of those obtained at room temperature[82]. Another survey conducted in 2003 showed that 30% of room temperature capacity is achievable at -40 ^oC [83]. In addition to electrolyte effect, the poor low-temperature

performance is also attributed to factors such as: increase of the surface film resistance between the electrode and electrolyte [82-86], increase of the charge-transfer resistance at the electrode/electrolyte interface [22, 23, 87], and increase of the diffusion impedance of the lithium ion into graphite anodes [88,89].

To overcome these limitations, researchers are trying to develop mixed-solvent electrolyte systems with improved performance at low temperature. The focus is on replacing the EC component, or at least reducing its concentration in the electrolyte, which will improve the low-temperature performance. However, reduction products of EC are known to be responsible for forming an effective solid electrolyte interface (SEI), and complete elimination of EC will affect negatively the performance of lithium-ion batteries. Many researchers have focused on reducing the EC content because EC is blamed for poor performance of the state-of-art lithium-ion cells at low temperature. The high melting point of EC (~36^{o}C) also has a detrimental effect on low-temperature performance since the EC component will precipitate at low temperature [90-92].

An attempt was made by Ein-Eli et al. [91] to make an electrolyte for low-temperature applications. They used methyl formate (MF), which has a low melting point ~ -99 ^{o}C, with EC at a volume ratio of 1:3. The reported conductivity for that electrolyte using $LiC(SO_2CF_3)_3$ [lithium tris(trifluoromethanesulfonyl)methide], (LiMe) salt, at -40 ^{o}C was excellent (5.4 mS cm^{-1}) [91]. Although it has a high ionic conductivity, the performance of the anode half cell was poor since only 50% of the room-temperature capacity is obtained at -2 ^{o}C. Other attempts to improve the low-temperature performance by using EC with alkyl carbonates that have a low melting point (e.g., EMC, DEC and DMC) were reported by many

researchers [81, 85, 86, 93-96]. However, these electrolytes have failed to give a satisfactory performance below -30 ^{o}C [96]. Because of limited improvements using alkyl carbonate, linear alkyl esters have been examined by Smart et al. [81, 94]. Since MF has a negative effect on battery performance, they chose to use other alkyl esters such as methyl acetate (MA) and ethyl acetate (EA) [81,94]. The addition of MA or EA improved the low-temperature performance; however, both components have a detrimental effect on anode and cathode stability[81]. However, the work of Herreyre et al. [97] showed that EA and MA can be used as co-solvents for low-temperature electrolytes. They reported excellent results using EA or MA. For example, by using EC/DMC/EA with 1M $LiPF_6$ with vinylene carbonate as an additive in $LiCoO_2$/graphite cells, the charge capacity at -30 ^{o}C was between 88-95% of that at room temperature. In addition, it was shown that capacity fading at high-temperature storage is comparable with cells using state-of-art electrolytes (0.05 % per cycle).

3.5. Fumed silica

Fumed silica, which is marketed under trade names such as Aerosil® and Cab-o-sil®, is a white amorphous, nonporous form of silicon dioxide (SiO_2) prepared by flame hydrolysis of silicon tetrachloride ($SiCl_4$) as shown in Figure 3.1 [98-102].

Fumed silica predominant particle structures are branch-like aggregates (ca. 0.1-μm long), which consist of partially fused primary particles (ca. 12-nm diameter) that cannot be disrupted by shear[98,101,103].

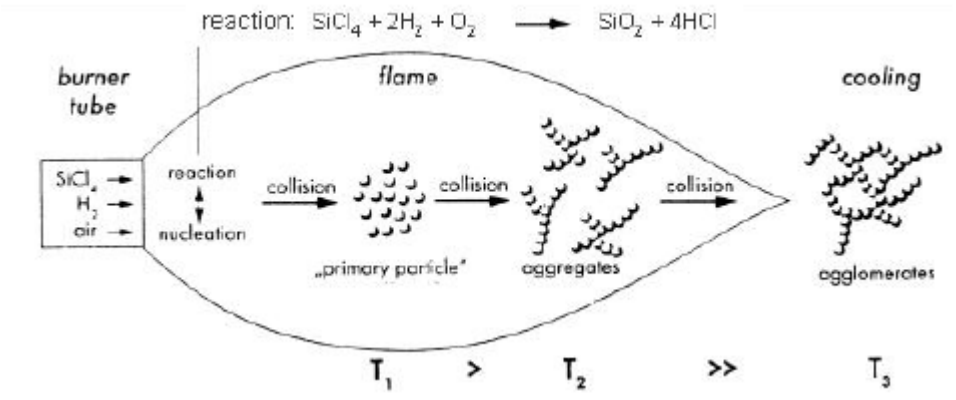

Figure 3.1. Schematic of fumed silica synthesis [101]

Native fumed oxides are hydrophilic due to surface hydroxyl groups, which determine many of physicochemical properties of these materials[104]. However, fumed silica morphology and surface chemistry can be easily modified by changing the synthesis conditions [99]. Hydrophobic fumed oxides can be easily produced by chemically treating the surface hydroxyl groups on fumed silica with alkylsilanes, polysiloxanes, or organofunctional silanes[102,105-109]. After surface treatment, surface hydroxyl groups are replaced by hydrophobic groups. For example, Evonik R805, is made by treating the hydrophilic silica, Evonik A200, with octa-methyl silazane. As a result of that, octyl chains replace about 50% of the hydroxyl groups. Other groups such as ethylene oxide (FS-EG3) and methyl groups (Evonic R974) can be attached to the surface also[110]. The surface chemistry of different types of fumed silica is shown in Figure 3.2.

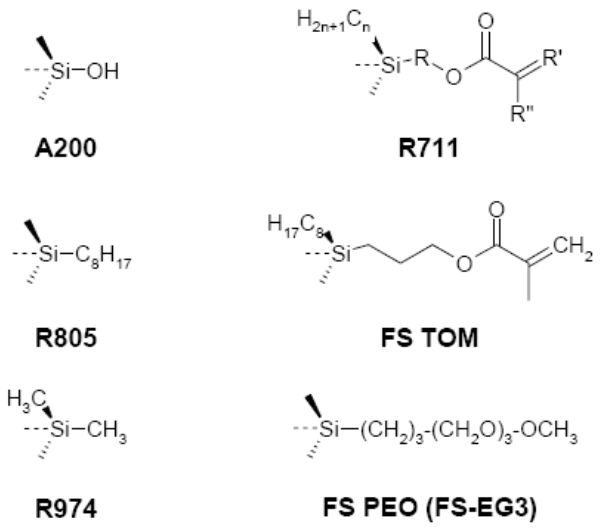

Figure 3.2. Overview of the types of fumed silica surface groups

Silanol groups have the ability to interact with polar molecules via hydrogen bonding, so, in general, if native fumed silica is dispersed in a weak polar solvent, silanol groups will hydrogen bond each other which will result in strong and rigid network [111-112]. In contrast if it dispersed in polar solvent, silanol group may hydrogen bond with the solvent molecules and form a sol. As a result of these interactions (particle-particle and particle-solvent), fumed silica is commonly used as a filler to modify the rheology of a variety of systems because of its ability to form three–dimensional network structures of interacting fumed silica aggregates, which enhance the mechanical strength of these systems.

3.5.1. Advantages of fumed silica

As we mentioned before, one of the advantages of fumed silica is that its surface can be easily modified from the native silanol (Si-OH). By modifying the surface group of fumed silica, the mechanical and electrochemical properties of fumed silica composite can be

tailored and controlled. Different types of fumed silica have been studied in various lithium battery electrolytes [113-117] and in addition to the increase in the conductivity noticed after adding fumed silica to some polymer electrolyte due to decrease in crystallinity, fumed silica based electrolyte are able to effectively stabilize the lithium interface compared to system without fumed silica [117,118-120]. The improved interface is due to several factors such as (i) the ability of fumed silica to scavenge impurities (ii) interaction between the polymer and fumed silica which prevents the polymer from interacting with lithium and (iii) morphology changes[118], (addition of hydrophobic fumed silica results in a nanoporous film morphology in PVDF-HFP [120] and crystallinity decreases from 70% for pure PEO to 9 or 22% for samples containing 30 wt.% hydrophilic and hydrophobic silica, repectively[117]). In PEGdm(250)-based electrolyte, addition of fumed silica has improved the mechanical properties with a little decrease in conductivity, as shown in Figure 3.3, so basically mechanical and electrochemical properties are decoupled and can be optimized independently [116,121].

The addition of 10 wt% R805 or 10 wt% A200 also increases the discharge capacity relative to the unfilled system, as shown in Figure 3.4[122]. In addition to previous advantages, the shear-thinning behavior of the fumed silica composites, as shown in Figure 3.5, is highly desirable and allows easy processing of the fumed silica composite[121].

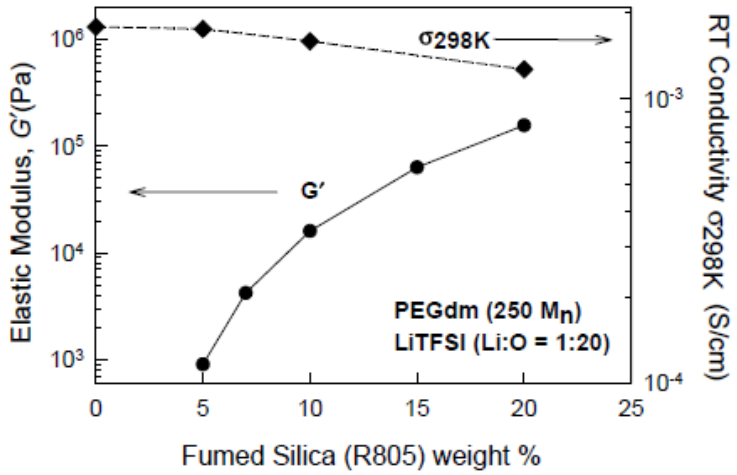

Figure 3.3. Elastic modulus and conductivity of PEGdm composites with R805[121]

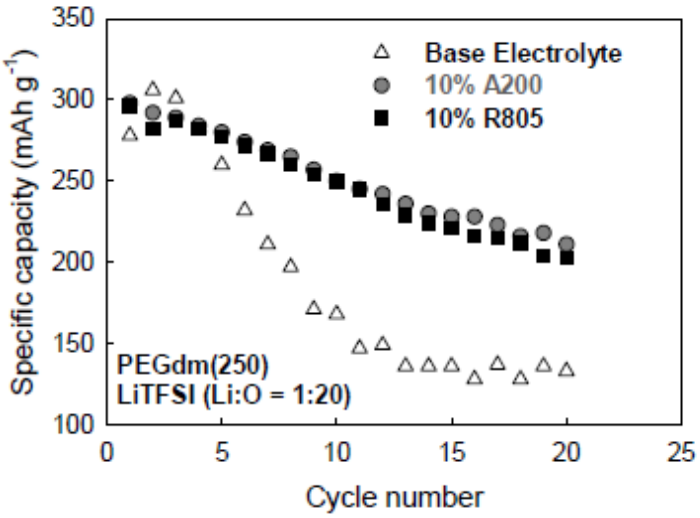

Figure 3.4. Cycling behavior for Li/V_6O_{13} cells w/o F.S (1.8-3 V, C/15, RT)[122]

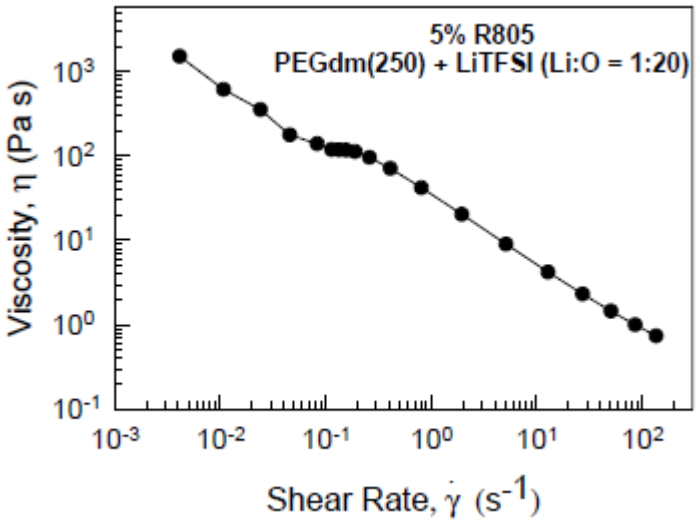

Figure 3.5. Steady-shear behavior of R805 composites[121]

3.6. References

1. K. Xu, Chem. Rev. 2004, 104.

2. D. Aurbach, "Nonaqueous Electrochemistry", Marcel Dekker, Inc., New York (1999).

3. K. Sawai, Y. Iwakoshi, and T. Ohzuhu, Solid State Ionics 69, (1994), 273.

4. I. Uchida, H. Sato, J. Electrochem. Soc. 142, (1995), L139.

5. J. Yamaura, Y. Ozaki, A. Morita, and A. Ohta, J. Power Sources 43/44, (1993), 233.

6. J. M. Tarascon, D. Guyomard, and G. L. Baker, J. Power Sources, 43/44, (1993), 689.

7. V. R. Koch, and J. H. Young, J. Electrochem. Soc. 125, (1978), 1371.

8. V. R. Koch, J. L. Goldman, C. J. Mattos, and M. J. Mulvaney, Electrochem. Soc. 129, (1982), 1.

9. K. M. Abraham, J. L. Goldman, and D. L. Natwig, J. Electrochem. Soc. 129, (1982), 2404.

10. F. W. Dampier, J. Electrochem. Soc. 128, (1981), 2501.

11. E. Plichta, S. Slane, M. Uchiyama, M. Salomon, D. Chua, W. B. Ebner, and H. W. Lin, J.Electrochem.Soc.136,(1989),1865.

12. G. J. Methlie, U.S. Patent 3,415,687, (1968).

13. R. A. Wiesboeck, U.S. Patent 3,654,330, (1972).

14. K. Takata, M. Morita, and Y. Matsuda, J. Electrochem. Soc. 132, (1985), 126.

15. A. Webber, J. Electrochem. Soc. 138, (1991),2586.

16. M. Armand, W.Gorecki, and R. Andreani, Proceedings of the 2nd International Meeting on Polymer Electrolytes, Scrosati, B., Ed., Elsevier: London, (1989), p 91.

17. R. Jasinski, and S. Carroll, J. Electrochem. Soc. 117, (1970), 218.

18. C. Nanjundiah, J. L. Goldman, L. A. Dominey, and V. R. Koch, J. Electrochem. Soc. 135, (1988), 2914.

19. V. R. Koch, J. Electrochem. Soc. 126, (1979), 181.

20. S. S. Zhang, K. Xu, and T. R. Jow, J. Electrochem. Soc. 149, (2002), A586.

21. N. Takami, T. Ohsaki, H. Hasebe, and M. Yamamoto, J. Electrochem. Soc. 149, (2002), A9.

22. S. S. Zhang, K. Xu, and T. R. Jow, Electrochem. Commun. 4, (2002), 928.

23. S. S. Zhang, K. Xu, and T. R. Jow, J. Solid State Electrochem. 7, (2003), 147.

24. F. Croce, A. D'Aprano, C. Nanjundiah, V. R. Koch, C. Walker, and M. Salomon, J. Electrochem. Soc. 143,(1996), 154.

25. M. Ue, J. Electrochem. Soc 141, (1994), 3336.

26. L. J. Krause, W. Lamanna, J. Summerfield, M. Engle, G. Korba, R. Loch, and R. Atanasoski, J. Power Sources 68, 1997, 320.

27. D. Aurbach, O. Youngman Chusid, Y. Carmeli, M. Babai, Y. Ein-Eli, J.power Source 43 ,(1993), 47.

28. D. Aurbach, B. Markovsky, Y. Ein-Eli, Y. Carmeli, H. Yamin, S. Luski, Electrochim. Acta 39, (1994), 2559.

29. R. Yazami, Electrochim. Acta 45 ,(1999), 87.

30. Lithium-Ion Batteries: Fundamentals and Performance, M. Wakihara and O. Yamamoto, Editors, Wiley-VCH, New York (1998).

31. D. Guyomard, J. M. Tarascon, J. Power Source 54 ,(1995), 92.

32. J. M. Tarascon, and D. Guyomard, Solid State Ionics 69 ,(1994), 293.

33. D. Guyomard, J. M. Tarascon, J. Electrochem. Soc. 140 ,(1993), 3071.

34. D. Aurbach, A. Schechter, B. Markovsky, Y. Ein-Eli, V. Koch, J. Electrochem. Soc. 143 ,(1996), L273.

35. Y. Ein-Eli, S. F. McDevitt, B. Markovsky, A. Schechter, D. Aurbach, J. Electrochem. Soc. 144 ,(1997), L180.

36. M. Winter, J. O. Besenhard, in Handbokk of Battery Materials, J. O. Besenhard, Ed., Wiley-VCH, Weinheim, New York, Chapter 5, (1990), p.383.

37. D. Aurbach, B. Markovsky, K. Gamolsky, E.Levi, Y. Ein-Eli, Electrochimica Acta, 45 ,(1999), 67.

38. E. Buiel, and J. R. Dahn, Electrochimica. Acta 45 ,(1999), 121.

39. D. Aurbach, H. Teller, E. Levi. J. Electrochem. Soc. 149 ,(2002), A1255.

40. S. E. Sloop, J. K. Pugh, S. Wang, J. B. Kerr, K. Kinoshita, Electrochem. Solid-State Lett. 4 ,(2001), A42.

41. K. Nagayama, K. Kamioka, E. Iwata, H. Oka, Y. Tokunaga and T. Okada, Electrochemistry 69 ,(2001), 6.

42. A.A. Smagin, V.A. Matyuka and V.P. Korobtsev, J. Power Sources 68 ,(1997), 326.

43. X. Zhang, P.N. Ross, R. Kostecki, F. Kong, S. Sloop, J.B. Kerr, K. Streibel, E.J. Cairns and F. McLarnon, J. Electrochem. Soc. 148 ,(2001), A463.

44. S. E. Sloop, J. B. Kerr, and K. Kinoshita, J. Power Sources 119-121, (2003), 330.

45. B. Ravdel, K. M. Abraham, R. Gitzendanner, J. DiCarlo, B. L. Lucht, and C. Campion, J. Power Sources 119-121, (2003), 805.

46. C. L. Campion, W. Li, W. B. Euler, B. L. Lucht, B. Ravdel, J. F. DiCarlo, R. Gitzendanner, and K. M. Abraham, Electrochem. Solid-State Lett. 7, (2004), A194.

47. K. Tasaki, K. Kanda, S. Nakamura, and M. Ue, J. Electrochem. Soc. 150, (2003), A1628.

48. G. E. Bloomgren, in Lithium Batteries,(ed): J. Gabano, Academic Press, New York (1983), P13.

49. H. J. Gores, J. Barthel, J. Solution Chem. 9, (1980), 939.

50. Y. Matsuda, J. Power Source 20, (1987), 19.

51. J. T. Dudley, D. P. Wilkinson, G. Thomas, R. LeVae, Woo, H. Blom, C. Horvath, M. W. Juzkow, B. Denis, P. Juric, P. Aghakinan, and J. R. Dahn, J. Power Sources 35, (1991), 59.

52. H. Watanabae, T. Nohma, I. Nakane, S. Yoshimura, K. Nishio, and T. Saito, J. Power Sources 43, (1993), 217.

53. P. V. S. S. Prabhu, T. P. Kumar, P. N. N. Namboodiri, and R. J. Gangadharan, Appl. Electrochem. 23, (1993), 151.

54. D. Aurbach, M. Daroux, P. Faguy, and E. B. Yeager, J. Electroanal. Chem. 225, (1991), 297.

55. S. K. Lee, Y.B. Zu, A. Herrmann, Y. Geerts, K. Mullen, and A. J. Bard, J. Am Chem. Soc. 121, (1999), 3513.

56. R. Oesten, U. Heider, and M. Schmidt, Solid State Ionics 148, (2002), 391.

57. U. Lischka, U. Wietelmann, and M. Wegner, Ger. DE 19829030 C1 (1999).

58. W. Xu, and C. A. Angell, Electrochem. Solid-State Lett. 4, (2001), E1.

59. K. Xu, S. S. Zhang, T. R. Jow, W. Xu, and C. A. Angell, Electrochem. Solid-State Lett., 5, (2002), A26.

60. K. Xu, S. Zhang, B. A. Poese, and T. R. Jow, Electrochem. Solid-State Lett. 5, (2002), A259.

61. K. Xu, S. Zhang, and T. R. Jow, Electrochem. Solid-State Lett. 6, (2003), A117.

62. K. Xu, U. Lee, S. Zhang, M. Wood, and T. R. Jow, Electrochem. Solid-State Lett. 6, (2003), A144.

63. K. Xu, U. Lee, S. Zhang, J. Allen, and T. R. Jow, Electrochem. Solid-State Lett. 7, (2004), A273.

64. K. Xu, U. Lee, S. Zhang, and T. R. Jow, J. Electrochem. Soc. 151, (2004), A2106.

65. S.S Zhang, K. Xu, and T.R. Jow, "LiBOB-based gel electrolyte Li-ion battery for high temperature operation ", J. Power Source, in press.

66. S. Zhang, K. Xu, and T.R. Jow, ARL Pat. Disclosure, (2002).

67. Z.H. Chen and J. R. Dahn, Electrochem. Solid-State Lett. 7, (2004), A11.

68. J. R. Dahn, U. von Sacken, M. W. Juzkow, and H. al-Janaby, J. Electrochem.Soc. 138, (1991), 2207.

69. J.O. Besenhard, M. Winter, J. Yang and W. Biberacher, J. Power Sources 54, (1995), 228.

70. R. Yazami and S. Genies, Denki Kagaku 66, (1998), 1293.

71. G. Chung, H. Kim, S. Yu, S. Jun, J. Choi and M. Kim, J. Electrochem. Soc.147, (2000), 4391.

72. T. R. Jow, M. S. Ding, K. Xu, S. S. Zhang, J. L. Allen, K. Amine, and G. L. Henriksen, J. Power Sources 119/121, (2003), 343.

73. J. Jiang, and J. R. Dahn, Electrochem. Solid-State Lett. 6, (2003), A180.

74. W. Xu, and C. A. Angell, Electrochim. Acta 48, (2003), 2029.

75. W. Xu, L.Wang, and C. A. Angell, Electrochim. Acta 48, (2003), 2037.

76. B. G. Nolan, and S. H. Strauss, J. Electrochem. Soc. 150, (2003), A1726.

77. W. Xu, A. J. Shusterman,R. Marzke, and C. A. Angell, Abstract 295, The Electrochemical Society Meeting Abstracts, Vol. 2003 Orlando, FL, Oct 12-16, (2003).

78. G. V. Zhuang, K. Xu, T. R. Jow, and P. N. Ross, Jr., Electrochem. Solid-State Lett. 7, (2004), A224.

79. M. C. Smart, B. V. Ratnakumar, and S. Surampudi, J. Electrochem. Soc. 146, (1999), 486.

80. H. C. Shiao, D. Chua, H. Lin, S. Slane, and M. Salomon, J. Power Sources 87, (2000), 167.

81. K. Sawai, snd T. Ohzuku, J. Electrochem. Soc. 150, (2003), A674.

82. Nagasubramanian, G., J. Appl. Electrochem. 31, (2001), 99.

83. J. Fan, J. Power Sources 117, (2003), 170.

84. M. C. Smart, B. V. Ratnakumar, S. Surampudi, Y.Wang, X. Zhang, S. G. Greenbaum, A. Hightower, C. C. Ahn, and B. Fultz, J. Electrochem. Soc. 146, (1999), 3963.

85. E. J. Plichta, M. Hendrickson, R. Thompson, G. Au, W. K. Behl, M. C. Smart, B. V. Ratnakumar, S. Surampudi, J. Power Sources 94. (2001), 160.

86. C. Wang, A. J. Appleby, and F. E. Little, J. Electrochem. Soc. 149, (2002), A754.

87. S. S. Zhang, K. Xu, and T. R. Jow J. Power Sources 115, (2003), 137.

88. H. P. Lin, D. Chua, M. Salomon, H. C. Shiao, M. Hendrickson, E. Plichta, and S. Slane, Electrochem. Solid-State Lett. 4, (2001), A71.

89. C.-K. Huang, J. S. Sakamoto, J. Wolfenstine, and S. Surampudi, J. Electrochem. Soc. 147, (2000), 2893.

90. A. Ohta, H. Koshina, H. Okuno, and H. Murai, J. Power Sources 54, (1995), 6.

91. Y. Ein-Eli, S. R. Thomas, R. Chadha, T. J. Blakely, and V. R. Koch, J. Electrochem. Soc. 144, (1997), 823.

92. S. P. Ding, K. Xu, and T. R. Jow, J. Electrochem. Soc. 147, (2000), 1688.

93. R. Hamlen, G. Au, M. Brundage, M. Hendrickson, E. Plichta, S. Slane, and J. Barbarello, J. Power Sources 97/98, (2001), 22.

94. M. C. Smart, B. V. Ratnakumar, and S. Surampudi, J. Electrochem. Soc. 149, (2002), A361.

95. M. C. Smart, B. V. Ratnakumar, V. S. Ryan-Mowrey, S. Surampudi, G. K. S. Prakash, J. Hu, and I. Cheung, J. Power Sources 119/121, (2003), 359.

96. M. C. Smart, B. V. Ratnakumar, L. D. Whitcanack, K. B. Chin, S. Surampudi, H. Croft, D. Tice, and R. Staniewicz, J. Power Sources 119/121, (2003), 349.

97. S. Herreyre, O. Huchet, S. Barusseau, F. Perton, J. M. Bodet, and Ph. Biensan, J. Power Sources 97/98, (2001), 576.

98. H. Barthel, Colloid Surf. A-Physicochem. Eng. Asp., 101, 217 (1995).

99. V. M. Gun'ko, I. F. Mironyuk, V. I. Zarko, V. V. Turov, E. F. Voronin, E. M. Pakhlov, E. V. Goncharuk, R. Leboda, J. Skubiszewska-Zieba, W. Janusz, S. Chibowski, Y. N. Levchuk, and A. V. Klyueva, J. Colloid Interface Sci., 242, 90 (2001).

100. Degussa Technical Bulletin No. 6, "Hydrophobic Aerosil: Manufacture, Properties and Applications," Degussa Corp., Akron, OH (1991).

101. H. Barthel, L. Rosch, and J. Weis, "Fumed Silica- Production, Properties, and Applications", in Organosilicon Chemistry II: From Molecules to Materials; N. Auner and J. Weis, Ed.; VCH Publishers, Weinheim, Germany, 761 (1996).

102. G. Michael and H. Ferch, Basic Characteristics of Aerosil, Degussa Technical Bulletin Pigment No. 11, (1998).

103. V. Khavryutchenko, H. Barthel, and E. Nikitina, Macromol. Symp., 169, 7 (2001).

104. V. M. Gun'ko, V. I. Zarko, V. V. Turov, R. Leboda, E. Chibowski, E. M. Pakhlov, E. V. Goncharuk, M. Marciniak, E. F. Voronin, and A. A. Chuiko, J. Colloid & Interf. Sci., 220, 302 (1999).

105. M. Ettlinger, T. Ladwig, and A. Weise, Prog. in Organic Coatings, 40, 31 (2000).

106. V. M. Gun'ko, D. J. Sheeran, S. M. Augustine, and J. P. Blitz, J. Colloid & Interf. Sci., 249, 123 (2002).

107. M. Ettlinger, Highly Dispersed Metallic Oxides Produced by the AEROSIL® Process, Degussa Technical Bulletin Pigments No. 56, Akron, OH (2002).

108. B. B. Boonstra, H. Cochrane, and E. M. Dannenberg, Rubber Chem. Technol., 48, 558 (1976).

109. Cabot Technical Brochure, "Cab-O-Sil Properties and Functions," Cabot Corp., Tuscola, IL (1987).

110. J. Hou, Composite Polymer Electrolytes Using Functionalized Fumed Silica and Low Molecular Weight PEO: Synthesis and Characterization, Michigan State University, Lansing, MI (1997).

111. H. Barthel, M. Dreyer, T. Gottschalk-Gaudig, V. Litvinov, and E. Nikitina, Macromol. Symp., 187, 573 (2002).

112. S. R. Raghavan, H. J. Walls, and S. A. Khan, Langmuir, 16, 7920 (2000).

113. G. Eichinger and M. Fabian, J. Power Sources, 68, 381 (1997).

114. G. Eichinger and M. Fabian, J. Power Sources, 68, 387 (1997).

115. H. P. Fritz, K. Stein, and R. Herr, J. Power Sources, 37, 315 (1992).

116. J. Fan, S. R. Raghavan, X. Y. Yu, S. A. Khan, P. S. Fedkiw, J. Hou, and G. L. Baker, Solid State Ion., 111, 117 (1998).

117. J. Przyluski, K. Such, H. Wycislik, W. Wieczorek, and Z. Florianczyk, Synth. Met., 35, 241 (1990).

118. Y. Fu, X. Ma, Q. Yang, and X. Zong, Mater Lett, 57, 1759 (2003).

119. H. P. Wang, H. T. Huang, and S. L. Wunder, J. Electrochem. Soc., 147, 2853 (2000).

120. K. M. Kim, K. S. Ryu, S. G. Kang, S. H. Chang, and I. J. Chung, Macromol. Chem. Phys., 202, 866 (2001).

121. S. R. Raghavan, M. W. Riley, P. S. Fedkiw, and S. A. Khan, Chem. Mat., 10, 244 (1998).

122. Y. X. Li, P. S. Fedkiw, and S. A. Khan, Electrochim. Acta, 47, 3853 (2002).

CHAPTER 4: EXPERIMENTAL AND METHODS

This section summarizes methods for material preparation and characterization of LiBOB-based electrolytes (gel and liquid electrolytes). Material preparations include liquid and composite electrolyte preparation, cathode and anode fabrication, and coin-cell assembly. Material characterizations include electrochemical (conductivity, and cell cycling), rheological (dynamic measurments), and Fourier transform infrared spectroscopy (FTIR) measurements.

4.1. Material preparation

4.1.1. Composite electrolyte preparation

The solvents used in this study are ethylene carbonate (EC), ethyl acetate (EA), and γ-butyrolactone (GBL) at the following weight compositions (GBL: EA: EC): 1:1:1, 1:1:0.1, and 1:1:0. For each composition, the following LiBOB concentrations (mol/L) are prepared: 0.2, 0.7, and 1.0 M. The salt concentration and solvent composition are varied in order to study the effects of salt concentration and EC content on conductivity, rheological properties, and cycling performance. The solubility of LiBOB in GBL, EA, and EC is 1.55, 0.98, and 1.03 mol/kg, respectively[1]. Table 4.1 lists the various electrolytes investigated.

Ethylene carbonate, ethyl acetate, and γ-butyrolactone are obtained from Aldrich and dried over 4 Å molecular sieves (Fisher Scientific) for at least one week. Lithium bis(oxalato)borate is obtained from Chemetall as a gift and dried in a vacuum oven at 150 ^{o}C for at least 48 hours before it is added to the solvents. Fumed silica is donated by Degussa

Corporation (Akron, OH) (currently known as Evonik) as Aerosil A200 (silanol, -OH groups) and Aerosil R805 (octyl, $-C_8H_{17}$ groups). Fumed silica w dried in a vacuum oven at 120 ^oC for 1 week before it is added to the solvents inside an Argon-filled glove box.

Table 4.1. Liquid electrolytes used in gel electrolyte preparation.

	LiBOB Concentration (mol L^{-1})		
	0.2	**0.7**	**1**
Solvent Composition GBL:EA:EC	1:1:0	1:1:0	1:1:0
	1:1:0.1	1:1:0.1	1:1:0.1
	1:1:1	1:1:1	1:1:1

The water content of solvents is measured to be below 20 ppm using a Mitsubishi CA-06/VA-06 Karl-Fisher titrator. To check the water content of the salt, a known amount of LiBOB (~ 0.1g) is placed in the oven boat of the Karl fisher titrator, as opposed to direct injection into the K-F reagent since it is known that LiBOB reacts with methanol in the K-F reagent to give water[2]. The amount of water in the dried LiBOB is around 350 ppm. The water content of the electrolyte solution is calculated as approximately 70 ppm from the measured water content in the salt and solvents.

Electrolyte formulation is performed under an argon atmosphere in a LABCONCO 50800 glove box. Liquid electrolytes are prepared by weighing an amount of LiBOB in a volumetric flask and adding an appropriate amount of solvent. Mixing of the liquid

electrolytes is performed by sealing the flask and gently shaking by hand until the salt dissolves.

Composite electrolytes are prepared in an argon-filled glove box by adding a certain weight of fumed silica (R805 and A200 varied from 10 to 20 wt %) to the baseline electrolyte and dispersed by use of a high-shear mixer (Tissue TearorTM, Model 398, BioSpec Products, Inc.)[3]. The gel electrolyte is then taken outside the glove box in a sealed vial and centrifuged (IEC HN-SII centrifuge, Damon/IEC Division) for twenty minutes at speed of 3000 rpm to remove gas bubbles

4.1.2. Cathode preparation

Three types of cathodes are used in this study: $LiCoO_2$, $LiMn_2O_4$, and $LiFePO_4$. The $LiCoO_2$ is obtained from OMG and LICO Technology Corp (Japan). The $LiMn_2O_4$ is obtained from Merck (Germany) and LICO. The $LiFePO_4$ is obtained from Hydro Quebec (Canada). Poly (vinylidene fluoride) (PVDF, $KYNAR_{TM}$) is obtained from Elf Atochem. Synthetic flake graphite (SFG 15 and SFG 6) is obtained from Timcal America. Carbon black (Ketjenblack (KJB) EC-600JD) is obtained from Akzo Nobel Inc . The solvent 1-methyl-2-pyrrolidinone (NMP) is obtained from Aldrich. Two types of carbon additives are used in this study: KJB graphite, which consists of round particles and the SFG type, which is in the form of flat flakes. All these components are used as received.

The typical compositions for $LiCoO_2$, $LiFePO_4$, and $LiMn_2O_4$ are given in Table 4.2. In these electrodes, carbon additives are used as the electronic conductor and PVDF is used as the binder. Aluminum foil (0.024-mm thick, Fisher Scientific) is used as the current

collector for $LiCoO_2$, $LiMn_2O_4$, and $LiFePO_4$ cathodes. Cathode half-cells are used with various $LiPF_6$- and LiBOB-based electrolytes. Electrolyte compositions that are used in cathode half-cells study are shown in Table 4.3.

Table 4.2 Typical composition for the cathodes in this study.

Cathode Type	Active Material wt%	PVDF wt%	SFG 15 wt%	KJB EC-600JD wt%
$LiCoO_2$	90	5	3	2
$LiFePO_4$	80	10	5	5
$LiMn_2O_4$	80	10	5	5

A fixed amount of metal oxide and carbon additives are thoroughly hand ground and mixed using a mortar and pestle, typically thirty minutes. The mixture of metal oxide and carbons is dispersed into a 11-ml glass vial containing PVDF in NMP. The vial then is placed in a rotator for 48-72 hr to mix the slurry thoroughly. The resulting slurry is coated onto the current collector using a "MICROM II" film applicator (Paul N. Gardner Co., Inc.). The film is dried at 80 °C overnight and cut into 1.27-cm diameter disks that are hot compacted by a hydraulic press at 150 °C and 700 MPa. After compaction, cathode disks are dried at 150 °C under vacuum for 24 hr.

Table 4.3. Electrolyte compositions that are used in cycling study.

	Fumed Silica Type and Content (wt %)						
		A200			R805		
	Liquid	10%	15%	20%	10%	15%	20%
$LiCoO_2$ GBL:EA:EC (LiBOB mole/L)	1:1:0 (0.7) 1:1:0 (1.0) 1:1:1 (0.7) 1:1:1 (1.0)	1:1:0 (0.7) 1:1:0 (1.0) 1:1:1 (0.7) 1:1:1 (1.0)	---- 1:1:0 (1.0) ---- ----	---- ---- ---- ----	1:1:0 (0.7) 1:1:0 (1.0) 1:1:1 (0.7) 1:1:1 (1.0)	1:1:0 (0.7) ---- ---- 1:1:1 (1.0)	---- 1:1:0 (1.0) 1:1:1 (0.7) 1:1:1 (1.0)
$LiMn_2O_4$ GBL:EA:EC (LiBOB mole/L)	1:1:0 (0.7) 1:1:0 (1.0) 1:1:1 (0.7) 1:1:1 (1.0)	1:1:0 (0.7) 1:1:0 (1.0) 1:1:1 (0.7) 1:1:1 (1.0)	---- ---- ---- 1:1:1 (1:0)	---- ---- ---- ----	1:1:0 (0.7) 1:1:0 (1.0) 1:1:1 (0.7) 1:1:1 (1.0)	1:1:0 (0.7) ---- ---- 1:1:1 (1.0)	1:1:0 (0.7) ---- ---- 1:1:1 (1.0)
$LiFePO_4$ GBL:EA:EC (LiBOB mole/L)	1:1:0 (0.7) 1:1:0 (1.0) 1:1:1 (0.7) 1:1:1 (1.0)	1:1:0 (0.7) 1:1:0 (1.0) 1:1:1 (0.7) 1:1:1 (1.0)	1:1:0 (0.7) ---- 1:1:1 (0.7) 1:1:1 (1.0)	1:1:0(0.7) ---- ---- ----	1:1:0 (0.7) 1:1:0 (1.0) 1:1:1 (0.7) 1:1:1 (1.0)	---- ---- ---- ----	1:1:0 (0.7) 1:1:0 (1.0) ---- 1:1:1 (1.0)

4.1.3. Preparation of coin cells

Coin cells in which an electrolyte/separator is sandwiched between lithium metal and a metal-oxide composite cathode or graphite anode are used in the cycling measurements

(Figure 4.1[4]). In these cells, a Celgard 2400 separator (Hoechst Celanese) (25-µm thick) was wetted by the electrolyte. A stainless steel spacer and spring are used to maintain good contact of electrolyte, electrode, and current collector.

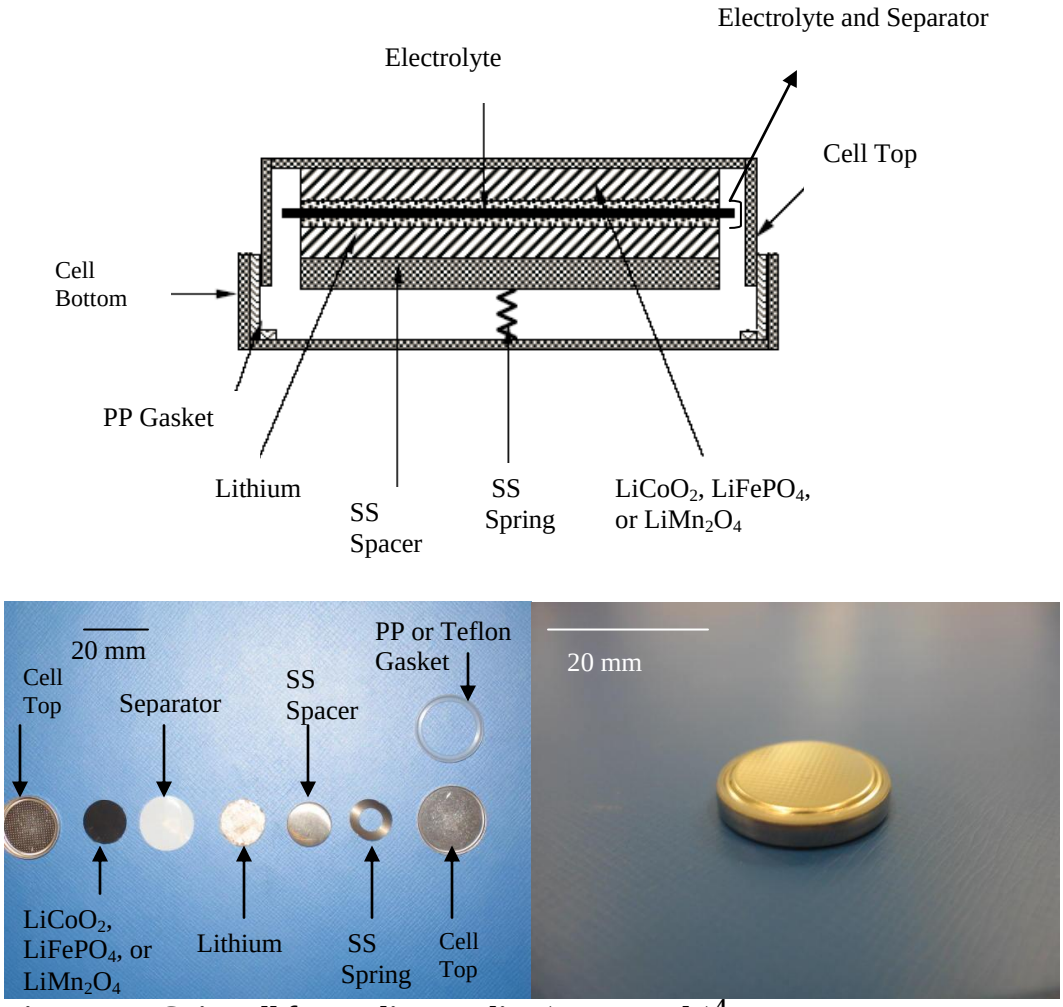

Figure 4.1. Coin cell for cycling studies (not to scale)[4].

4.2. Electrochemical measurements

Electrochemical impedance spectroscopy (EIS) is used to evaluate the electrochemical characteristics of the system under study by applying an alternating potential (AC signal) at varying frequencies and measuring the current response. The AC impedance measurements are made using PowerSine software (Princeton Applied Research). AC data obtained from the measurements reflect ion migration and ionic polarization that occurs within the cell. Electrical information of the cell is obtained using a circuit model.

4.2.1. Electrolyte resistance

The resistance of an ionic solution depends on the ionic concentration, type of ions, temperature and cell geometry. In a rectangular bounded area with area A and length l carrying a uniform current the resistance is defined as:

$$R = \rho \frac{l}{A} \tag{4.1}$$

where ρ is the solution resistivity. The conductivity of the solution, σ (S cm^{-1}), is more commonly used in solution resistance calculations. Its relationship with solution resistance is:

$$R = \frac{l}{A\sigma} \Rightarrow \sigma = \frac{l}{RA} \tag{4.2}$$

If we take the ratio of conductivity for two solutions, we have the following:

$$\frac{\sigma_1}{\sigma_2} = \frac{l_1 R_2 A_2}{R_1 A_1 l_2} \tag{4.3}$$

If the geometry is fixed, then

$$\frac{\sigma_1}{\sigma_2} = \frac{R_2}{R_1} \tag{4.4}$$

We can calculate the conductivity for any sample by using a standard solution with a known conductivity and measure the resistance for the standard sample. Upon measurement of the resistance for the unknown sample, the conductivity of the unknown sample can be calculated using Equation 4.4

4.2.2. Conductivity measurements

Ionic conductivity is a measure of total charge species in the electrolyte. High-conductivity electrolytes are favorable because they have lower Ohmic potential losses. Conductivity of gel electrolytes is measured using EG&G Princeton Applied Research PowerSine software to control an EG&G Model 273 potentiostat and EG&G Model 5210 lock-in amplifier in the frequency range 100 kHz to 100 mHz. The cell constants is found using a KCl standard solution (1409 μS cm^{-1} at 25 °C, Fisher Scientific) prior to and after each measurement.

The conductivity cell that is used in conductivity measurements consists of a glass cell containing two blocking platinum wire electrodes (0.64-mm diameter, Alfa Aesar), a thermocouple opening, an o-ring seal, and glass vial. The conductivity cell has a diameter of ~1.5 cm and height of 5 cm. The design of the cell is described by Riley[5], and a schematic of the conductivity cell is shown in Figure 4.2[4-5]

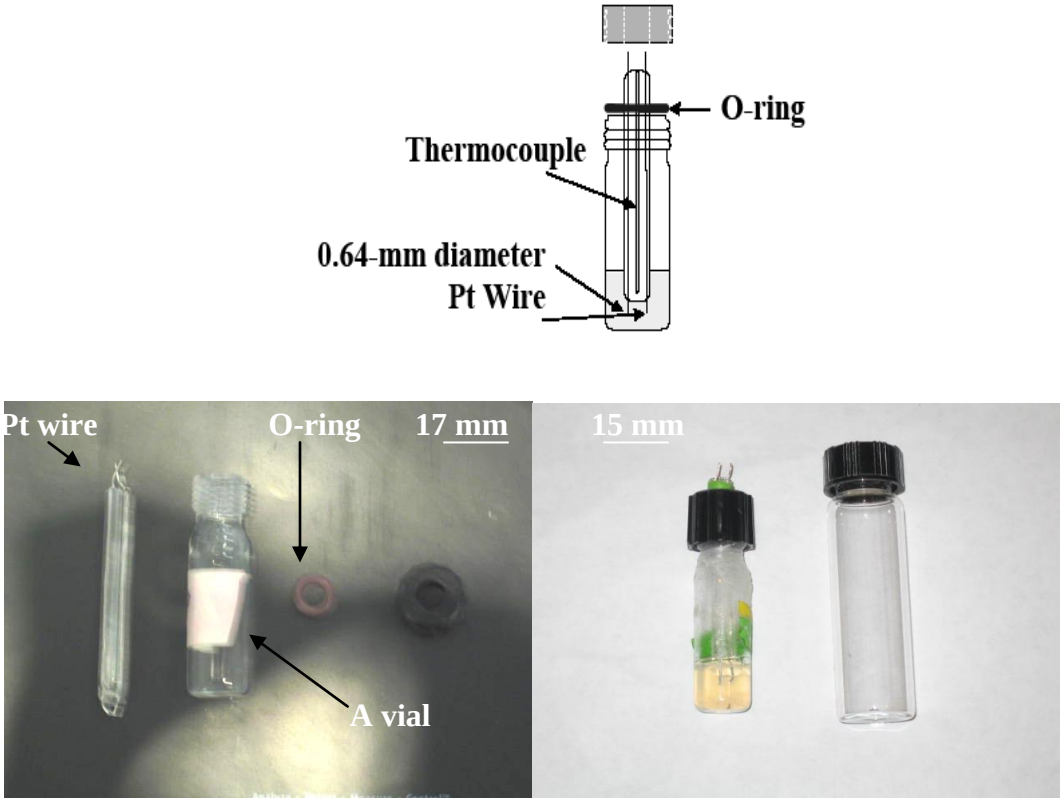

Figure 4.2. Two-electrode cell for conductivity measurement[5].

The empty conductivity cells are placed in an oven at 80 ^{o}C for 1 day to remove moisture and then moved to the glove box where the electrolyte sample is inserted. Samples are added to the conductivity cells within the glove box to ensure low-moisture content. The measurements are performed over the temperature range from -2 to 60 °C. Temperature is controlled by placing conductivity cells inside wells in an insulated aluminum block with an internal-coolant circuit connected to a temperature-controlled circulating water bath with accuracy of ±0.5 °C (Isotope 1016P Fisher Scientific). The temperature of each sample is measured using a T-type thermocouple (Omega) placed in a sealed glass compartment fully

submerged in the sample. The data acquisition system consists of a National Instruments Field point Module (FP 1000) connected to two National Instruments 8-channel thermocouple modules (FP-TC-120). Table 4.4 shows the electrolyte compositions that are used in conductivity measurements.

Table 4.4. Gel electrolyte compositions.

	Fumed Silica Type and Content (wt %)					
	R805			A200		
	10 %	15%	20%	10 %	15%	20%
Base Electrolyte Composition GBL:EA:EC (LiBOB Concentration mol/L)	1:1:0 (0.2,0.7, and 1M)	1:1:0 (0.2,0.7, and 1M)	1:1:0 (0.2,0.7, and 1M)	1:1:0 (0.2,0.7, and 1M)	1:1:0 (0.2,0.7, and 1M)	1:1:0 (0.2,0.7, and 1M)
	1:1:0.1 (0.2,0.7, and 1M)	1:1:0.1 (0.2,0.7, and 1M)	1:1:0.1 (0.2,0.7, and 1M)	1:1:0.1 (0.2,0.7, and 1M)	1:1:0.1 (0.2,0.7, and 1M)	1:1:0.1 (0.2,0.7, and 1M)
	1:1:1 (0.2,0.7, and 1M)	1:1:1 (0.2,0.7, and 1M)	1:1:1 (0.2,0.7, and 1M)	1:1:1 (0.2,0.7, and 1M)	1:1:1 (0.2,0.7, and 1M)	1:1:1 (0.2,0.7, and 1M)

Two methods are used to calculate the resistance of the electrolyte Z_{RE} from the EIS data:

1. Take the intercept on a Nyquist plot of Z with the real impedance axis at high frequency
2. Use a program (ZSimpWin from EG&G Prinston Applied Research) to calculate equivalent-circuit parameters. The equivalent circuit used for the calculation is shown in Figure 4.3.

The first method is used in this study but checked periodically using the second method. The resistance determined between the two methods differed by no more than two percent.

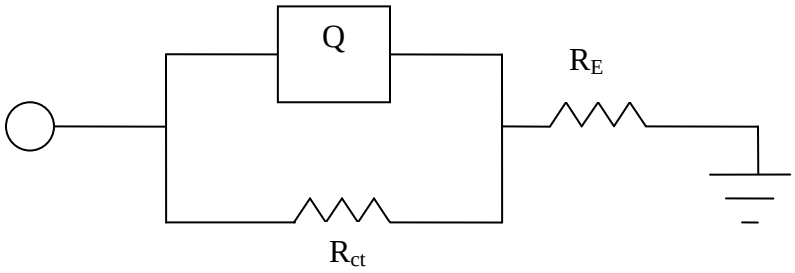

Figure 4.3. Equivalent circuit used for electrolyte resistance calculation, where R_E is bulk electrolyte resistance, R_{ct} is charge transfer resistance, and Q is constant phase element.

For each sample, electrolyte conductivity for three different mixtures (same electrolyte composition) is measured with the reported value representing the average. The electrolyte conductivity is obtained from the cell constant and measured resistance using equation 4.5

$$\sigma_i = \frac{\sigma_{KCl} \times Z_{RE,KCl}}{Z_{RE,i}} \quad (4.5)$$

where σ_{KCl} is the conductivity of KCl the standard [1409 µS cm^{-1} at 25 ^{o}C], $Z_{RE,KCl}$ is the measured intercept of the real impedance axis for the KCl standard [ohm], and $Z_{RE,i}$ is the measured intercept of the real impedance axis for sample *i* [ohm].

4.2.3. Cell cycling

An Arbin battery cycler (Model BT2042 and BT2043) controlled by Arbin ABTS software is employed to carry out constant-current cell cycling in Li/electrolyte/X cells, where X is $LiCoO_2$, $LiMn_2O_4$, or $LiFePO_4$. A C-rate of C/10 is used in all measurements. Cell cycling is terminated upon reaching a typical cycle number of 20-50. The cutoff voltage for each cathode is shown below in Table 4.5

Table 4.5. Cutoff voltages for cathodes in this study.

Cathode Type	Discharge voltage (V)	Charge Voltage (V)
$LiCoO_2$	2.5	4.2
$LiFePO_4$	2.5	4.2
$LiMn_2O_4$	3	4.2

4.3 Rheological measurements

Rheological measurements on the gels were conducted using a stress controlled rheometer (Rheometrics DSR II and TA instrument AR2000). A parallel-plate geometry with 20-mm diameter plates is used for the measurements. The gap between the plates was set at 1000-μm. All measurements are performed at room temperature and ambient air.

4.3.1 Dynamic measurements

Dynamic measurements are primarily used to probe the gel microstructure with minimal disturbance of samples[6]. The relative magnitude and shapes of elastic (G') and viscous (G") moduli as a function of rotation frequency indicate the type and extent of microstructure of samples[7]. The gel electrolyte compositions that are used in dynamic measurement are shown in Table 4.6. Gel samples are allowed to sit overnight in a closed glass vial inside the glove box prior to rheological measurement. A pre-shear step (between 0.4-40 rad s^{-1} at 25 °C) followed by a recovery step (5 min at zero shear) is applied to each sample in order to establish a uniform shear history.

After loading the sample, it is allowed to equilibrate for five minutes. A dynamic stress sweep at a constant frequency of 1 rad s^{-1} is performed to determine the range of stresses within the linear-viscoelastic (LVE) region for each sample. After that, a new sample is loaded and a dynamic frequency sweep (0.01 rad s^{-1} to 100 rad s^{-1}), using the pre-determined LVE stress, is performed to examine the elastic (G') and viscous (G") moduli in the LVE regime.

Table 4.6. Gel electrolyte compositions used in dynamic measurements.

	Fumed Silica Type and Content (wt %)					
	R805			A200		
	10 %	15%	20%	10 %	15%	20%
GBL:EA:EC (LiBOB Concentration mol/L)	1:1:0 (0.2, 0.7, and 1 M)	1:1:0 (0.2, 0.7, and 1 M)	1:1:0 (0.2, 0.7, and 1 M)	1:1:0 (0.2, 0.7, and 1 M)	1:1:0 (0.2, 0.7, and 1 M)	1:1:0 (0.2, 0.7, and 1 M)
	1:1:1 (0.2, 0.7, and 1 M)	1:1:1 (0.2, 0.7, and 1 M)	1:1:1 (0.2, 0.7, and 1 M)	1:1:1 (0.2, 0.7, and 1 M)	1:1:1 (0.2, 0.7, and 1 M)	1:1:1 (0.2, 0.7, and 1 M))

4.4. FTIR-ATR measurements

FTIR is used in order to develop a chemical understanding of the salt concentration effect on the elastic modulus of A200-containg electrolyte. Spectra are collected using a Bio-Rad-Digilab FTS-3000 Fourier transform infrared (FT-IR) spectrometer using a mounted crystalline Germanium, attenuated total internal reflection (ATR) sample attachment (Pike Technologies inc., MIRacle™ Single Reflection ATR) with a normal spectral response of 650 to 5500 cm^{-1}. The infrared light is focused onto the photodiode of a liquid nitrogen-

cooled, narrow band mercury-cadmium-telluride (MCT) detector with a normal spectral response of 650 to 7000 cm^{-1}. There is nominally one reflection with a spot size of approximately 100 μm. The spectrometer and attachment where purged with dry compressed air, which reduces the possibility of atmospheric water or CO_2 contamination of the spectra and samples.

The spectra presented are an average of 64 scans. All spectra are recorded at room temperature, approximately 23° ± 0.5° C, with a resolution of 2 cm^{-1}. The data are transferred to a data processing program (OriginPro, v8.0) where numerical treatment and graphs are prepared. FTIR-ATR samples that are used in FTIR-ATR measurements are shown in Table 4.7.

Table 4.7. Samples used in FTIR-measurements.

	Fumed Silica Type and Content (wt %)					
	R805			A200		
	0 %	10%	15%	0 %	10%	15%
GBL:EA (LiBOB Concentration mol/L)	1:0, 0:1, and 1:1 (0, 0.2, and 0.7 M)	1:0, 0:1, and 1:1 (0, 0.2, and 0.7 M)	1:0, 0:1, and 1:1 (0, 0.2, and 0.7 M)	1:0, 0:1, and 1:1 (0, 0.2, and 0.7 M)	1:0, 0:1, and 1:1 (0, 0.2, and 0.7 M)	1:0, 0:1, and 1:1 (0, 0.2, and 0.7 M)
AN (LiBOB Concentration mol/L)	(0 and 0.2 M)	(0 and 0.2 M)	(0 and 0.2 M)	(0 and 0.2 M)	(0 and 0.2 M)	(0 and 0.2 M)

4.5. References

1. Chemtall, Technical brochure "Lithium bis(oxalate)borate (LiBOB) a halogen-free conductive salt for lithium batteries", (2004).

2. H. G. Schweiger, M. Multerer, U. Wietelmann, J. C. Panitz, T. Burgemeister, and H. J. Gores, J. Electrochem. Soc., (2005), 152, A622.

3. H. J. Walls, J. Zhou, J. A. Yerian, P. S. Fedkiw, S. A. Khan, M. K. Stowe, and G. L. Baker, J. Power Sources, 89, 156 (2000).

4. J. Zhou, PhD" Fumed Oxide-Based Nanocomposite Polymer Eelectrolyte For Rechargeable Lithium Batteries" North Carolina State University, (2002).

5. M. Riley, P. S. Fedkiw, and S. A. Khan, J. Electrochem. Soc. 149, (2002), A667.

6. S. R. Raghavan, M. W. Riley, P. S. Fedkiw, and S. A. Khan, Chem. Mater., 10, 244 (1998).

7. C. W. Macosko, Rheology: Principles, Measurements, and Applications, VCH publishers, Inc., New York (1994).

CHAPTER 5: CONDUCTIVITY OF LIBOB-BASED ELECTROLYTE FOR LITHIUM-ION BATTERIES

Fadhel Azeez and Peter S. Fedkiw*

Department of Chemical & Biomolecular Engineering, North Carolina State University, Raleigh, NC 27695-7905, USA

In preparation for submission to

Journal of Power Sources

* Corresponding author. Tel.: +1-919-515-3572; Fax: +1-919-515-3456
E-mail address: fedkiw@eos.ncsu.edu

Abstract

This work reports the use of mixtures of γ-butyrolactone (GBL) and ethyl acetate (EA), with and without ethylene carbonate (EC), as solvents for lithium bis(oxalato)borate (LiBOB) salt as potential electrolytes for Li-ion cells. The effects of salt concentration, ethylene carbonate (EC) content, and temperature on the conductivity and viscosity of the mixture are reported. Results indicate that the best electrolyte for high-temperature application is that which contains 1 M LiBOB in GBL+EA+EC of composition 1:1:0.1 (wt). For low-temperature applications, the best electrolyte is that which contains 0.7 M LiBOB in GBL+EA+EC of composition 1:1:0 (wt). The product of conductivity with viscosity was essentially independent of temperature but was dependent on solvent composition showing that at fixed salt concentration, the viscosity is the major criteria affecting electrolyte conductivity rather than dielectric constant.

5.1. Introduction

Li-ion batteries are used in many applications such as portable electronics, cellular phones and laptop computers. In addition, there is interest in using Li-ion batteries in electric vehicles (EVs) and hybrid electric vehicles (HEVs) due to their high- energy and –power density compared to alternatives such as Ni-Cd and Ni-MH [1].

Currently, the state-of-art electrolyte for a Li-ion battery is composed of lithium hexafluorophosphate ($LiPF_6$) salt dissolved in a mixture of ethylene carbonate (EC) and linear esters such as dimethyl carbonate (DMC), diethyl carbonate (DEC), and ethyl methyl carbonate (EMC). Lithium hexafluorophosphate has been used as the salt in Li-ion batteries for more than a decade because of its unique balance of properties such as good ionic conductivity and ability to passivate an aluminum current collector. However, $LiPF_6$ is thermally unstable and it decomposes into undesired products such as LiF and PF_5 that can trigger detrimental reactions on the electrode surfaces [2, 3]. In addition, $LiPF_6$ and PF_5 react with trace of water to form HF [4]

$$LiPF_6 \Leftrightarrow LiF + PF_5 \quad (1)$$

$$LiPF_6 + H_2O \rightarrow POF_3 + LiF + 2HF \quad (2)$$

$$PF_5 + H_2O \rightarrow POF_3 + 2HF \quad (3)$$

The LiF deposits on the electrode surface and results in high-interfacial impedance and is an impediment for Li^+ insertion and deinsertion processes, which lead to cell capacity fade [5].

Also, HF causes dissolution and migration of the cathode's transition metals which leads to structural changes and capacity fade [6, 7].

Efforts have been devoted to develop alternative lithium salts to replace $LiPF_6$, including lithium perchlorate ($LiClO_4$), lithium arsenate ($LiAsF_6$), lithium tetrafluoroborate ($LiBF_4$), lithium triflate ($LiCF_3SO_3$), and lithium bis(trifluoromethane sulfone)imide ($LiN(SO_2CF_3)_2$). However, each salt has its own challenges that prevent it from being used in commercial Li-ion batteries. For example, $LiClO_4$ and $LiAsF_6$ cannot be used because of explosion risks of ClO_4^- [8] and toxicity of AsF_6^- and its degradation products[9-12], respectively. The main challenge with $LiBF_4$ is its low conductivity, although it was observed recently that electrolytes with $LiBF_4$ have good performance at low temperature[13-16]. Lithium triflate has two shortcomings. First, it has poor ion conductivity in nonaqueous solvents, which is attributed to the low-dissociation constant of $LiCF_3SO_3$ in solvents with a low-dielectric constant[12, 17] and the moderate ion mobility of $CF_3SO_3^-$ as compared to other salts anions[18]. The second problem with using $LiCF_3SO_3$ is the aluminum current-collector corrosion that occurs with it[19], which is also a problem with $LiN(SO_2CF_3)_2$[19].

Recently, LiBOB, which was independently disclosed by Lischka *et al.* in Germany and Angell *et al.* in the USA [20, 21], has attracted attention as a promising candidate for Li-ion batteries [22-26]. The LiBOB salt has many advantages such as high thermal stability (up to 302 ^oC), ability to passivate aluminum, and ability to form a solid electrolyte interface (SEI) on graphite even in the absence of EC [27, 28], which is a major solvent component due to its ability to form the SEI. On the other hand, EC is believed to be at least partially responsible for the low-temperature limit of Li-ion batteries [29]. Although LiBOB has many advantages,

it also has disadvantages when used with linear carbonate co-solvents that are used to lower viscosity. The problems of using LiBOB with linear carbonate solvents come from LiBOB essentially being insoluble in these solvents [30] and, consequently, practical solvents must be EC- or PC-rich. However, high-EC or -PC content in an electrolyte increases its viscosity, which renders the electrolyte with poor low-temperature performance and rate capability. There is a need to find a proper solvent mixture that is tailored for LiBOB to give high conductivity and good solubility for the salt. In this work, we used mixtures of γ-butyrolactone (GBL), ethyl acetate (EA), and ethylene carbonate (EC) to dissolve LiBOB and studied the conductivity and viscosity of the electrolyte. The effects of salt concentration, solvent composition, and temperature on conductivity and viscosity are reported here.

Gamma-butyrolactone (GBL) is chosen as a co-solvent because it has a reasonably high-dielectric constant (~39), a relatively moderate viscosity (~1.7 cP at 25^{o}C), a similar structure to EC, and good solubility for LiBOB[31-33]. In addition, it was reported that GBL can improve the low-temperature performance of a LiBOB-based electrolyte [34-36]. Ethyl acetate is chosen because it has a low-melting point (~-84 ^{o}C), which will increase the liquid range of the electrolyte. In addition, the low viscosity (~0.5 cP at 25^{o}C) of EA will improve conductivity. Also, it has been reported that EA enhances the low-temperature performance of Li-ion cells because of improved solution transport properties[37-40]

5.2. Experimental

Ethylene carbonate, ethyl acetate, and γ-butyrolactone are obtained from Aldrich and dried over 4 Å molecular sieves (Fisher Scientific) for at least one week. Lithium

bis(oxalato)borate is obtained from Chemetall and used as is. Fumed silica is donated by Evonic as Aerosil A200 (silanol, -OH groups) and Aerosil R805 (octyl, $-C_8H_{17}$ groups). Fumed silica is dried in a vacuum oven at 120 ^oC for 1 week before it is added to the solvents inside a glove box with an Ar atmosphere.

The water content of solvents is measured to be below 20 ppm using a Mitsubishi CA-06/VA-06 Karl-Fisher titrator. The water content of the electrolyte solution is calculated as approximately 70 ppm from the measured water content in the salt and solvents.

5.2.1. Conductivity measurements

Conductivity is measured using EG&G Princeton Applied Research PowerSine software to control an EG&G Model 273 potentiostat and EG&G Model 5210 lock-in amplifier in the frequency range 100 kHz to 100 mHz. The cell constants are found using a KCl standard solution (1409 $\mu S\ cm^{-1}$ at 25°C) (Fisher Scientific) prior to and after each measurement.

The conductivity cell consists of a glass cell containing two blocking platinum wire electrodes (0.64-mm diameter, Fisher Scientific), a thermocouple opening, an O-ring seal, and glass vial. The conductivity cell has a diameter of ~1.5 cm and height of 5 cm. The design of the cell is described by Riley [41], and a schematic of the conductivity cell is shown in Figure 5.1.

[Figure 5.1]

Temperature is controlled by putting the conductivity cells inside wells in an insulated aluminum block with an internal-coolant circuit connected to a temperature-

controlled circulating water bath (Isotope 1016P Fisher Scientific). Conductivities are measured over the temperature range of -3 to 60°C and the temperature of each sample is measured using a T-type thermocouple (Omega) placed in a sealed glass compartment fully submerged in the sample. The data acquisition system consists of a National Instruments Field point Module (FP 1000) connected to two National Instruments 8-channel thermocouple modules (FP-TC-120).

Two methods are used to calculate the resistance of the electrolyte Z_{RE} from the electrochemical impedance spectroscopy (EIS) data: From the intercept on a Nyquist plot of Z with the real impedance axis at high frequency; and use of a program (ZSimpWin from EG&G Princeton Applied Research) to calculate equivalent-circuit parameters, as shown in Figure 5.2. The first method is used in this study with the second method periodically used to verify the results. There is a small difference in the resistance between two methods (<2%).

[Figure 5.2]

For each electrolyte sample, the conductivity in five separate cells is measured with the reported value representing the average. The electrolyte conductivity is obtained from the cell constant and measured resistance using Equation 4

$$\sigma_i = \frac{\sigma_{KCl} \times Z_{RE,KCl}}{Z_{RE,i}} \tag{4}$$

where σ_{KCl} is the conductivity of KCl the standard, $Z_{RE,KCl}$ is the measured intercept of the real impedance axis for the KCl standard [ohm], and $Z_{RE,i}$ is the measured intercept of the real impedance axis for sample i [ohm].

5.2.2. Viscosity measurement

Rheological measurements are conducted using a TA AR2000 stress rheometer over a temperature range of 10-25 ^{o}C. The liquid viscosities are determined using conical concentric cylinders. The inner radius of the outer stator cylinder is 15 mm; the outer radius of the inner rotor is 14 mm; and the cylinder immersed height is 42 mm. Typically, the liquid sample volume is 19.6 ml.

Liquid viscosities are measured by a steady-state flow mode. Typical Newtonian behavior is observed for the liquid sample: viscosity does not vary with shear stress or shear rate; viscosity is constant with time of shearing; and stress in fluid immediately falls to zero when shear is stopped.

5.3. Result and Discussion

5.3.1. Salt concentration effect on conductivity and viscosity

As evident from Figure 5.3, conductivity increases with salt concentration at low- salt concentrations, which is attributable to the number of free ions increasing with salt concentration. After achieving a maximum conductivity, an increase in salt concentration results in higher ion aggregation and higher viscosity of the solution, which reduces the free-ion number and the ionic mobility, respectively. It is a universal phenomenon for liquid electrolytes to have a maximum in conductivity at a certain salt concentration, and it has been reported for many electrolytes of lithium salts [42-46].

[Figure 5.3]

The concentration at the maximum in conductivity was ~ 0.7 M LiBOB at 0 ^{o}C for all solvent compositions studied. At 60 ^{o}C the system with GBL:EA:EC at 1:1:0 shows a broad maximum around 1.0 M LiBOB. The salt concentration at the maximum in conductivity increases with EC content. For the system with solvent composition of 1:1:0.1 (GBL:EA:EC), the maximum in conductivity occurs between 0.7 and 1.2 M LiBOB. The system with GBL:EA:EC at 1:1:0.5 has the maximum conductivity around 1.0 M LiBOB, and finally for the system with solvent composition of 1:1:1, there is no maximum in the studied range of salt concentration. As seen in Equation 5, the required distance q for ion-pair formation decreases as temperature increases [47].

$$q = \frac{\left|z_i z_j\right|}{8\pi\varepsilon_o \varepsilon kT} e^2 \qquad (5)$$

A decrease in q means that more salt can be dissolved without ion pairing, which will shift the maximum conductivity to a higher salt concentration than the same electrolyte at lower temperature. At high temperature (60^{o}C), the maximum conductivity occurs at higher salt concentration as the EC content increases because of the higher dielectric constant of the solvent mixture. The maximum conductivity at 0 ^{o}C occurs around 0.7 M LiBOB irrespective of EC content. Although addition of EC increases the solvent dielectric constant, the high

viscosity of EC decreases conductivity; that is, at low temperature the viscosity effect appears to dominate over the dielectric-constant effect.

The molar conductivity Λ is shown as a function of salt concentration in Figure 5.4. The molar conductivity decreases with increase of salt concentration because of the two negative factors (viscosity and ion association). That is, as the salt concentration increases, the viscosity and ion association increases. A viscosity increase will lower ion mobility and an ion association increase will lower the number density of free ions, both which will lower conductivity.

[Figure 5.4]

The relation between the viscosity and the salt concentration is shown in Figure 5.5 for GBL:EA:EC of 1:1:0.1. As the salt concentration increases so does the viscosity because of the increasing intermolecular force between ions and molecules. This trend is typical for other solvent compositions.

[Figure 5.5]

Figure 5.6 shows the product of conductivity and viscosity as a function of temperature for the solvent compositions studied. The product is nearly temperature independent, although there is a slight increase at the lowest temperature shown. At fixed temperature, increasing values of the product $\sigma\eta$ indicate increasing salt disassociation[46]. Figure 5.6 shows that the highest $\sigma\eta$ value is for GBL:EA:EC of 1:1:1 and the smallest value

is for solvent composition of 1:1:0. The increase of the $\sigma\eta$ product with EC content is due to the increase of the mixture's dielectric constant[48], leading to an increase of ion disassociation. Although it is reasonable to expect that the solvent composition of 1:1:1 (GBL:EA:EC) should produce the highest ion disassociation, its conductivity is the lowest (Figure 5.3) because of the high viscosity of EC. From Figures 5.3 and 5.6, we deduce that viscosity is the dominate factor in our electrolyte.

[Figure 5.6]

5.3.2. EC content effect on conductivity and viscosity

At fixed temperature and salt concentration, the solvent viscosity and dielectric constant change with solvent composition[48], which affects the conductivity of the electrolyte through its dependence on viscosity and dielectric constant; however, the temperature and salt concentration influence the degree of the effect. For example, at 0.2 M LiBOB and 0 ^{o}C (Figure 5.7), the conductivity decreases as EC content increases. The conductivity decrease is due to the dominant role of viscosity over dielectric constant at low temperature. In comparison at 60 ^{o}C, initially the conductivity slightly increases with EC content and reaches a maximum at 1:1:0.1 (GBL: EA: EC); at higher EC content it decreases. The initial increase of conductivity with EC content occurs because the number of free ions increases upon addition of the high-dielectric constant EC (ε ~ 89.6). At the same time, however, the solution viscosity increases because of the high viscosity of EC (Figure 5.8). At the combination condition of low-EC content, low-salt concentration, and high temperature, the

effect of free ions dominates over the viscosity effect. However, as the EC content increases the viscosity effect dominates.

[Figures 5.7 and 5.8]

Similarly, salt concentration also affects the dependence of conductivity on solvent composition. For example, at 60 ^{o}C and 0.2 M LiBOB (Figure 5.7), conductivity increases with EC content up to a GBL:EA:EC composition of 1:1:0.1 but decreases at higher EC content. For 1.2 M LiBOB at 60 ^{o}C (Figure 5.7), the conductivity increases with increasing EC content up to a solvent composition of 1:1:0.1 but decreases more slowly at higher EC content. At low-salt concentration, the positive effect of EC is effective only for low-EC content since a low-salt concentration does not require a high-dielectric solvent to disassociate the salt. This is because the distance between ions in the electrolyte is already large, which reduces the effect of dielectric constant on ion disassociation. So, as the EC content increases, its effect on ion dissociation will not be significant; however, the viscosity increases with EC content (Figure 5.8) and reaches a value where the viscosity effect is more important than the free-ion effect. In the case of high-salt concentration (1.2 M), the conductivity initially increases with EC content until it reaches the point where conductivity decreases because the viscosity effect becomes dominant over the number density of free ions; however, as the EC content continues to increase, the number-of-free-ions effect opposes the effect of viscosity so the two effects counter one another and conductivity levels off at high-salt concentration. For low temperature, the viscosity effect of EC is always more important than the effect of free ions generated by adding more EC.

5.3.3. Temperature effect on conductivity

At a given salt concentration and solvent composition, the conductivity of LiBOB-containing electrolytes increases with temperature, as shown in Figure 5.9. As the temperature increases, the viscosity and dielectric constant decrease. In the studied temperature range, the effect of viscosity outweighs the effect of dielectric constant. Although the dielectric constant increases with a decrease in temperature, at low temperature ion conductivity is predominately determined by electrolyte viscosity. As the salt concentration increases, the drop in conductivity with decreasing temperature increases since the increasing salt concentration contributes to a higher viscosity. High viscosity resulted from high-salt concentration and low temperature causes more rapid decrease in conductivity compared to the low-salt concentration electrolytes as seen in Figures 5.9. Solvent composition also has an influence on the temperature dependence of ion conductivity. From Figure 5.9, we see that the rate of change of conductivity with temperature increases as the EC content increases.

[Figure 5.9]

5.4. Summary

The trends observed in conductivity of LiBOB in GBL:EA:EC solvent mixtures with changing salt concentration, solvent composition, and temperature can be interpreted in terms of the variation in dielectric constant and viscosity with these same variables. Since these factors and their effect on ion conductivity are not unique to the LiBOB/GBL+EA+EC

system, these trends provide general guidance how ion conductivities of other electrolyte systems with similar solvent compositions would change with these same variables, and they should constitute a useful database for the understanding of more complex systems, such as quaternary mixtures.

The electrolyte conductivity depends on the solvent composition (GBL:EA:EC ratio), LiBOB concentration, and temperature. For example, the best electrolyte for high-temperature application is that which contains 1 M LiBOB in GBL+EA+EC of composition 1:1:0.1. For low-temperature applications, the best electrolyte is that which contains 0.7 M LiBOB in GBL+EA+EC of composition 1:1:0. In terms of conductivity, the co-solvent EC is not recommended at low temperature because its high viscosity and melting point affects the ion mobility and decreases conductivity.

Acknowledgments

The authors gratefully acknowledge funding from Kuwait University, the BATT program, U.S. Department of Energy, and the DOE Office of FreedomCar. The authors express their gratitude toward Professor Saad Khan (NCSU) for use of his lab's rheometer and Dr. Yangxing Li for help in measuring viscosity.

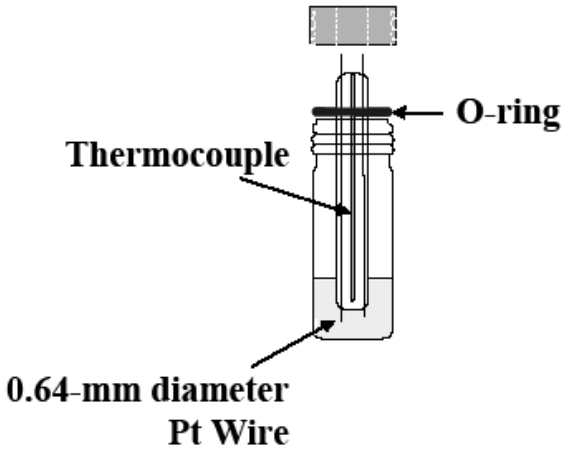

Figure 5.1. Conductivity cell

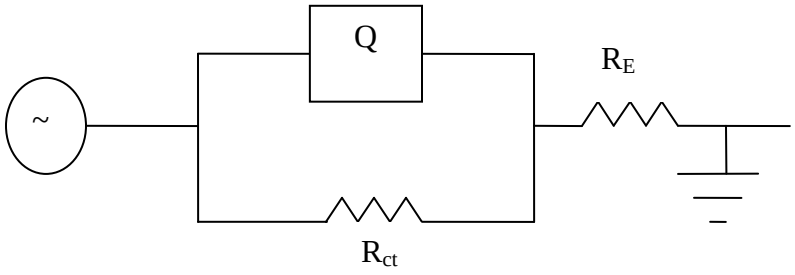

Figure 5.2. Equivalent circuit used for electrolyte resistance calculation, where R_E is bulk electrolyte resistance, R_{ct} is charge transfer resistance, and Q is a constant phase element.

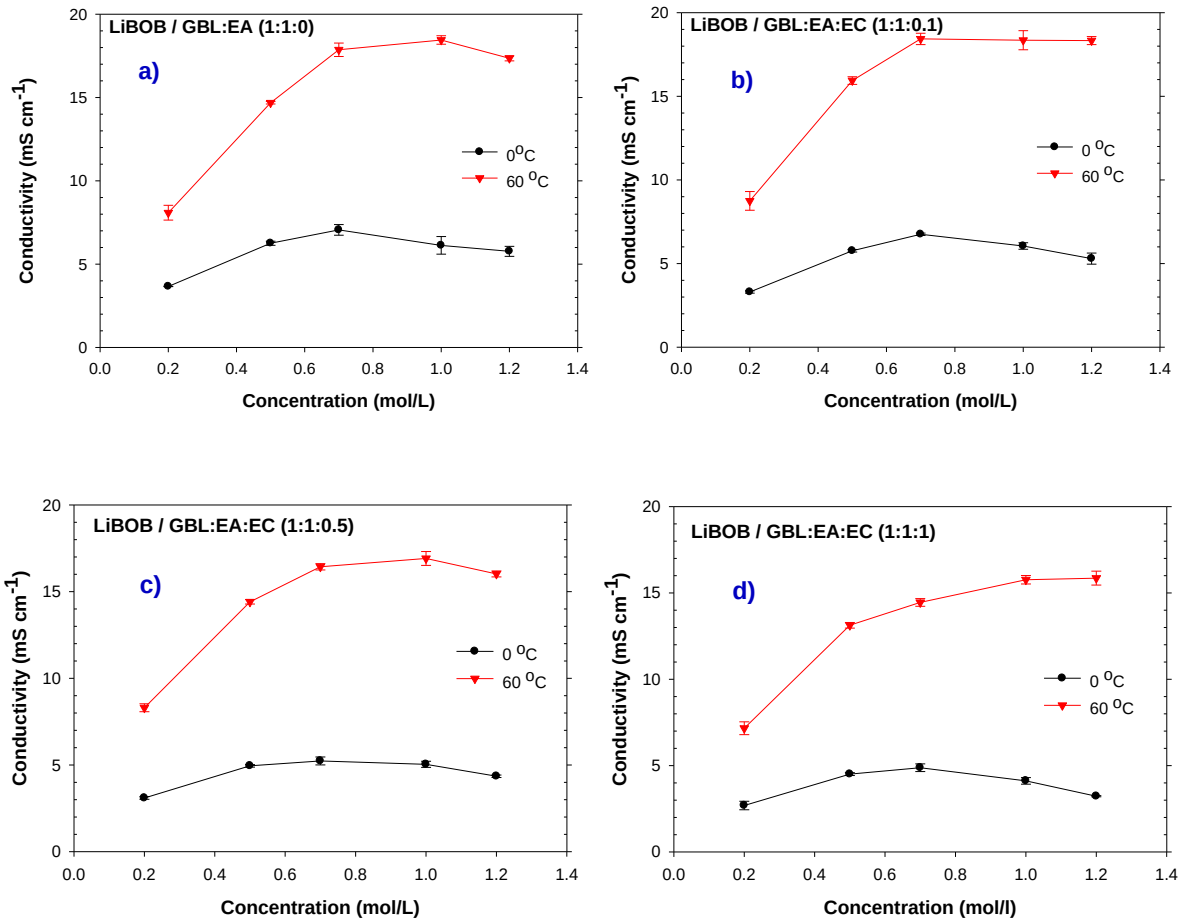

Figure 5.3. Concentration dependence of conductivity for electrolytes containing LiBOB in GBL:EA:EC of a) 1:1:0, b) 1:1:0.1, c) 1:1:0.5, and d) 1:1:1 (wt) composition at 0 and 60 °C.

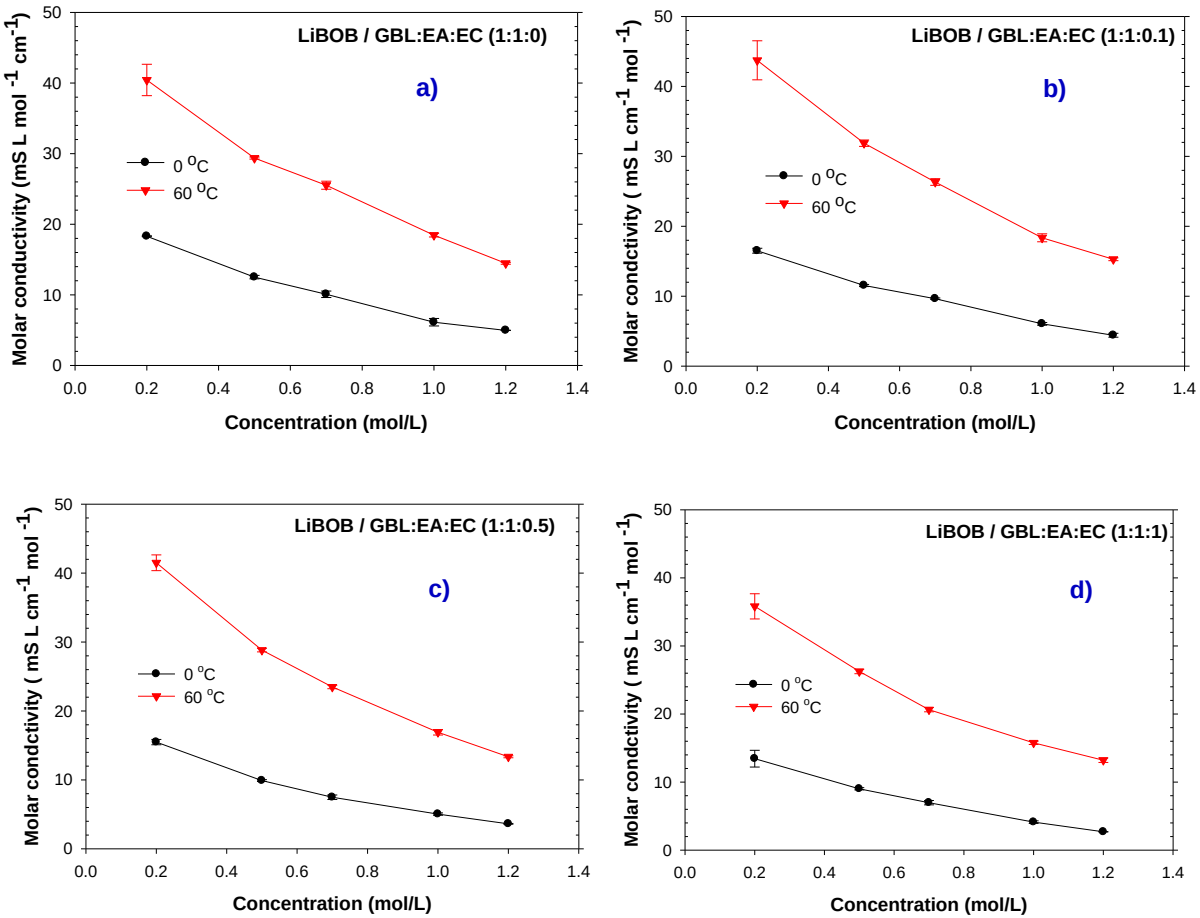

Figure 5.4. Concentration dependence of molar conductivity for electrolytes containing LiBOB in GBL:EA:EC of a) 1:1:0, b) 1:1:0.1, c) 1:1:0.5, and d) 1:1:1 (wt) compositions at 0 and 60 °C.

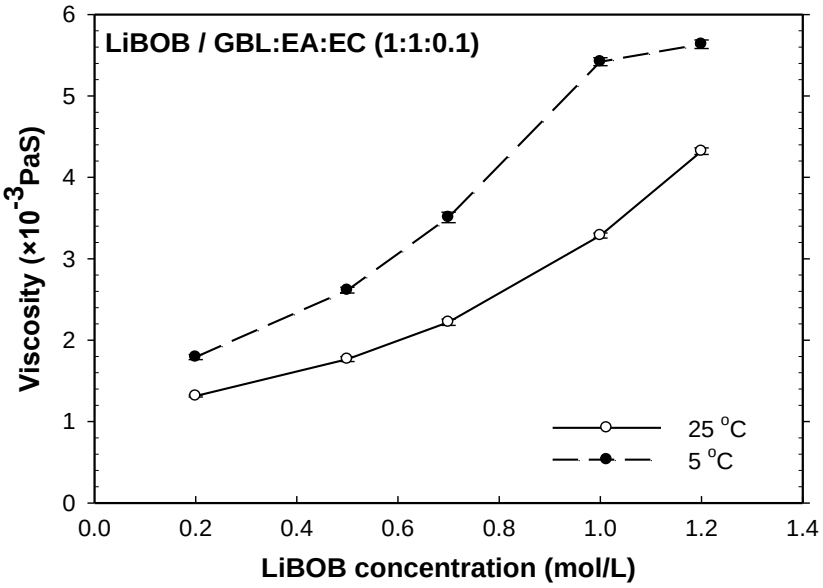

Figure 5.5. Concentration dependence of viscosity for electrolytes containing LiBOB in GBL:EA:EC composition of 1:1:0.1 (wt) at 5 and 25°C.

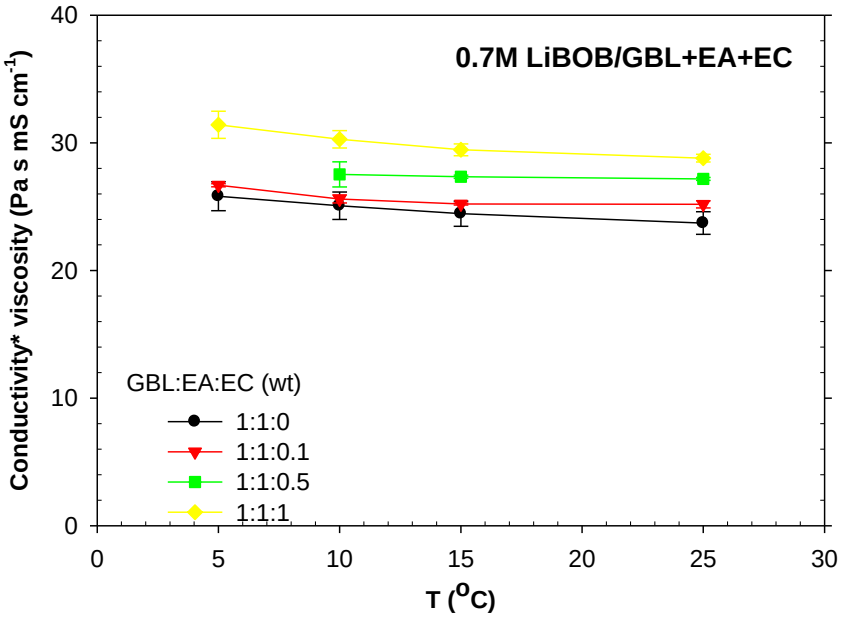

Figure 5.6. Product of viscosity and conductivity for 0.7 M LiBOB dissolved in GBL:EA:EC as a function of temperature for various solvent compositions.

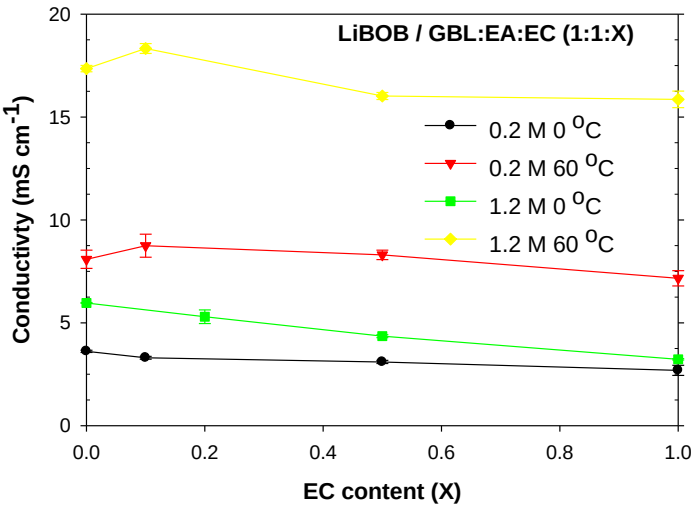

Figure 5.7. Dependence of conductivity on EC content for 0.2 and 1.2 M LiBOB dissolved in GBL:EA:EC at 0 and 60 ^{o}C.

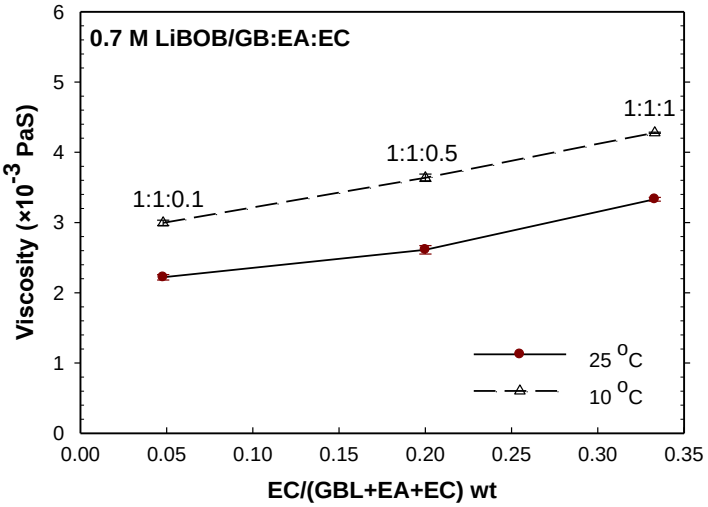

Figure 5.8. Dependence of viscosity on EC content in 0.7 M LiBOB in GBL:EA:EC at 10 and 25 °C.

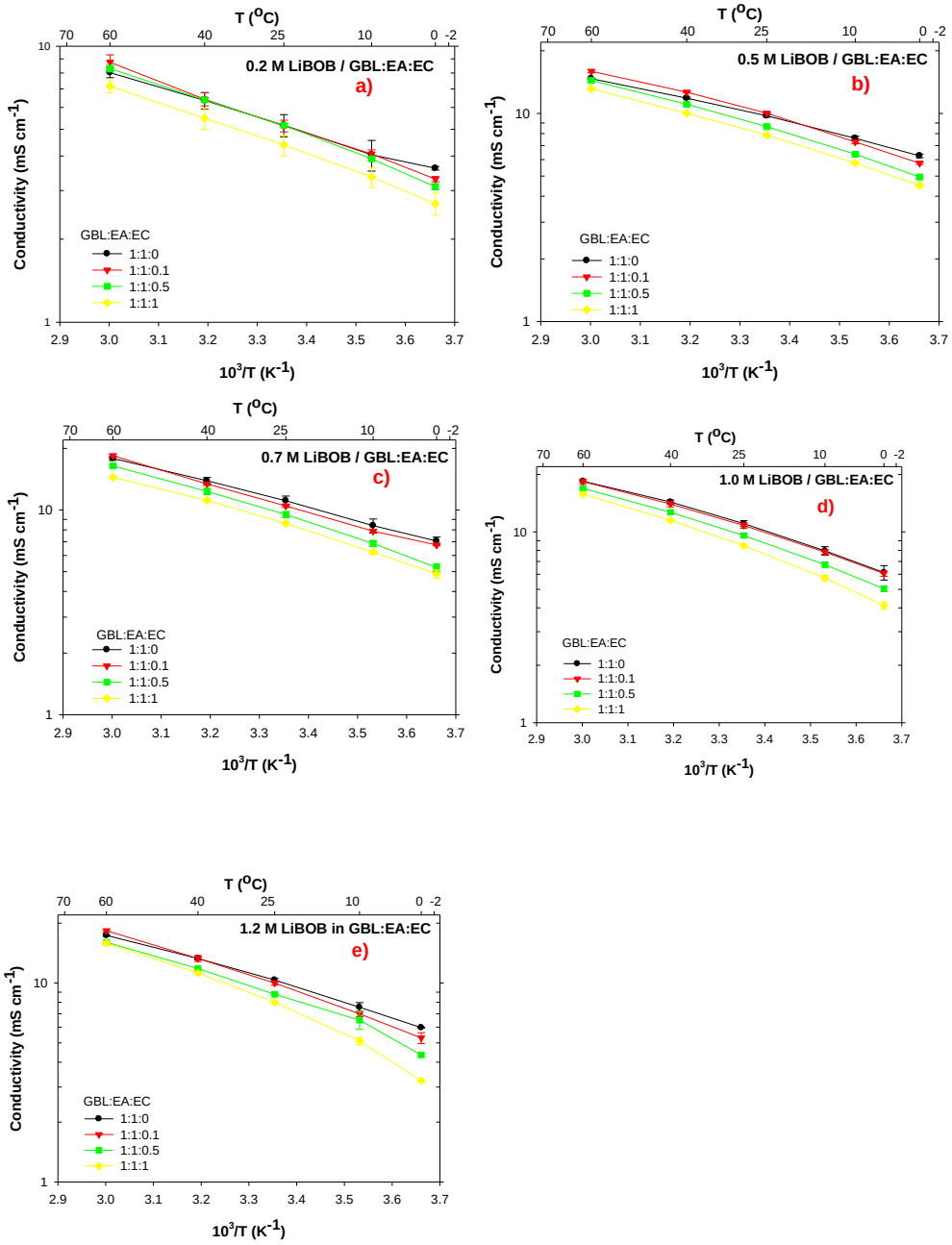

Figure 5.9. Temperature dependence of conductivity for a) 0.2, b) 0.5, c) 0.7, d) 1.0, and e) 1.2 M LiBOB in a GBL:EA:EC solvent mixture of varying EC content.

5.5. References

1. J. M. Tarascon and M. Armand, Nature (London), 414, 395 (2001).

2. S. E. Sloop, J. K. Pugh, S. Wang, J. B. Kerr and K. Kinoshita, Electrochem Solid-State Lett 4, A42 (2001).

3. E. Zinigrad, L. Larush-Asraf, J. S.Gnanaraj, M. Sprecher and D. Aurbach, Thermochim Acta 438, 184 (2005).

4. A. M. Andersson and K. Edstrom, J Electrochem Soc., 148, A1100 (2001).

5. D. Aurbach, K. Gamolsky, B. Markovsky, G. Salitra and Y. Gofer, J Electrochem Soc., 147, 1322 (2000).

6. A. D. Pasquier, A. Blyr, P. Courjal, G. Armatucci, B. Gerand and J. M. Tarascon, J Electrochem Soc, 146, 428 (1999).

7. K. Amine, J. Liu, S. Kang, I. Belharouak, Y. Hyung, D. Vissers, and G. Henriksen, J. Power Sources, 129, 14 (2004).

8. R. Jasinski, and S. Carroll, J. Electrochem. Soc. 117, (1970), 218.

9. K. M. Abraham, J. L. Goldman, and D. L. Natwig, J. Electrochem. Soc. 129, (1982), 2404.

10. C. Nanjundiah, J. L. Goldman, L. A. Dominey, and V. R. Koch, J. Electrochem. Soc. 135, (1988), 2914.

11. V. R. Koch, J. Electrochem. Soc. 126, (1979), 181.

12. A. Webber, J. Electrochem. Soc. 138, (1991), 2586.

13. S. S. Zhang, K. Xu, and T. R. Jow, J. Electrochem. Soc. 149, (2002), A586.

14. N. Takami, T. Ohsaki, H. Hasebe, and M. Yamamoto, J. Electrochem. Soc. 149, (2002), A9.

15. S. S. Zhang, K. Xu, and T. R. Jow, Electrochem. Commun. 4, (2002), 928.

16. S. S. Zhang, K. Xu, and T. R. Jow, J. Solid State Electrochem. 7, (2003), 147.

17. F. Croce, A. D'Aprano, C. Nanjundiah, V. R. Koch, C. Walker, and M. Salomon, J. Electrochem. Soc. 143,(1996), 154.

18. M. Ue, J. Electrochem. Soc 141, (1994), 3336.

19. L. J. Krause, W. Lamanna, J. Summerfield, M. Engle, G. Korba, R. Loch, and R. Atanasoski, J. Power Sources 68, 1997, 320.

20. U. Lischka, U. Wietelmann, and M. Wegner, German Pat. DE 19829030 C1 (1999) doi:10.1149/1.1701584.

21. W. Xu and C. A. Angell, Electrochem. Solid-State Lett., 4, E1 (2001).

22. Zhang SS, J Power Sources 162: 1379 (2006).

23. Xu K, Zhang SS, Lee U, Allen JL and Jow TR, J Power Sources 146: 79 (2005).

24. Xu W and Angell CA, Solid State Ionics 147: 295 (2002).

25. Yu BT, Qiu WH, Li FS and Xu GX, Electrochem Solid-State Lett 9: A1 (2006).

26. K. Xu, S. Zhang, B. A. Poese, and T. R. Jow, Electrochem. Solid-State Lett., 5, A259 (2002)

27. J. S. Gnanaraj, M. D. Levi, Y. Gofer, D. Aurbach and M. Schmidt, J Electrochem Soc 150, (2003), A445.

28. K. Xu Chem. Rev., 104 (10), (2004), 4303.

29. K. Xu, J. Electrochem Soc, 155, (2008), A733.

30. M. Salomon, and E. Plichta, J. Electrochim. Acta 30,(1985), 113.

31. A. Chagnes. B. Carre, P. Willmann, and D. Lemordant, J. Power Sources 109,(2002), 203.

32. T. Fukushima, Y. Matsuda, H. Hashimoto, and R. Arakawa, J. Power Sources 110, (2002), 34.

33. A. Chagnes, B. Carre, P. Willmann, R. Dedryvere, D. Gonbeau, and D. Lemordant, J. Electrochem. Soc. 150, (2003), A1255.

34. T.R. Jow, K. Xu, M.S. Ding, S.S. Zhang, J.L. Allen, and K. Amine, J. Electrochem. Soc 151, (2004), A1702.

35. K. Sawai, snd T. Ohzuku, J. Electrochem. Soc. 150, (2003), A674.

36. M. C. Smart, B. V. Ratnakumar, and S. Surampudi, J. Electrochem. Soc. 149, (2002), A361.

37. S. Herreyre, O. Huchet, S. Barusseau, F. Perton, J. M. Bodet, and Ph. Biensan, J. Power Sources 97/98, (2001), 576.

38. J. Vetter, and P. Novak, J. Power Sources 119/121, (2003), 338.

39. M. Riley, P. S. Fedkiw, and S. A. Khan, J. Electrochem. Soc. 149, (2002), A667.

40. A. Cisak and L. Werblan, High-Energy Non-aqueous Batteries, Chap. 7, Ellis Horwood, New York (1993).

41. H. P. Chen, J. W. Fergus, and B. Z. Jang, J. Electrochem. Soc. 147, (2000), 399.

42. Y. Choquette, G. Brisard, M. Parent, D. Brouillette, G. Perron, J. E. Desnoyers, M. Armand, D. Gravel, and N. Slougui, J. Electrochem. Soc. 145, (1998), 3500.

43. J. Barthel, R. Buestrich, E. Carl, and H. J. Gores, J. Electrochem. Soc. 143, (1996), 3565.

44. J. Barthel, H. J. Gores, and G. Schmeer, and B. Bunsenges. Phys. Chem. 83, (1979), 911.

45. B. E. Conway, Electrochemical Super capacitors-Scientific Fundamentals and Technological Applications, chap. 13, Kluwer Academic/Plenum Publishers, New York (1999).

46. I. Geoffroy, P. Willmann, K. Mesfae, B. Carré, and D. Lemordant, Electrochimica Acta 45,(2000), 2019.

47. F Bockris, J. O'M.; Reddy, A. K. N. Modern Electrochemistry, 2nd ed.; Plenum Press: New York, 2000; Vol. 2.

48. F. Azeez, Master Thesis, “ Transport properties of lithium bis(oxalate)borate-based electrolyte for lithium-ion cells” , North Carolina State University

CHAPTER 6: RHEOLOGICAL PROPERTIES OF LIBOB-BASED GEL ELECTROLYTE FOR LITHIUM-ION BATTERIES

Fadhel Azeez, Saad Khan*, and Peter S. Fedkiw

Department of Chemical & Biomolecular Engineering, North Carolina State University, Raleigh, NC 27695-7905, USA

In preparation for submission to

Langmir

***** Corresponding author. Tel.: +1-919-515-4519; Fax: +1-919-515-3456
E-mail address: khan@eos.ncsu.edu

Abstract

In this work, rheological properties of gel electrolytes consisting of lithium bis(oxalato)borate (LiBOB) dissolved in a solvent mixture of γ-butyrolactone (GBL) and ethyl acetate (EA), with and without ethylene carbonate (EC), with two types (hydrophobic and hydrophilic) of fumed silica are studied. The effects of salt concentration, EC content, fumed silica surface chemistry, and fumed silica content on the rheology of the mixture are reported. A three-dimensional network structure is formed upon adding fumed silica to the liquid base electrolyte. The elastic modulus of the hydrophobic R805-contaning electrolyte is independent of salt concentration and solvent composition. However, the elastic modulus the of hydrophilic A200-containg electrolytes is affected by salt concentration and solvent composition. FTIR-ATR was used to understand the effect of salt concentration on the elastic modulus of A200-containg electrolyte. The intensity of stretching vibration of BOB^- carbonyl groups decreases upon adding A200 fumed silica to 0.2 M LiBOB dissolved in acetonitrile (AN) but is unaffected by R805 fumed silica. The silanol groups on A200 interact with carbonyl groups of BOB^- anion, which cause the reduction in the vibration intensity of the carbonyl groups. The increase of salt concentration leads to have more BOB^- anion which increases the probability of interaction between BOB^- and silanol and lower the probability of the interaction between silanol and solvent molecules. The result of these interactions is the increase of gel strength.

6.1. Introduction

Li-ion batteries are used in many applications such as portable electronics, cellular phones, and laptop computers. In addition, there is interest in using Li-ion batteries in electric vehicles (EVs) and hybrid electric vehicles (HEVs) due to their high- energy and –power density compared to alternatives such as Ni-Cd and Ni-MH[1].

Currently, the state-of-art electrolyte for a Li-ion battery is composed of lithium hexafluorophosphate ($LiPF_6$) dissolved in a mixture of ethylene carbonate (EC) and linear esters such as dimethyl carbonate (DMC), diethyl carbonate (DEC), and ethyl methyl carbonate (EMC). Lithium hexafluorophosphate has been used as the salt in Li-ion batteries for more than a decade, because of its unique balance of properties such as good ionic conductivity and ability to passivate an aluminum current collector. However, $LiPF_6$ is thermally unstable and it decomposes into undesired products such as LiF and PF_5 that can trigger detrimental reactions on the electrode surfaces [2, 3]. In addition, $LiPF_6$ and PF_5 react with trace of water to form HF. [4]

$$LiPF_6 \Leftrightarrow LiF + PF_5 \quad (1)$$

$$LiPF_6 + H_2O \rightarrow POF_3 + LiF + 2HF \quad (2)$$

$$PF_5 + H_2O \rightarrow POF_3 + 2HF \quad (3)$$

The LiF deposits on the electrode surface and results in high-interfacial impedance and is an impediment for Li^+ insertion and deinsertion processes, which lead to cell capacity fade [5].

Also, HF causes dissolution and migration of the cathode's transition metals which leads to structural changes and capacity fade [6, 7].

Efforts have been devoted to develop alternative lithium salts to replace $LiPF_6$, including lithium perchlorate ($LiClO_4$), lithium arsenate ($LiAsF_6$), lithium tetrafluoroborate ($LiBF_4$), lithium triflate salt ($LiCF_3SO_3$), and lithium bis(trifluoromethane sulfone)imide ($LiN(SO_2CF_3)_2$). However, each salt has its own challenges that prevent it from being used in commercial Li-ion batteries. For example, $LiClO_4$ and $LiAsF_6$ cannot be used because of explosion risks of ClO_4^- [8] and toxicity of AsF_6^- and its degradation products[9-12], respectively. The main challenge with $LiBF_4$ is its low conductivity, although it was observed recently that electrolytes with $LiBF_4$ have good performance at low temperature[13-16]. Lithium triflate has two shortcomings. First, it has poor ion conductivity in nonaqueous solvents, which is attributed to the low-dissociation constant of $LiCF_3SO_3$ in solvents with a low-dielectric constant[12, 17] and the moderate ion mobility of $CF_3SO_3^-$ as compared to other salts anions[18]. The second problem with using $LiCF_3SO_3$ is the aluminum current-collector corrosion that occurs with it[19], which is also a problem with $LiN(SO_2CF_3)_2$[19].

Recently, LiBOB, which was independently disclosed by Lischka *et al.* in Germany and Angell *et al.* in the USA [20, 21], has attracted attention as a promising candidate for Li-ion batteries [22-26]. The LiBOB has many advantages such as high thermal stability (up to 302 ^oC), ability to passivate aluminum, and ability to form a solid electrolyte interface (SEI) on graphite even in the absence of EC [27, 28], which is a major solvent component due to its ability to form the SEI. On the other hand, EC is believed to be at least partially responsible for the low-temperature limit of Li-ion batteries [29]. Although LiBOB has many advantages,

it also has disadvantages when used with linear carbonate co-solvents that are used to lower viscosity. The problems of using LiBOB with linear carbonate solvents come from LiBOB essentially being insoluble in these solvents [30] and, consequently, practical solvents must be EC- or PC-rich. However, high-EC or -PC content in an electrolyte tends to increase its viscosity, which renders the electrolyte with poor low-temperature performance and rate capability. There is a need to find a proper solvent mixture that is tailored for LiBOB to give high conductivity and good solubility for the salt. In this work, we used mixtures of γ-butyrolactone (GBL), ethyl acetate (EA), and ethylene carbonate (EC) to dissolve LiBOB and added fumed silica to form a gel and enhance the mechanical properties of the electrolyte. The conductivity of LiBOB-based gel and liquid electrolyte using the same solvent mixture is reported elsewhere [31]. In this work we report the effect of salt concentration, solvent composition, fumed silica content, and fumed silica surface chemistry on the rheological properties of the gel electrolyte. Understanding how these variables affect rheological properties, along with knowledge how the same variables affect conductivity, provides a foundation to formulate electrolyte with strong mechanical properties and good conductivity.

Gamma-butyrolactone (GBL) is chosen as a co-solvent because it has a reasonably high-dielectric constant (~39), a relatively moderate viscosity (~1.7 cP at 25^{o}C), a similar structure to EC, and good solubility for LiBOB[32-34]. In addition, it was reported that GBL can improve the low-temperature performance of a LiBOB-based electrolyte [35-37]. Ethyl acetate is chosen because it has a low-melting point (~-84 ^{o}C), which will increase the liquid range of the electrolyte. In addition, the low viscosity (~0.5 cP at 25^{o}C) of EA will improve

conductivity. Also, it has been reported that EA enhances the low-temperature performance of Li-ion cells because of improved solution transport properties[38-41]

Fumed silica is added to improve the mechanical properties of the electrolyte by forming a 3-D network structure which enhances the safety of Li-ion batteries by eliminating leakage problems associated with liquid electrolytes. Fumed silica is a filler that can be used to modify the rheological properties of systems. The unique features of fumed silica are its branched, primary structure consisting of fused SiO particles (Figure 6.1) and the ability to tailor the surface functionalities of the fumed silica. Fumed silica is synthesized by the flame hydrolysis of silicon tetrachloride in a flame of hydrogen and oxygen [42]. Initially, spherical particles of silica (7-40 nm diameter) are formed, and these particles fuse irreversibly into aggregates. Fumed silica particles can interact with each other by hydrogen bonds between the silanol groups after fumed silica is dispersed in liquids. As a result of that interaction, a larger floc structure forms. At high silica concentrations a 3-D network of flocs extends throughout the volume of the sample and the suspension is considered to be a "physical gel" [43]. Several factors have an influence on the rheological properties of fumed silica suspensions: fumed silica concentration, solvent polarity, and fumed silica surface chemistry.

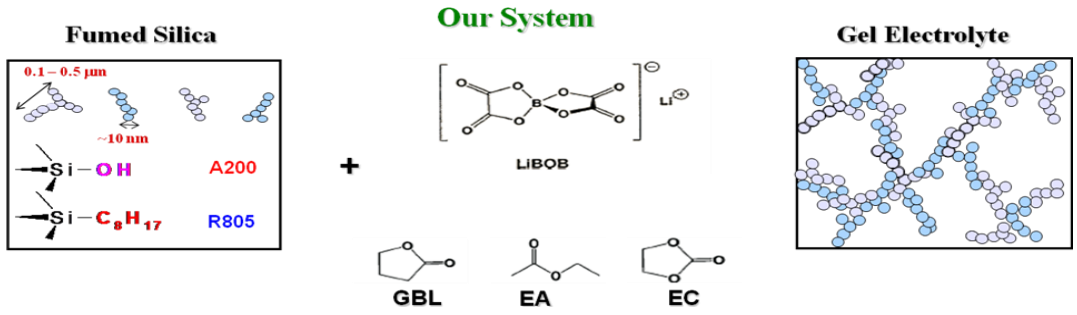

Figure. 6.1. Components of studied gel electrolytes.

6.2. Experimental

6.2.1. Materials

Ethylene carbonate, ethyl acetate, and γ-butyrolactone are obtained from Aldrich and dried over 4 Å molecular sieves (Fisher Scientific) for at least one week. Lithium bis(oxalato)borate is obtained from Chemetall and used as is. Fumed silica is donated by Evonic as Aerosil A200 (silanol, -OH groups) and Aerosil R805 (octyl, $-C_8H_{17}$ groups). Fumed silica is dried in a vacuum oven at 120 ^oC for 1 week before it is added to the solvents inside a glove box with an Ar atmosphere. The primary particle size of silica is about 12 nm. The R805 fumed silica contains octyl surface group at 48% coverage and silanol surface group at 52% coverage. The A200 fumed silica contains only native silanol on the surface. The water content of solvents is measured to be below 20 ppm using a Mitsubishi CA-06/VA-06 Karl-Fisher titrator.

Composite electrolytes are prepared in an argon-filled glove box by adding a certain weight of fumed silica (R805 and A200 varied from 10 to 20 wt%) to the baseline electrolyte and dispersed by use of a high-shear mixer (Tissue Tearor$_{TM}$, Model 398, BioSpec Products, Inc.)[44]. The gel electrolyte is taken outside the glove box and centrifuged (IEC HN-SII centrifuge, Damon/IEC Division) for twenty minutes at speed of 3000 rpm to remove air bubbles. After centrifuging, sample is returned to the glove box.

6.2.2. Rheological measurement

Rheological measurements are conducted using a AR2000 stress rheometer from TA Instrument at room temperature. Dynamic measurements are primarily used to probe the gel

microstructure with minimal disturbance of samples[45]. The relative magnitude and shapes of elastic modulus (G') and viscous modulus (G") data as a function of rotation frequency indicate the type and extent of microstructure of samples[46]. Dynamic rheology involves applying a low-amplitude sinusoidal deformation (γ) to the sample at some frequency (ω) and maximum strain amplitude γ_o

$$\gamma = \gamma_o \sin(\omega t) \tag{4}$$

The sinusoidal-stress response (τ) of the sample may be written as an in-phase and out-of-phase component as shown in:

$$\tau = G'\gamma_o \sin(\omega t) + G''\gamma_o \cos(\omega t) \tag{5}$$

The in-phase component is attributed to energy stored in the sample and thus defines the elastic modulus G'. The out-of-phase component is attributed to energy dissipated and thus defines the viscous modulus G". For a liquid-like sample G" dominates, and for a solid-like sample G' dominates. [46.]

Gel samples are allowed to sit overnight in a closed glass vial inside the glove box prior to rheological measurements to insure the full gel structure was formed. After loading the sample, it is allowed to equilibrate for five minutes. A dynamic stress sweep at a constant frequency of 1 rad s^{-1} was performed to determine the range of stresses within the linear-viscoelastic (LVE) region for each sample. A new sample is loaded and a dynamic frequency sweep (0.01 rad s^{-1} to 100 rad s^{-1}), using the pre-determined LVE stress, is performed to examine the elastic (G') and viscous (G") moduli in the LVE regime.

6.2.3. FTIR-ATR measurements

FTIR is used in order to develop a chemical understanding of the salt concentration effect on the elastic modulus of A200-containg electrolyte. Spectra are collected using a Bio-Rad-Digilab FTS-3000 Fourier transform infrared (FT-IR) spectrometer using a mounted crystalline Germanium, attenuated total internal reflection (ATR) sample attachment (Pike Technologies inc., MIRacle™ Single Reflection ATR) with a normal spectral response of 650 to 5500 cm^{-1}. The infrared light is focused onto the photodiode of a liquid nitrogen-cooled, narrow band mercury-cadmium-telluride (MCT) detector with a normal spectral response of 650 to 7000 cm^{-1}. There is nominally one reflection with a spot size of approximately 100 µm. The spectrometer and attachment where purged with dry compressed air, which reduces the possibility of atmospheric water or CO_2 contamination of the spectra and samples.

The spectra presented are an average of 64 scans. All spectra are recorded at room temperature, approximately 23° ± 0.5° C, with a resolution of 2 cm^{-1}. The data are transferred to a data processing program (OriginPro, v8.0) where numerical treatment and graphs are prepared.

6.3. Result and Discussion

6.3.1. Effect of fumed silica content on rheological properties

Figures 6.2 and 6.3 present the effect of fumed silica content and type, A200 and R805, respectively, on elastic (G') modulus for LiBOB-based electrolyte with 0.2 M LiBOB

in a solvent mixture of GBL:EA:EC at 1:1:0. The R805 fumed silica contains octyl surface group at 48% coverage and silanol surface group at 52% coverage, and the A200 fumed silica contains only native silanol on the surface. Figure 6.2, shows that adding fumed silica (A200) improved the elastic modulus and the mixture exhibits a frequency-independent elastic modulus G' with its elastic modulus larger than its viscous modulus G", indicating that a solid-like (gel) structure is formed upon adding A200. In addition, it's clear that increasing fumed silica content from 10 to 15% leads to an increase in the elastic modulus by an order of magnitude. Figure 6.3 shows that after adding fumed silica (R805) to the liquid electrolyte, a gel electrolyte is also formed. In all gel samples studied in this work, elastic modulus increases with increasing fumed silica content for A200- and R805-containing electrolyte implying an increase in strength of the solid-like structure. In general, at a low salt concentration and fumed silica content, the R805-containg electrolytes are stronger than A200-containg electrolytes as shown in Figures 6.2 and 6.3. However, this can be changed as the salt concentration and/or fumed silica content increase. The effect of salt concentration is discussed in more detail later.

6.3.2. Effect of solvent composition on rheological properties

The rheological behavior of the R805-and A200-containing electrolytes is determined by the colloidal interactions dominant in the system, which in turn are strongly affected by the fumed silica surface chemistry. In a given system, there will be competitive interactions between the surface groups and the solvent molecules. A mismatch in chemical nature (e.g., polarity) between the surface layer and surrounding liquid will lead to strong interactions between surface groups on adjacent particles [47]. Thus, for hydrophobic octyl-modified fumed

silica in GBL:EA:EC, the non polar octyl groups prefer to interact with other octyl groups rather than with the more polar solvent molecules. This favored interaction leads to the formation of three-dimensional network of particles and thus to a gel. As the weight fraction of R805 silica increases, the density of crosslinks in the gel increases, and therefore the gel elastic modulus (G') also increases. Adding A200 fumed silica to 0.2M LiBOB dissolved in GBL:EA:EC (1:1:0) leads to a formation of gel electrolyte (Figure 6.2), but increasing EC content, which increases mixture's dielectric constant, precludes flocculation of fumed silica particles (Figure 6.4) since silanol groups prefer to interact with solvent rather than each other. Consequently, a suspension of distinct entities is formed with no gel structure. The effect of solvent composition is also seen in Figure 6.5, which presents elastic modulus for 1M LiBOB dissolved in GBL:EA:EC (1:1:0 and 1:1:1) + 10% A200 and R805 as a function of frequency. It's clear that upon adding EC (33%) the elastic modulus reduced by almost one order of magnitude. On the other hand, it's clear that there is no effect of EC content on the elastic modulus of R805-containg electrolyte. The difference in the elastic modulus behavior between R805- and A200-containg electrolytes originates from the fact that EC presence is increasing the interaction between silanol groups on A200 particles and solvent molecules, which weakens the gel strength (lower G'). The EC content has no effect on elastic modulus of R805-containg electrolyte because octyl groups in R805 particles act as a shield and protect the silanol groups from interacting with solvent molecules and thus any effect of increasing EC on R805-contaning electrolyte is eliminated.

6.3.3. Effect of salt concentration on rheological properties

The results in Figure 6.6 show essentially no effect of increasing salt concentration from 0.2 to 1.0 M LiBOB on the elastic modulus of R805-containing electrolyte. However, the G' (gel strength) increases by one order of magnitude for A200-containing electrolyte upon increasing the salt concentration from 0.2 to 1 M LiBOB.

The elastic modulus (G') increasing with salt concentration for A200-containing electrolyte suggests an increase in strength of the solid-like structure. One possible reason for this effect is that the probability of interaction between hydroxyl groups on fumed silica and carbonyl groups on GBL decreases as the LiBOB concentration increases, which yields a high chance for hydroxyl groups on adjacent fumed silica to hydrogen bond leading to a stronger solid-like structure. The probability of interaction between hydroxyl groups on fumed silica and carbonyl groups of GBL decreases because GBL prefers to solvate Li^+ rather than interact with hydroxyl groups on fumed silica. Each Li^+ cation can be solvated by 3 GBL molecules [33]. Another possibility explaining why gel strength is increasing with salt concentration is that BOB^- anions hydrogen bond with silanol groups and act as a bridge between fumed silica particles. In order to study the role of BOB^- anion and solvent molecules in improving the mechanical properties, we measured the elastic modulus for 0.2 and 0.7 M LiTFSI in GBL:EA:EC (1:1:0). As shown in Figure 6.7, there is no effect of increasing LiTFSI concentration on elastic modulus (G'). Given the order of magnitude increase in G' with LiBOB concentration (Figure 6.6), we infer that BOB^- anion has an essential role in the increase of G' and its role is greater than the role of the increase in solvating Li^+ by GBL. We find support for this hypothesis through the FTIR measurement.

We measured the spectra for GBL, EA and their mixtures with LiBOB and fumed silica. However, it was not possible to distinguish between the salt and solvent bands because the carbonyl bands overlapped. Thus, we used acetonitrile (AN) for these FTIR studies.

Figure 6.8 reports FTIR-ATR spectra for gel electrolytes containing A200 and R805 dispersed in 0.2M LiBOB in AN and spectra for AN and 0.2M LiBOB in AN. Figure 6.8 shows that 0.2M LiBOB introduces two peaks with wave numbers of 1808 and 1780 cm^{-1}. These peaks represent the stretching vibration of carbonyl on BOB^-. Upon adding A200 to 0.2M LiBOB in AN, the peaks intensity dropped by more than 40 %. A decrease in the stretching vibration amplitude of the carbonyl group intensity means a decrease in its dipole moment. The decrease in intensity may occur because as A200 content changes from 0 to 10%, some of BOB^- anions may interact with silanol groups on A200 particles. In contrast to the decrease in the vibration intensity of carbonyl groups the A200-contaning electrolyte, the vibration intensity of carbonyl for R805-containg electrolyte is not affected by the salt increase because the octyl groups act as a shield protecting silanol groups in fumed silica particles from interacting with BOB^-.

As a result of these interactions between A200 and BOB^-, the probability of interactions between solvent molecules and hydroxyl group on fumed silica decreases, which gives a better chance for hydroxyl groups on fumed silica to hydrogen bond with each other. As the hydrogen bonding strengthens, the elastic modulus increases and the gel electrolyte become mechanically stronger.

Figure 6.9 shows the difference in the elastic modulus R805 and A200 for 0.2 M LiBOB dissolved in GBL:EA:EC with solvent composition of 1:1:0. It’s clear that the G' for

R805-containing electrolyte is higher. However, the difference decreases as the salt concentration and fumed silica content increase. In the case of salt concentration and low-fumed silica content, more BOB^- anion will be generated from the salt disassociation with increasing salt concentration. Thus the likelihood of silanol groups to interact with BOB^- will be greater and the strength of the gel will increase. Also, as Li^+ concentration increases, more GBL molecules will be needed to solvate the cation and hence, becomes less available to interact with the silanol. Since the increase in salt concentration will affect only A200-containg electrolyte (raise G') and there will be negligible effect on R805-containing electrolyte, eventually the difference in G' between the two will decrease, which is why at high salt concentration and low fumed silica content the difference get smaller (Figure 6.6). In addition to the decrease in the difference in G' between R805- and A200-containg electrolyte as the salt concentration increases, we see the same effect in the case of increasing fumed silica content (Figures 6.2,6.3 and 6.10). One possible explanation is that as the A200 content increases, the probability for silanol groups on A200 particles to interact with each other increases, which leads to formation of a stronger gel. This suggests that the surface chemistry of fumed silica has an effect on mechanical properties: G' for LiBOB-based electrolyte containing 10% R805 > 10% A200 for low-salt concentration and low-fumed silica content and the difference keep decreasing as the salt concentration or fumed silica content increase.

6.4. Summary

Adding fumed silica to LiBOB-based electrolyte yields a mixture that exhibits a frequency-independent elastic modulus G' with an elastic modulus larger than its viscous modulus G". These features suggest that a 3-D network structure (solid-like structure) is formed upon adding fumed silica to LiBOB-based electrolyte. The formation of this structure (gel) improves the rheological properties of the electrolyte and hence is anticipated to improve safety of Li-ion batteries. In addition, the enhancement in rheological properties does not greatly affect the conductivity of these gel electrolytes in our previous work. The rheological properties of A200-containing electrolyte were affected greatly by solvent composition and salt concentration. On other hand, there was no effect of solvent composition and salt concentration on the rheological properties of R805-containg electrolyte. FTIR shows that BOB^- anions interact with silanol groups on A200 particles which helps in the formation of the gel structure. On the other hand, BOB^- anions do interact with silanol groups on R805 particles because octyl groups act as a shield and protect hydroxyl groups from any interaction with the anions. These results encourage us to continue studying LiBOB-based electrolyte, and we believe that LiBOB-based electrolyte may enhance the safety of lithium-ion batteries.

Acknowledgment

The FTIR work was conducted at The Laser Imaging and Vibrational Spectroscopy Facility located at NC State University in the Department of Chemistry. The authors gratefully

acknowledge Evonik and Chemetall for donated material; Kuwait University for support of Fadhel Azeez; and Dr. Simon Leppi for the assistance with the FTIR work.

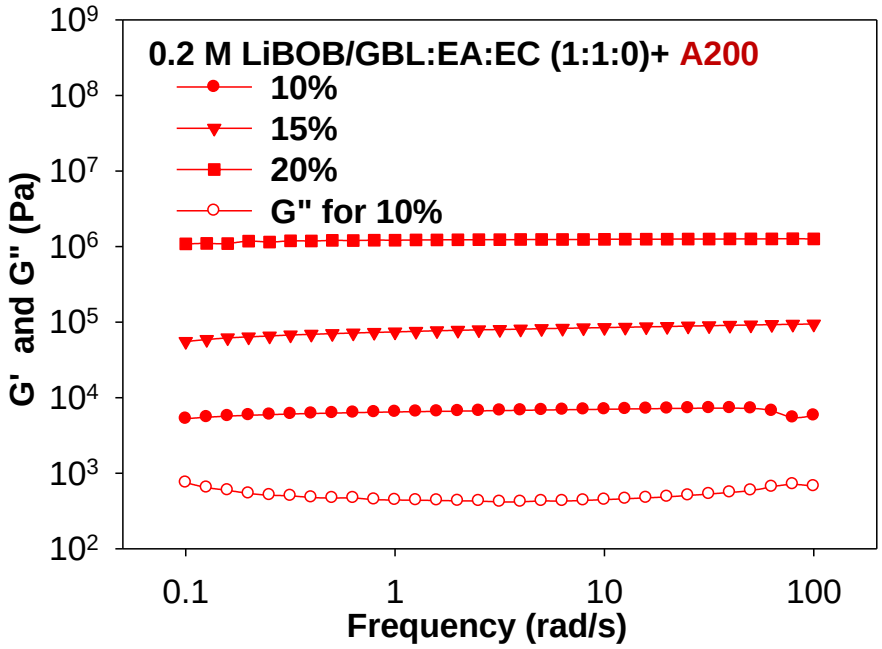

Figure 6.2. Elastic and viscous moduli for 0.2 M LiBOB in GBL:EA:EC (1:1:0) + various content of A200.

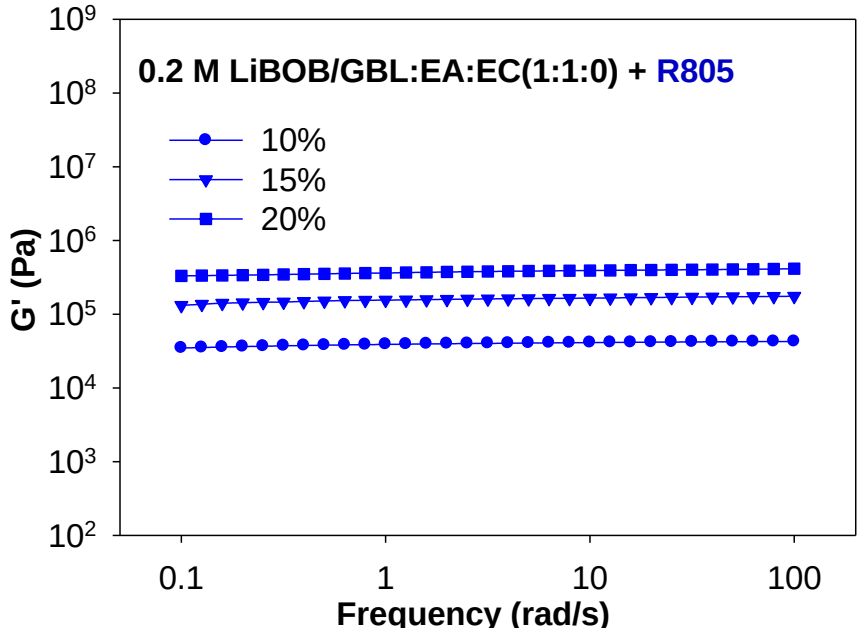

Figure 6.3. Elastic modulus for 0.2 M LiBOB in GBL:EA:EC (1:1:0) + various content of R805.

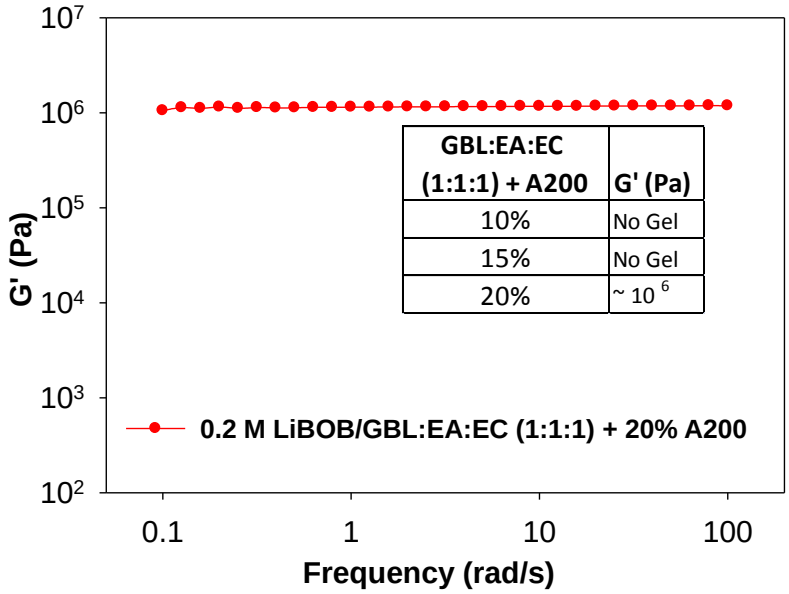

Figure 6.4. Elastic modulus for 0.2 M LiBOB in GBL:EA:EC (1:1:1) + A200.

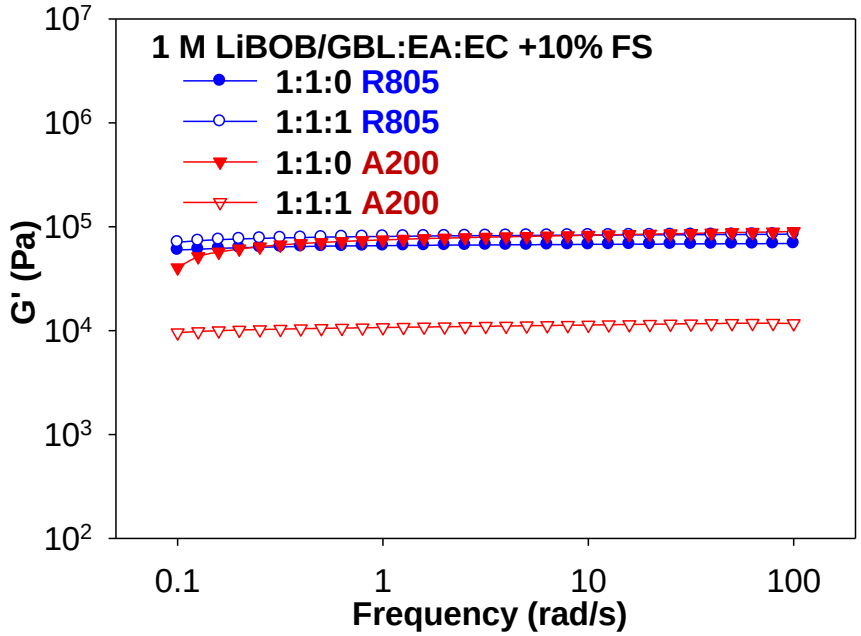

Figure 6.5. Elastic modulus for 1.0 M LiBOB dissolved in various composition of GBL:EA:EC + 10% fumed silica (FS).

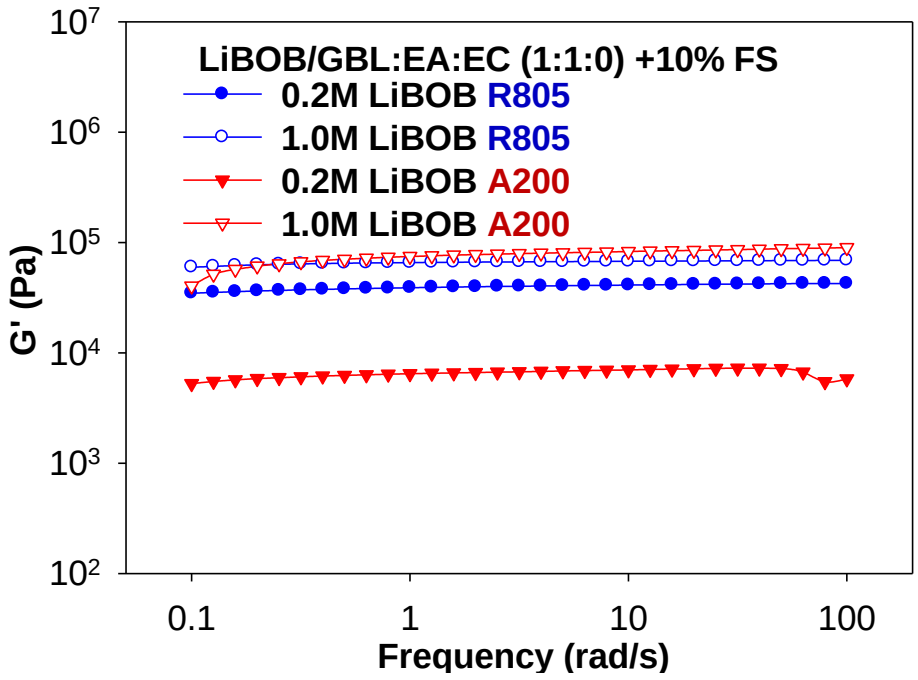

Figure 6.6. Elastic modulus for various LiBOB concentrations in GBL:EA:EC (1:1:0) + 10 % FS.

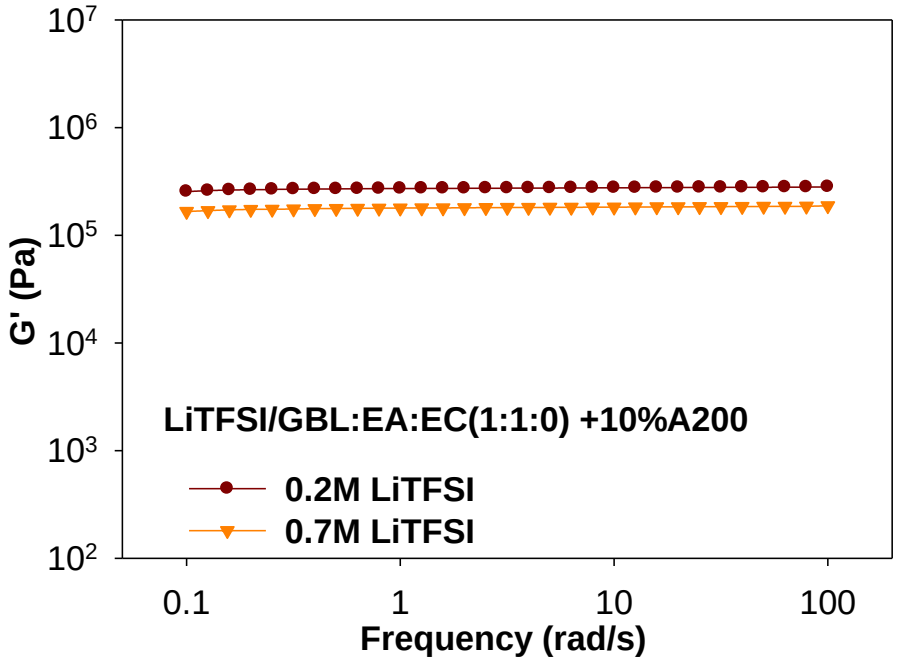

Figure 6.7. Elastic modulus for various LiTFSI concentration in GBL:EA:EC (1:1:0) + 10% + A200.

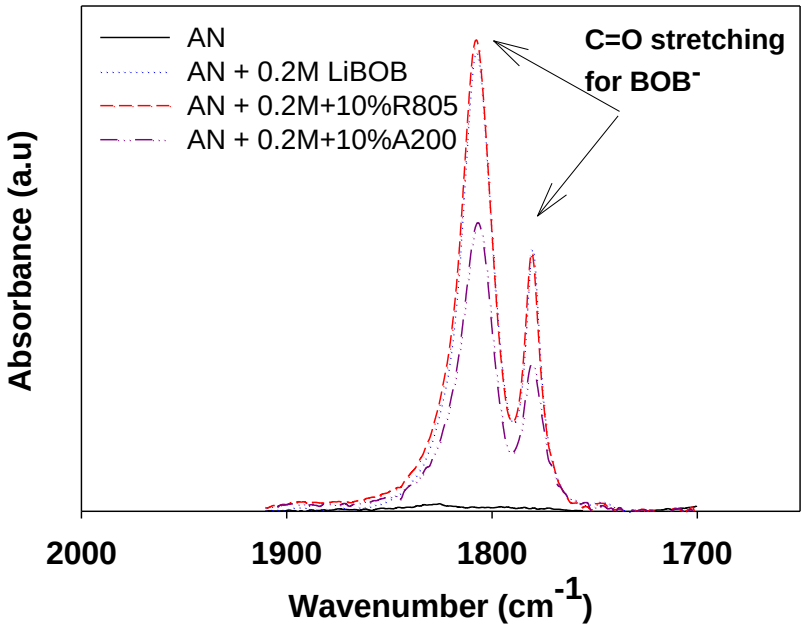

Figure 6.8. Spectra for acetonitrile (AN) with and without fumed silca and LiBOB between wavenumber of 1700-1910 cm^{-1}.

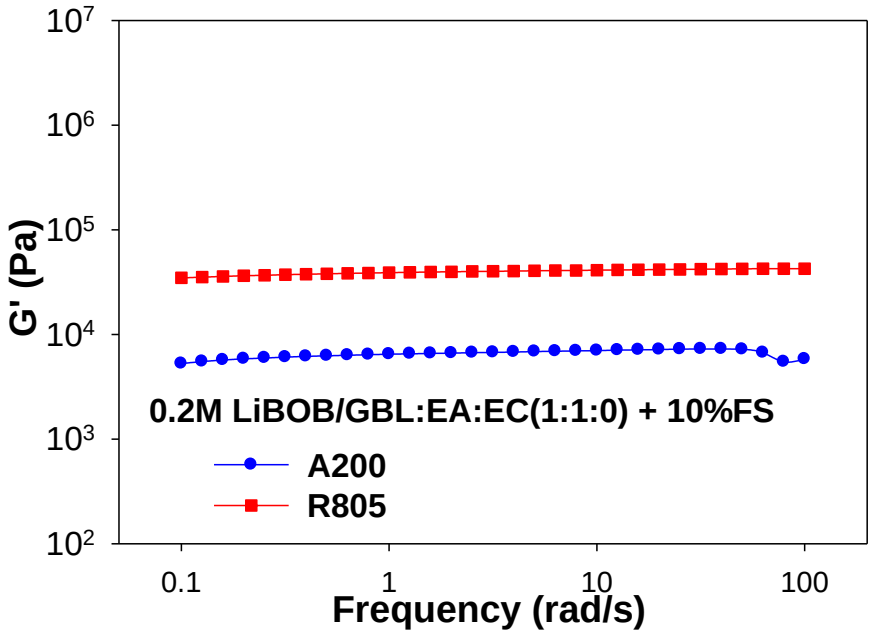

Figure 6.9. Elastic modulus for 0.2 M LiBOB in GBL:EA:EC (1:1:0) + 10 % fumed silica.

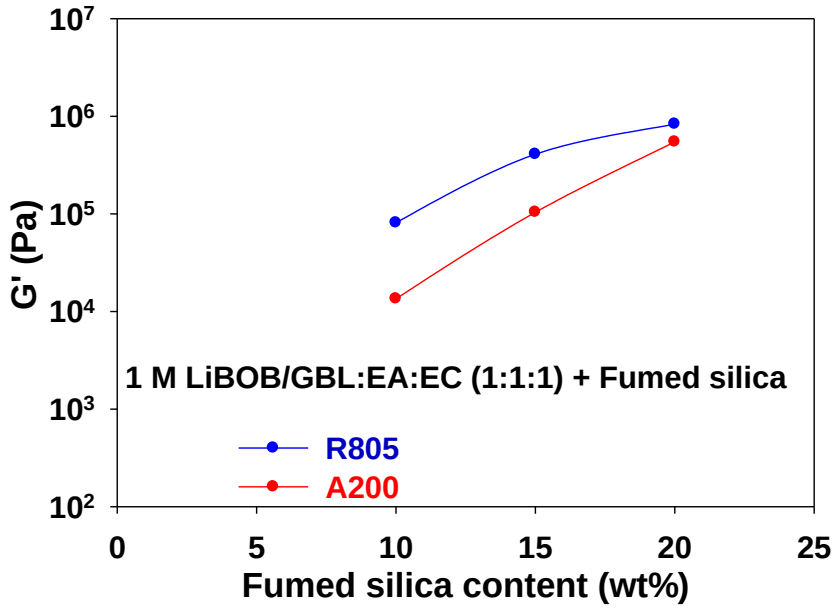

Figure 6.10. Elastic modulus for 1.0 M LiBOB in GBL:EA:EC (1:1:1) + fumed silica.

6.5. References

1. J. M. Tarascon and M. Armand, Nature (London), 414, 395 (2001).

2. S. E. Sloop, J. K. Pugh, S. Wang, J. B. Kerr and K. Kinoshita, Electrochem Solid-State Lett 4, A42 (2001).

3. E. Zinigrad, L. Larush-Asraf, J. S.Gnanaraj, M. Sprecher and D. Aurbach, Thermochim Acta 438, 184 (2005).

4. A. M. Andersson and K. Edstrom, J Electrochem Soc., 148, A1100 (2001).

5. D. Aurbach, K. Gamolsky, B. Markovsky, G. Salitra and Y. Gofer, J Electrochem Soc., 147, 1322 (2000).

6. A. D. Pasquier, A. Blyr, P. Courjal, G. Armatucci, B. Gerand and J. M. Tarascon, J Electrochem Soc, 146, 428 (1999).

7. K. Amine, J. Liu, S. Kang, I. Belharouak, Y. Hyung, D. Vissers, and G. Henriksen, J. Power Sources, 129, 14 (2004).

8. R. Jasinski, and S. Carroll, J. Electrochem. Soc. 117, (1970), 218.

9. K. M. Abraham, J. L. Goldman, and D. L. Natwig, J. Electrochem. Soc. 129, (1982), 2404.

10. C. Nanjundiah, J. L. Goldman, L. A. Dominey, and V. R. Koch, J. Electrochem. Soc. 135, (1988), 2914.

11. V. R. Koch, J. Electrochem. Soc. 126, (1979), 181.

12. A. Webber, J. Electrochem. Soc. 138, (1991), 2586.

13. S. S. Zhang, K. Xu, and T. R. Jow, J. Electrochem. Soc. 149, (2002), A586.

14. N. Takami, T. Ohsaki, H. Hasebe, and M. Yamamoto, J. Electrochem. Soc. 149, (2002), A9.

15. S. S. Zhang, K. Xu, and T. R. Jow, Electrochem. Commun. 4, (2002), 928.

16. S. S. Zhang, K. Xu, and T. R. Jow, J. Solid State Electrochem. 7, (2003), 147.

17. F. Croce, A. D'Aprano, C. Nanjundiah, V. R. Koch, C. Walker, and M. Salomon, J. Electrochem. Soc. 143,(1996), 154.

18. M. Ue, J. Electrochem. Soc 141, (1994), 3336.

19. L. J. Krause, W. Lamanna, J. Summerfield, M. Engle, G. Korba, R. Loch, and R. Atanasoski, J. Power Sources 68, 1997, 320.

20. U. Lischka, U. Wietelmann, and M. Wegner, German Pat. DE 19829030 C1 (1999) doi:10.1149/1.1701584.

21. W. Xu and C. A. Angell, Electrochem. Solid-State Lett., 4, E1 (2001).

22. Zhang SS, J Power Sources 162: 1379 (2006).

23. Xu K, Zhang SS, Lee U, Allen JL and Jow TR, J Power Sources 146: 79 (2005).

24. Xu W and Angell CA, Solid State Ionics 147: 295 (2002).

25. Yu BT, Qiu WH, Li FS and Xu GX, Electrochem Solid-State Lett 9: A1 (2006).

26. K. Xu, S. Zhang, B. A. Poese, and T. R. Jow, Electrochem. Solid-State Lett., 5, A259 (2002).

27. J. S. Gnanaraj, M. D. Levi, Y. Gofer, D. Aurbach and M. Schmidt, J Electrochem Soc 150, (2003), A445.

28. K. Xu Chem. Rev., 104 (10), (2004), 4303.

29. K. Xu, J. Electrochem Soc, 155, (2008), A733.

30. M. Salomon, and E. Plichta, J. Electrochim. Acta 30,(1985), 113.

31. F. Azeez, P.S. Fedkiw, submitted to Power source on 2009.

32. A. Chagnes. B. Carre, P. Willmann, and D. Lemordant, J. Power Sources 109,(2002), 203.

33. T. Fukushima, Y. Matsuda, H. Hashimoto, and R. Arakawa, J. Power Sources 110, (2002), 34.

34. A. Chagnes, B. Carre, P. Willmann, R. Dedryvere, D. Gonbeau, and D. Lemordant, J. Electrochem. Soc. 150, (2003), A1255.

35. T.R. Jow, K. Xu, M.S. Ding, S.S. Zhang, J.L. Allen, and K. Amine, J. Electrochem. Soc 151, (2004), A1702.

36. K. Sawai, snd T. Ohzuku, J. Electrochem. Soc. 150, (2003), A674.

37. M. C. Smart, B. V. Ratnakumar, and S. Surampudi, J. Electrochem. Soc. 149, (2002), A361.

38. S. Herreyre, O. Huchet, S. Barusseau, F. Perton, J. M. Bodet, and Ph. Biensan, J. Power Sources 97/98, (2001), 576.

39. J. Vetter, and P. Novak, J. Power Sources 119/121, (2003), 338.

40. M. Riley, P. S. Fedkiw, and S. A. Khan, J. Electrochem. Soc. 149, (2002), A667.

41. A. Cisak and L. Werblan, High-Energy Non-aqueous Batteries, Chap. 7, Ellis Horwood, New York (1993).

42. Degussa Tech. Bull., 1989

43. Kosinski and Caruthers, 1985; Khan and Zoeller, 1993

44. H. J. Walls, J. Zhou, J. A. Yerian, P. S. Fedkiw, S. A. Khan, M. K. Stowe, and G.L. Baker, J. Power Sources, 89, 156 (2000).

45. S. R. Raghavan, M. W. Riley, P. S. Fedkiw, and S. A. Khan, Chem. Mater., 10, 244 (1998).

46. C. W. Macosko, Rheology: Principles, Measurements, and Applications, VCH publishers, Inc., New York (1994).

47. S. R. Raghavan, J. Hou, G. L. Barker, and S. A. Kahn, Langmuir, 16, 1066 (2000).

CHAPTER 7: ELECTROCHEMICAL PROPERTIES OF LIBOB-BASED GEL ELECTROLYTE FOR LITHIUM-ION BATTERIES

Fadhel Azeez and Peter S. Fedkiw*

Department of Chemical & Biomolecular Engineering, North Carolina State University, Raleigh, NC 27695-7905, USA

In preparation for submission to

Journal of the Electrochemical Society

* Corresponding author. Tel.: +1-919-515-3572; Fax: +1-919-515-3456
E-mail address: fedkiw@eos.ncsu.edu

Abstract

This work reports electrochemical and rheological properties of gel electrolytes composed of lithium bis(oxalato)borate (LiBOB) dissolved in solvent mixtures of γ-butyrolactone (GBL), ethyl acetate (EA), and ethylene carbonate (EC) with two types of fumed silica. A three-dimensional gel network structure is formed upon adding fumed silica to the base-liquid electrolyte. The mechanical properties are improved by adding fumed silica to the liquid electrolytes, and the conductivity of gel electrolytes is slightly lower than that of the base-liquid electrolytes. Effects are reported of salt concentration, EC content, fumed silica surface chemistry, and fumed silica content on the conductivity and cycling behavior of cathode half-cells using the gel electrolyte. The cycling behavior of spinel $LiMn_2O_4$ cathode using LiBOB-based liquid and gel electrolytes is better than the performance obtained using state-of-art electrolyte ($LiPF_6$ in mixed carbonates). The cycling behavior of $LiFePO_4$ and $LiCoO_2$ cathodes using LiBOB-based electrolyte and state-of-art electrolyte are comparable. The average charge and discharge voltages for gel electrolyte are stable unlike the base-liquid electrolyte, which indicates a higher energy efficiency with less anticipated capacity fade. Based on the results obtained in this work, a LiBOB-based gel electrolyte appears to be a promising candidate for lithium-ion batteries

.

7.1. Introduction

Li-ion batteries are used in many applications such as portable electronics, cellular phones and laptop computers. In addition, there is interest in using Li-ion batteries in electric vehicles (EVs) and hybrid electric vehicles (HEVs) due to their high- energy and –power density compared to alternatives such as Ni-Cd and Ni-MH [1].

Currently, the state-of-art electrolyte for a Li-ion battery is composed of lithium hexafluorophosphate ($LiPF_6$) dissolved in a mixture of ethylene carbonate (EC) and linear esters such as dimethyl carbonate (DMC), diethyl carbonate (DEC), and ethyl methyl carbonate (EMC). Lithium hexafluorophosphate has been used as the salt in Li-ion batteries for more than a decade, because of its unique balance of properties such as good ionic conductivity and ability to passivate an aluminum current collector. However, $LiPF_6$ is thermally unstable and it decomposes into undesired products such as LiF and PF_5 that can trigger detrimental reactions on the electrode surfaces [2, 3]. In addition, $LiPF_6$ and PF_5 react with trace of water to form HF [4]

$$LiPF_6 \Leftrightarrow LiF + PF_5 \quad (1)$$

$$LiPF_6 + H_2O \rightarrow POF_3 + LiF + 2HF \quad (2)$$

$$PF_5 + H_2O \rightarrow POF_3 + 2HF \quad (3)$$

The LiF deposits on the electrode surface and results in high-interfacial impedance and is an impediment for Li^+ insertion and deinsertion processes, which lead to cell capacity fade [5]. Also, HF causes dissolution and migration of the cathode's transition metals which leads to structural changes and capacity fade [6, 7].

Efforts have been devoted to develop alternative lithium salts to replace $LiPF_6$, including lithium perchlorate ($LiClO_4$), lithium arsenate ($LiAsF_6$), lithium tetrafluoroborate ($LiBF_4$), lithium triflate ($LiCF_3SO_3$), and lithium bis(trifluoromethane sulfonyl)imide ($LiN(SO_2CF_3)_2$). However, each salt has its own challenges that prevent it from being used in commercial Li-ion batteries. For example, $LiClO_4$ and $LiAsF_6$ cannot be used because of explosion risks of ClO_4^- [8] and toxicity of AsF_6^- and its degradation products[9-12], respectively. The main challenge with $LiBF_4$ is its low conductivity, although it was observed recently that electrolytes with $LiBF_4$ have good performance at low temperature[13-16]. Lithium triflate has two shortcomings. First, it has poor ion conductivity in nonaqueous solvents, which is attributed to the low-dissociation constant of $LiCF_3SO_3$ in solvents with a low-dielectric constant[12, 17] and the moderate ion mobility of $CF_3SO_3^-$ as compared to other salts anions[18]. The second problem with using $LiCF_3SO_3$ is the aluminum current-collector corrosion that occurs with it[19], which is also a problem with $LiN(SO_2CF_3)_2$[19].

Recently, LiBOB, which was independently disclosed by Lischka *et al.* in Germany and Angell *et al.* in the USA [20, 21], has attracted attention as a promising candidate for Li-ion batteries [22-26]. The LiBOB has many advantages such as high thermal stability (up to 302 ^oC), ability to passivate aluminum, and ability to form a solid electrolyte interface (SEI) on graphite even in the absence of EC [27, 28], which is a major solvent component due to its ability to form the SEI. On the other hand, EC is believed to be at least partially responsible for the low-temperature limit of Li-ion batteries [29]. Although LiBOB has many advantages, it also has disadvantages when used with linear carbonate co-solvents that are used to lower viscosity. The problems of using LiBOB with linear carbonate solvents come from LiBOB

essentially being insoluble in these solvents [30] and, consequently, practical solvents must be EC- or PC-rich. However, high-EC or -PC content in an electrolyte tends to increase its viscosity, which imparts poor low-temperature performance and rate capability. There is a need to find a proper solvent mixture that is tailored for LiBOB to give high conductivity and good solubility for the salt. In this work, we used mixtures of γ-butyrolactone (GBL), ethyl acetate (EA), and ethylene carbonate (EC) to dissolve LiBOB and added fumed silica to enhance the mechanical properties of the electrolyte. Motivation for using gamma-butyrolactone (GBL) and ethyl acetate (EA) as solvent components are mentioned elsewhere [31]. Fumed silica is used as a filler in order to form a gel electrolyte, which is formed by interaction between fumed silica particles in the liquid.[32]Gel electrolytes are attractive for use in Li-ion batteries since they are anticipated to improve safety by eliminating leakage problems associated with liquid electrolytes.[33] Sony has already introduced Li-ion cells using gel electrolytes to the market.[34] Our group has been developing a type of nanocomposite gel electrolyte using fumed silica nanoparticles.[35-38]

The gelling mechanism in an electrolyte using fumed silica as a filler is different from polymer gels. One advantage of using solid filler over polymer, which depends on solvent swelling of polymer chains, (e.g., PVDF-HFP) [39], is that solid filler can inhibit crystallization at low temperature and yet still support a three-dimensional network at high temperature.[40] Silica-based composite gel electrolytes exhibit desirable mechanical elastic modulus (G') in excess of 10^5 Pa and are processable with shear thinning behavior.[36, 38]

Efforts to make a gel electrolyte comprised of $LiPF_6$ salt and fumed silica were not successful [41, 42] because $LiPF_6$ is sensitive to hydrolysis and the native silanol surface groups on silica inevitably absorb moisture.

We report here the effect of salt concentration, solvent composition, fumed silica content, and fumed silica surface chemistry on the cycling behavior of cathode half-cells using LiBOB-based liquid and gel electrolyte and state-of-art electrolyte. The conductivity of LiBOB-based gel and liquid electrolytes using the same solvent mixture used here is reported elsewhere[31]. Understanding how these variables affect the cycle performance of cathode half-cells inform the design of an improved Li-ion battery through selection of the right combination of solvent composition, salt concentration, fumed silica type and content and cathode.

7.2. Experimental

7.2.1. Materials

Ethylene carbonate, ethyl acetate, and γ-butyrolactone are obtained from Aldrich and dried over 4 Å molecular sieves (Fisher Scientific) for at least one week. Lithium bis(oxalato)borate is obtained from Chemetall and used as is. Fumed silica is obtained from Evonik as Aerosil A200 (silanol, -OH groups) and Aerosil R805 (octyl,-C_8H_{17} groups). Fumed silica is dried in a vacuum oven at 120 ^oC for 1 week before it is added to the solvents inside a glove box with an Ar atmosphere. The primary particle size of silica is about 12 nm. The R805 fumed silica contains octyl surface group at 48% coverage and silanol surface group at 52% coverage, and the A200 fumed silica contains only native silanol on the

surface. The water content of solvents is measured to be below 20 ppm using a Mitsubishi CA-06/VA-06 Karl-Fisher titrator.

Composite electrolytes are prepared in an argon-filled glove box by adding a certain weight of fumed silica (R805 and A200 varied from 10 to 20 wt %) to the baseline electrolyte and dispersed by use of a high-shear mixer (Tissue Tearor^{TM}, Model 398, BioSpec Products, Inc.)[43]. The gel electrolyte is taken outside the glove box in a sealed vial and centrifuged (IEC HN-SII centrifuge, Damon/IEC Division) for twenty minutes at speed of 3000 rpm to remove gas bubbles. After centrifuging, the sample is returned to the glove box.

7.2.2. Rheological measurement

Rheological measurements are conducted using a AR2000 stress rheometer (TA instrument) at room temperature. Dynamic measurements are primarily used to probe the gel microstructure with minimal disturbance of samples[44]. The relative magnitude and shape of elastic (G') and viscous (G'') moduli as a function of rotation frequency indicate the type and extent of microstructure of samples[45]. After loading the sample, it is allowed to equilibrate for five minutes. A dynamic stress sweep at a constant frequency of 1 rad s^{-1} is performed to determine the range of stresses within the linear-viscoelastic (LVE) region for each sample. A new sample is loaded and a dynamic frequency sweep (0.01 to 100 rad s^{-1}), using the pre-determined LVE stress, is performed to examine the elastic (G') and viscous (G'') moduli in the LVE regime.

7.2.3. Conductivity measurements

Conductivity is measured using EG&G Princeton Applied Research PowerSine software to control an EG&G Model 273 potentiostat and EG&G Model 5210 lock-in

amplifier in the frequency range 100 kHz to 100 mHz. The cell constants are found using a KCl standard solution (1409 μS cm^{-1} at 25°C) (Fisher Scientific) prior to and after each measurement.

The conductivity cell consists of a glass cell containing two blocking platinum wire electrodes (0.64-mm diameter, Fisher Scientific), a thermocouple opening, an O-ring seal, and glass vial. The conductivity cell has a diameter of ~1.5 cm and height of 5 cm. The design of the cell is described by Riley [46]. Details about the conductivity measurement are published elsewhere [31]

7.2.4. Cathode half-cell preparation and cell cycling

Three types of cathode materials are used in this work: $LiCoO_2$, $LiMn_2O_4$, and $LiFePO_4$. The $LiCoO_2$ is obtained from OMG and LICO Technology Corp (Japan); the $LiMn_2O_4$ is obtained from Merck (Germany) and LICO Technology Corp (Japan); the $LiFePO_4$ is obtained from Hydro Quebec (Canada), poly (vinylidene fluoride) (PVDF, KYNAR^{TM}) is obtained from Elf Atochem; synthetic flake graphite (SFG 6) is obtained from Timcal American; carbon black (Ketjenblack (KJB) EC-600JD) is obtained from Akzo Nobel Inc; and the solvent 1-methyl-2-pyrrolidinone (NMP) is obtained from Aldrich. Two types of carbon additives are used in this study: KJB graphite, which consists of round particles and the SFG type, which is in the form of flat flakes. All these components are used as received.

The typical composition for $LiCoO_2$ cathode is 90-5-3-2 (wt % active material-PVDF-KS6-KJB EC-600JD). For $LiFePO_4$ and $LiMnO_4$, the typical cathode composition is 80-10-5-5 (active material-PVDF-KS6-KJB EC-600JD). Aluminum foil (0.024-mm thick,

Fisher Scientific) is used as the current collector for $LiCoO_2$, $LiMn_2O_4$, and $LiFePO_4$ cathodes.

A fixed amount of metal oxide and carbon additives are thoroughly hand ground and mixed, typically thirty minutes using a mortar and pestle. The mixture of metal oxide and carbons is dispersed into a 11-ml glass vial containing PVDF in NMP. The vial then is placed in a rotator for 48-72 hr to mix the slurry thoroughly. The resulting slurry is coated onto the current collector using a "MICROM II" film applicator (Paul N. Gardner Co., Inc.). The film is dried at 80 °C overnight and cut into 1.27-cm diameter disks that are hot-compacted by a hydraulic press at 150 °C and 700 MPa. After compaction, cathode disks are dried at 150 °C under vacuum for 24 hr.

Coin cells in which an electrolyte/separator is sandwiched between lithium metal and a metal-oxide composite cathode are used in the cycling measurements (Figure 7.1 [47]). In these cells, a Celgard 2400 separator (Hoechst Celanese) (25-µm thick) is wetted by the electrolyte. A stainless steel spacer and spring are used to maintain good contact of electrolyte, electrode, and current collector.

An Arbin battery cycler (Model BT2042 and BT2043) controlled by Arbin ABTS software is employed to carry out constant-current cell cycling in $LiMO_X$/electrolyte/Li cells, where $LiMO_X$ is $LiCoO_2$, $LiMn_2O_4$, or $LiFePO_4$. A C-rate of C/10 was used in all measurements. Cell cycling is terminated upon reaching a typical cycle number of 20-50. The cutoff voltages for each cathode are 2.5-4.2 V for $LiFePO_4$ and $LiCoO_2$ and 3-4.2 V for $LiMn_2O_4$.

7.3. Result and Discussion

7.3.1. Fumed silica effects on conductivity and rheology

Two types of fumed silica (hydrophilic A200 and hydrophobic R805) are used to study the effects of fumed silica surface chemistry on conductivity and rheology. Each type is expected to form a three-dimensional network by hydrogen bonding (A200) or steric interactions (R805)[38]. Figure 7.2 shows conductivity for 0.7 M LiBOB in GBL:EA:EC with solvent composition of 1:1:0, with and without R805 or A200. Ionic conductivity for the liquid electrolyte is slightly higher than that for the gel electrolytes. The conductivities of LiBOB-based electrolytes at room temperature are all ~ 10^{-3} S/cm. As the figure shows, addition of either hydrophilic or hydrophobic fumed silica nanoparticles to the liquid electrolyte causes a slight decrease in conductivity (about 10%), which is the same trend seen when using PEO as the solvent with lithium salts such as $LiN(CF_3SO_3)_2$) and LiTFSI[35-37].

As expected, conductivity monotonically increases with temperature for both the gel and liquid electrolytes because both viscosity and ion association decrease with a consequential increase in ion mobility and number of free ions, respectively. The relatively small difference in conductivity between liquid and gel electrolytes stems from the fact that upon adding fumed silica to the liquid electrolyte a 3-D network structure is formed that allows Li^+ ion to move relatively free, thus causing low impedance for ion transport.

The evidence for the formation of a 3-D network structure is presented in Figure 7.3, which shows the elastic and viscous moduli for 1M LiBOB in GBL:EA:EC(1:1:1) + various content of R805. It is clear that elastic modulus dominates the viscous modulus over the

frequency range examined and is independent of frequency. The dominant elastic response indicates that the composites are a colloidal gel in which the silica nanoparticles are self-assembled into a volume-filling 3-D network structure. Figure 7.4 shows the elastic modulus of R805 and A200 in an electrolyte containing 0.7 M LiBOB in GBL:EA:EC with solvent composition of 1:1:0. In general at low fumed-silica content, R805-containing gel electrolytes are stronger than A200-containg electrolyte because of the mismatch of solubility factor between silica surface group and solvents[38], which is the same trend observed in poly(ethylene glycol) solvent[36,38]. However, this trend can change (G' for A200-containg electrolyte > G' for R805-containg electrolyte) with solvent composition, salt concentration, and fumed silica content as shown in our previous publication [48]. This suggests that the surface chemistry of fumed silica has an effect on mechanical properties: G' for LiBOB-based electrolyte containing 10% R805 > 10% A200.

The effect of R805 fumed silica content on conductivity is shown in Figure 7.5 for an electrolyte of 0.7 M LiBOB in GBL:EA:EC with composition of 1:1:1. As expected, conductivity decreases with the increase of fumed silica content; because of the volume effect of the insulating fumed silica, however, the decrease in the conductivity is small in comparison to the large increase in the mechanical properties for the gel electrolyte, as shown in Figure 7.3. From Figures 7.2-7.5, we conclude that the gel electrolytes show a relatively high conductivity and adding fumed silica to liquid electrolytes increases the elastic modulus without sacrificing conductivity. Safety of lithium-ion batteries is anticipated be enhanced as a result of improving the mechanical properties of lithium-ion electrolytes.

These features warrant further study of LiBOB-based gel electrolyte as a potential replacement for the state-of–art electrolyte.

7.3.2. Salt concentration effect on conductivity

Figure 7.6 shows the conductivity for LiBOB in GBL:EA:EC with composition of 1:1:0, 1:1:0.1, and 1:1:1 + 10% R805 as a function of salt concentration at 0 and 60^{o}C. The conductivity increases with salt concentration at low-salt concentrations because the number of free ions increases with salt concentration. After achieving a maximum conductivity, an increase in salt concentration results in higher ion aggregation and higher viscosity of the solution, which reduces the free-ion number and the ionic mobility, respectively. It is a universal phenomenon for electrolytes to have a maximum in conductivity at a certain salt concentration, and it has been reported for many electrolytes of lithium salts [49-53]. The concentration at the maximum in conductivity was ~ 0.7 M LiBOB at 0 ^{o}C for all solvent compositions. At 60 ^{o}C the three solvent mixtures show a broad maximum around between 0.7 and 1.0 M in LiBOB. This is expected since the required distance q for ion-pair formation decreases as temperature increases[47] as seen in Equation 1.

$$q = \frac{\left|z_i z_j\right|}{8\pi\varepsilon_o \varepsilon kT} e^2 \qquad (1)$$

The decrease in q means that more salt can be dissolved without ion pairing, which will shift the maximum conductivity to a higher salt concentration than the same electrolyte at lower temperature.

7.3.3. EC content effect on conductivity

At fixed temperature and salt concentration, the solvent viscosity and dielectric constant change with solvent composition [54], which affects the conductivity of the electrolyte through its dependence on viscosity and dielectric constant. Figure 7.7 shows conductivity for 1 M LiBOB in GBL:EA:EC + 10% A200 as a function of EC content. As EC content increases, both dielectric constant and viscosity increase. The increase in dielectric constant will aid in salt disassociation but increasing viscosity will hinder ion mobility. Increasing salt disassociation will increase conductivity and increasing viscosity will lower conductivity. The conductivity decrease with EC increase shows that viscosity has the dominant role over dielectric constant.

7.3.4. Cathodes half-cells using LiBOB- and $LiPF_6$- based electrolyte

We studied the effects of solvent composition, salt concentration and type, fumed silica content and type (surface chemistry) on cycling behavior of $LiCoO_2$, $LiMn_2O_4$, and $LiFePO_4$ cathodes. Figure 7.8 shows discharge capacity of Li/$LiFePO_4$ cells using LiBOB at 0.7 and 1 M in GBL:EA:EC (1:1:1 and 1:1:0) cycled at C/10 and room temperature. At low C-rate (C/10), both solvent composition and salt concentration have little effect on discharge capacity of Li/$LiFePO_4$ half cells. This trend is true for $LiCoO_2$ and $LiMn_2O_4$ cathodes (data not shown). At C/10 the cycling performance does not differ much among the condition reported. Changing the salt concentration from 0.7 to 1 M or solvent composition from 1:1:0 to 1:1:1 (GBL:EA:EC) does not affect appreciably the charge-transfer or interfacial film resistances, thus they will not affect cycling performance.

Spinel $LiMn_2O_4$ is an attractive cathode material because it is lower cost than $LiCoO_2$ and environmentally benign.[55] Spinel $LiMn_2O_4$ also has good rate capability and is a good candidate for a high-rate battery used in transportation technology.[56] However, spinel $LiMn_2O_4$ faces challenges that must be addressed. One of these challenges is capacity fading during cycling, especially at elevated temperature. One reason for capacity fade is manganese dissolution into the electrolyte with state-of-art electrolyte, which is caused by hydrofluoric acid (HF) generated from $LiPF_6$ hydrolysis. Hydrofluoric acid leads to disproportion reaction of Mn^{3+} to Mn^{2+}, which dissolves in the electrolyte. It is not possible to use spinel $LiMn_2O_4$ with current $LiPF_6$ salt. Figure 7.9 reports the cycle performances of $Li/LiMn_2O_4$ using 1 M LiBOB in GBL:EA:EC(1:1:1) and 1 M $LiPF_6$ in EC:EMC (1:1) electrolytes cycled at room temperature from 3 to 4.2 V at C-rate of C/10. The cell using LiBOB electrolyte has approximately the same initial capacity (~93 mAh g-1) as the cell using $LiPF_6$ electrolyte (~97 mAh g^{-1}). The discharge capacity (92.5 mAh g^{-1}) at the 20th cycle for the cells with LiBOB electrolyte is higher than the discharge capacity (85 mAh g^{-1}) for the cells using $LiPF_6$ electrolyte, which means that capacity fade is slower in LiBOB-based liquid electrolyte (0.025 mAh g^{-1} /cycle) than the state-of-art electrolyte (~ 0.6 mAh g^{-1} /cycle). The decreased capacity fading is attributed to less dissolved manganese with the LiBOB electrolyte since it is HF free

The performance of cathode half-cells using gel electrolyte is shown in Figures (7.9-7.11). As shown in Figure 7.9, the cycling performance of cells using gel electrolyte is comparable to cells using LiBOB-based electrolyte and better than cells using state-of-art

electrolyte. However, the average charge and discharge voltage for gel electrolyte are stable unlike those of liquid electrolyte. For example in the case of Li/$LiFePO_4$ half cells, the charge and discharge voltages for liquid changes from 3.52 to 3.61 V and from 3.31 to 3.21 V, respectively, over 20 cycles. On the other hand, these voltages are stable for gel electrolyte (3.52 for charge and 3.30 V for discharge). The stability of charge and discharge voltages indicate that gel electrolytes have higher energy efficiency with anticipated less capacity fade. The increase stability of gel electrolyte has been attributed to better interfacial stability than its liquid counterpart[57-59].

The effect of fumed silica content and type on cycling performance of $LiFePO_4$/Li cells using gel electrolyte cycled at C/10 at room temperature is reported in Figure 7.10. It is clear that neither fumed silica content nor type have little effect on the performance at low C-rate. Figure 7.11 shows the effects of solvent composition and salt concentrations on cathode half-cell cycling performance using LiBOB in GBL:EA:EC + 10% A200. Changing solvent composition from 1:1:0 to 1:1:1 (GBL:EA:EC) or LiBOB salt concentration from 0.7 to 1 M have no effect on the discharge capacity. This is agreement with what is observed for liquid electrolyte.

7.4. Summary

The results show that LiBOB-based electrolytes (liquid and gel) have good conductivity in a wide temperature range. In addition, adding fumed silica to LiBOB-based electrolyte yields a mixture that exhibits a frequency-independent elastic modulus G' with an elastic modulus larger than its viscous modulus G". These features mean that a 3-D network

structure (solid-like structure) forms that improves the rheological properties of the electrolyte and is anticipated to enhance safety of Li-ion batteries. In addition, the enhancements in rheological properties do not affect significantly conductivity of these gel electrolytes. In general, a hydrophobic surface group on the silica produces higher modulus than a hydrophilic group due to the solubility parameter mismatch of nonpolar surface group in the carbonate medium

The cycling behavior for cathode half-cells using LiBOB-based electrolytes show that the performance of spinel $LiMnO_4$ half cells using LiBOB-based electrolyte is better than those using state-of-art electrolyte. The HF-free media of a LiBOB electrolyte potentially produces a longer cycle life than $LiPF_6$ electrolyte, which is an objective for batteries in EV/HEV application. In addition, LiBOB-based electrolyte can be used with spinel $LiMn_2O_4$, which is less costly than $LiCoO_2$, which is anticipated to lower the cost of Li-ion batteries. There is no effect of solvent composition and salt concentration on cycling behavior of cathode half-cells at C/10 and room temperature are the condition studied. The average charge and discharge voltages for gel electrolyte are stable unlike these of liquid electrolyte, which indicates a higher energy efficiency with less anticipated it capacity fade. These results encourage further study of LiBOB-based electrolyte; there is a good possibility that LiBOB-based electrolyte may enhance the safety of Li-ion batteries and lower their cost.

Acknowledgments

The authors gratefully acknowledge funding from the BATT program, Lawrence Berkeley Laboratory, U.S. Department of Energy, and the DOE Office of FreedomCar and

Vehicle Technologies, and Basic Energy Sciences. The authors express their gratitude toward Dr. Karim Zaghib at Hydro-Quebec for supply of $LiFePO_4$, Timcal American for supplying SFG 6, LICO Technology Corp for supplying $LiMn_2O_4$, and Professor Saad Khan (NCSU) for use of his rheometer.

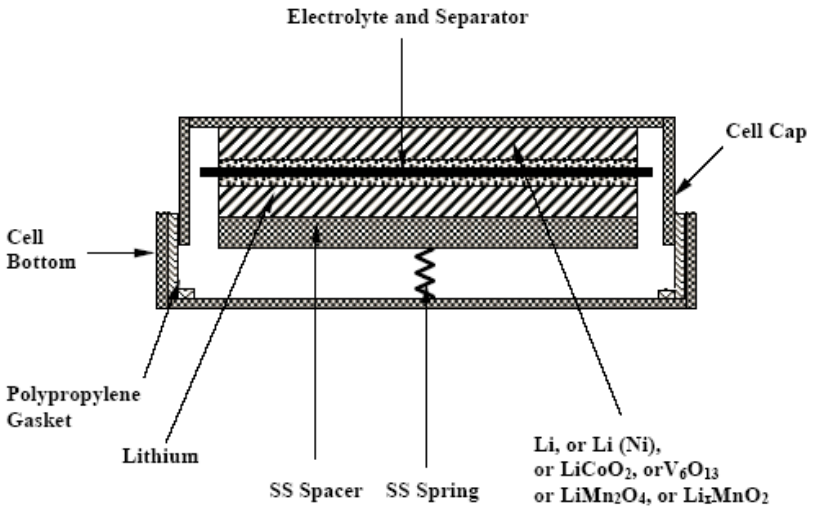

Figure 7.1. Coin cell for cycling studies (not to scale)[47].

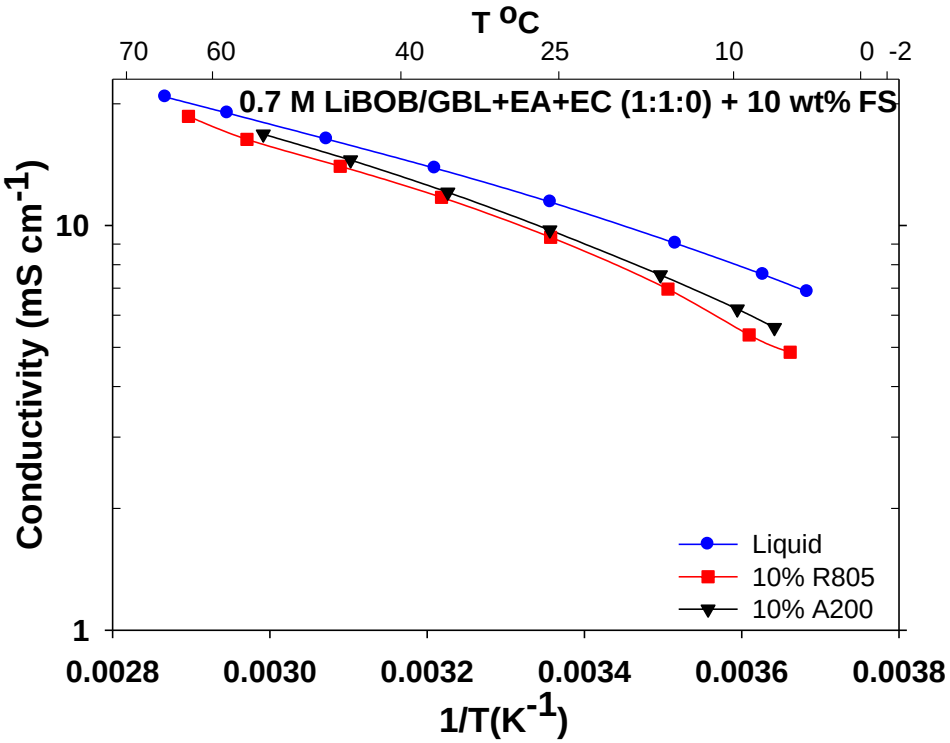

Figure 7.2. Temperature dependence of conductivity for 0.7 M LiBOB in mixture of GBL:EA:EC of 1:1:0 composition for liquid electrolyte with and without 10% fumed silica (R805 or A200).

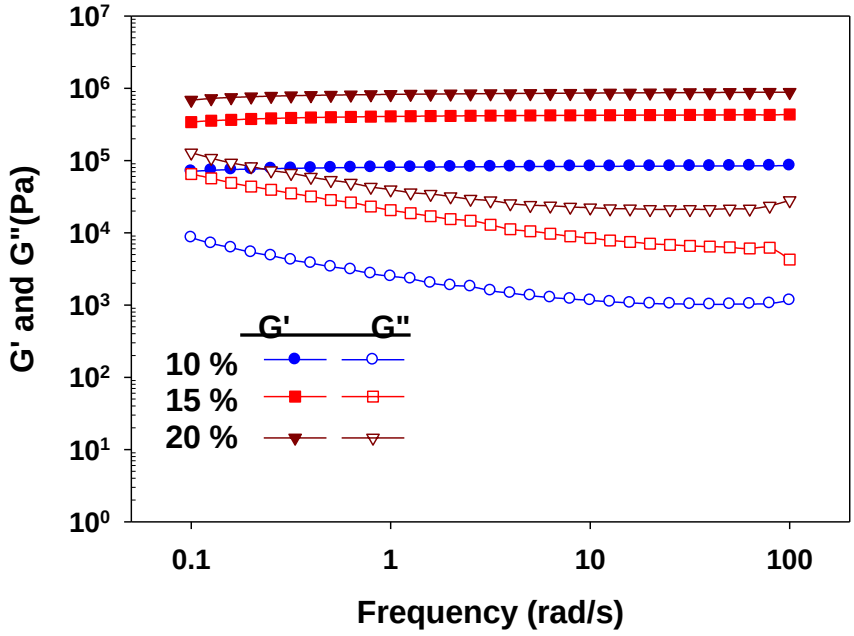

Figure 7.3. Elastic and viscous moduli for 1.0 M LiBOB in GBL:EA:EC (1:1:1) + various content of R805.

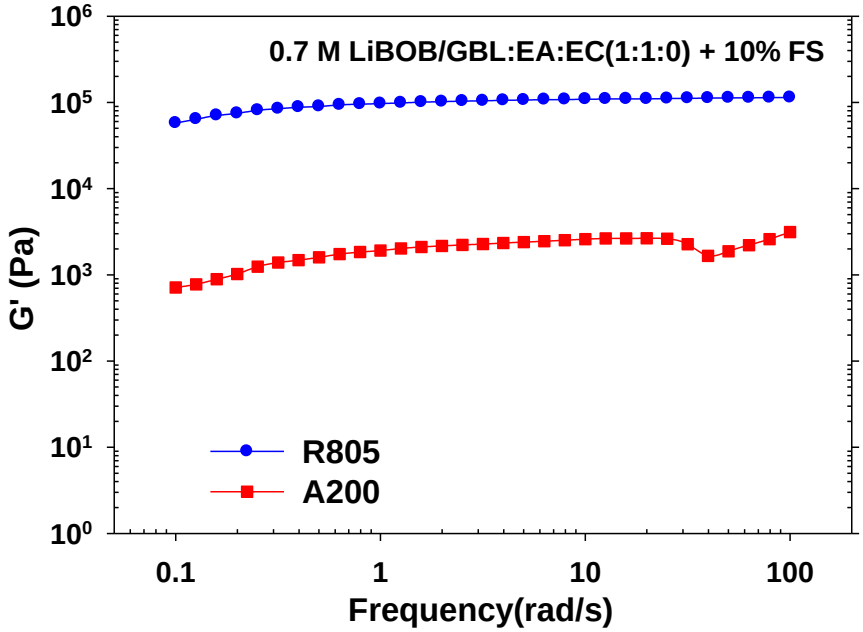

Figure 7.4. Elastic modulus (G') for 0.7 M LiBOB in mixture of GBL:EA:EC of 1:1:0 composition with 10% fumed silica (R805 or A200).

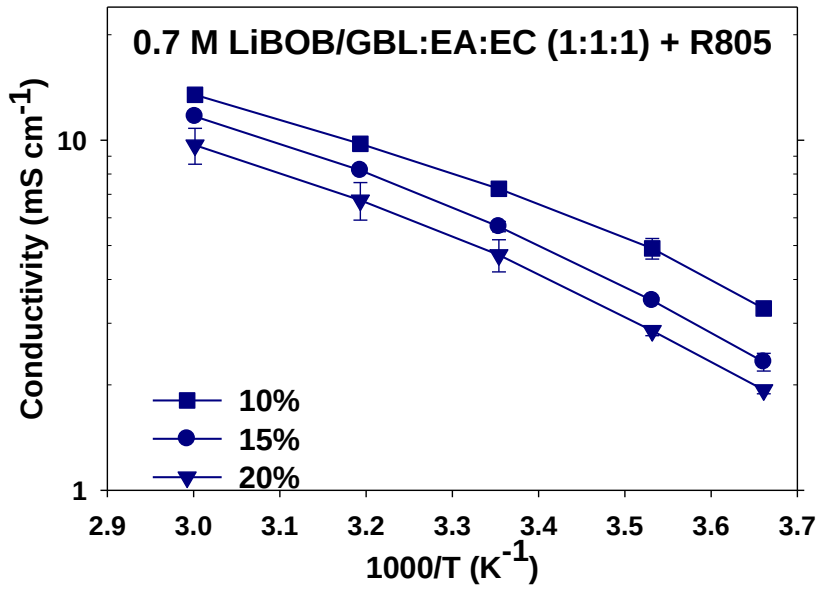

Figure 7.5. Conductivity for 0.7 M LiBOB in mixture of GBL+EA+EC of 1:1:1 composition with various fumed silica content (R805).

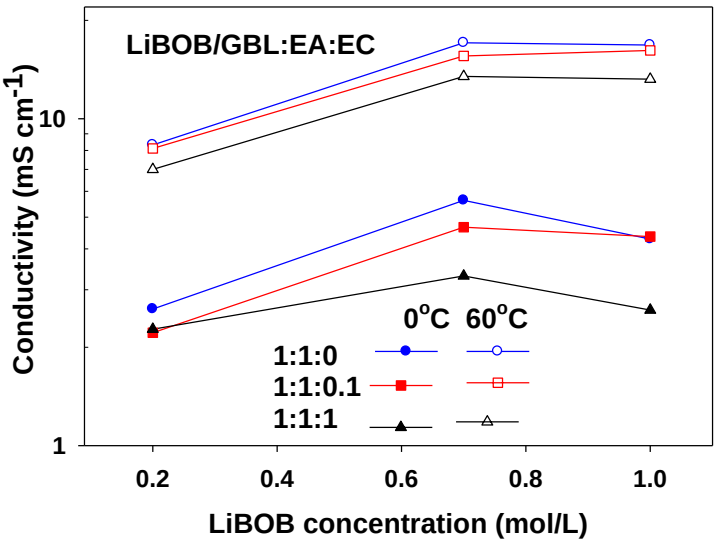

Figure 7.6. Conductivity of LiBOB in GBL:EA:EC +10% R805 at 0 and 60°C.

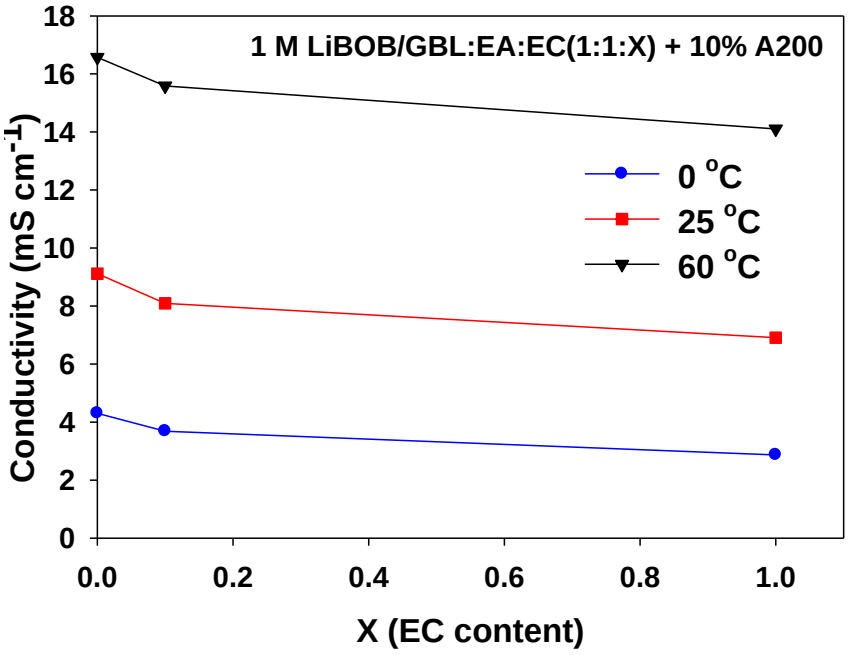

Figure 7.7. Conductivity of 1 M LiBOB in GBL:EA:EC +10% A200 at 0, 25, and 60°C.

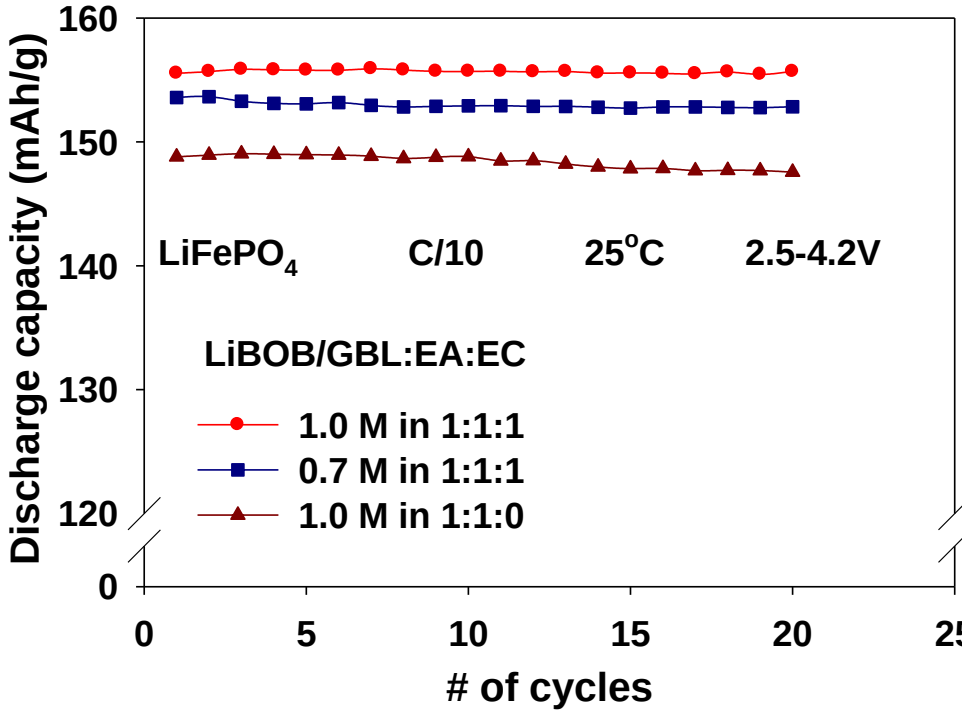

Figure 7.8. Discharge capacity for Li/$LiFePO_4$ half cells using LiBOB-based electrolyte.

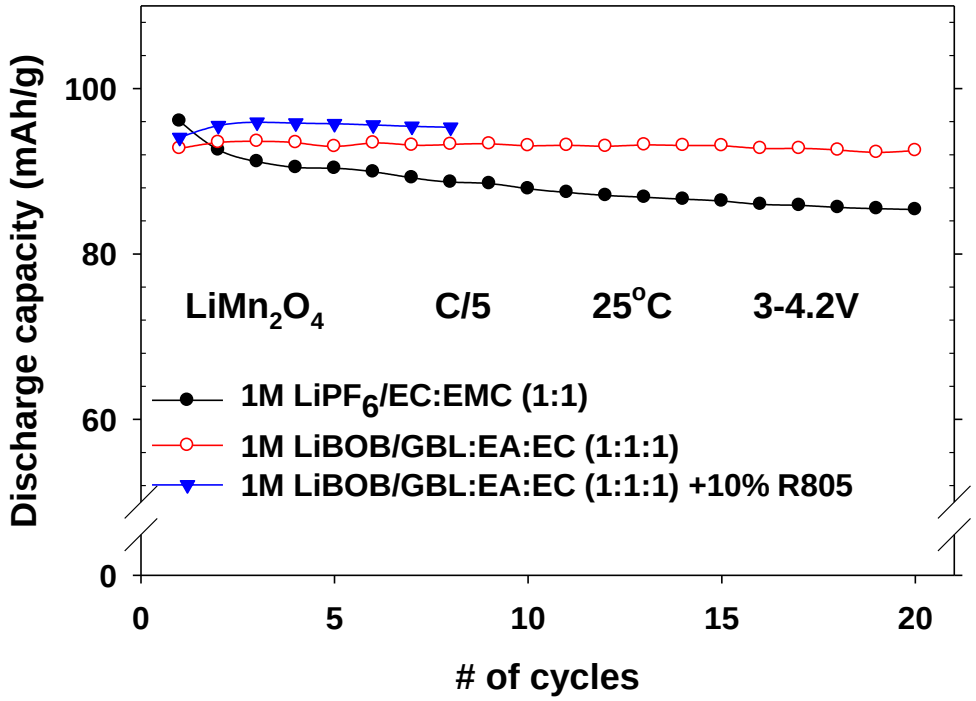

Figure 7.9. Discharge capacity of Li/$LiMn_2O_4$ half cells using LiBOB-based liquid and gel electrolytes.

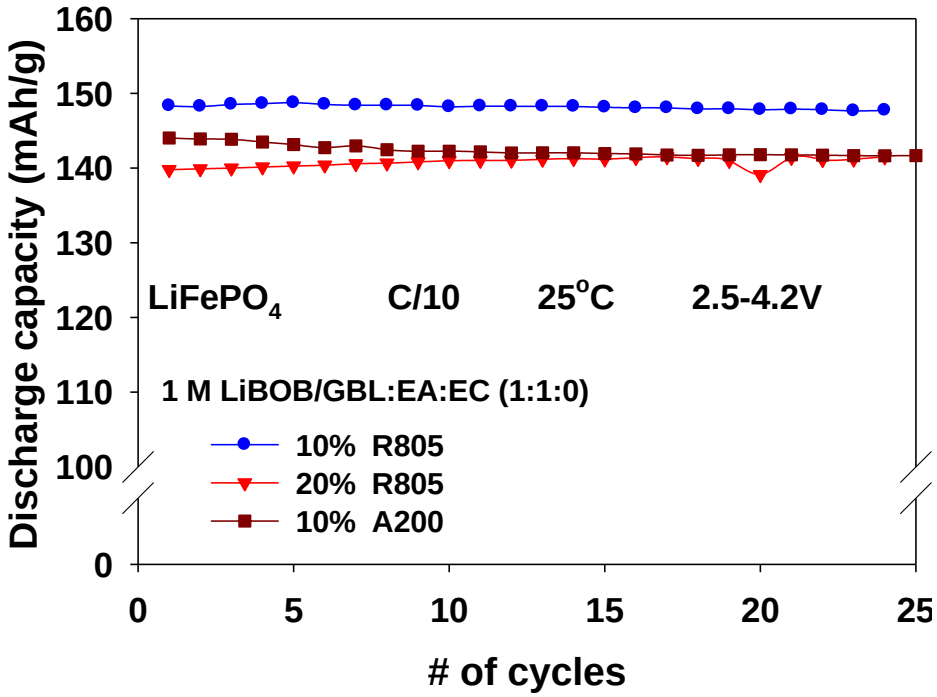

Figure 7.10. Discharge capacity of Li/$LiFePO_4$ half cells using 1 M LiBOB/GBL:EA:EC (1:1:0) + fumed silica.

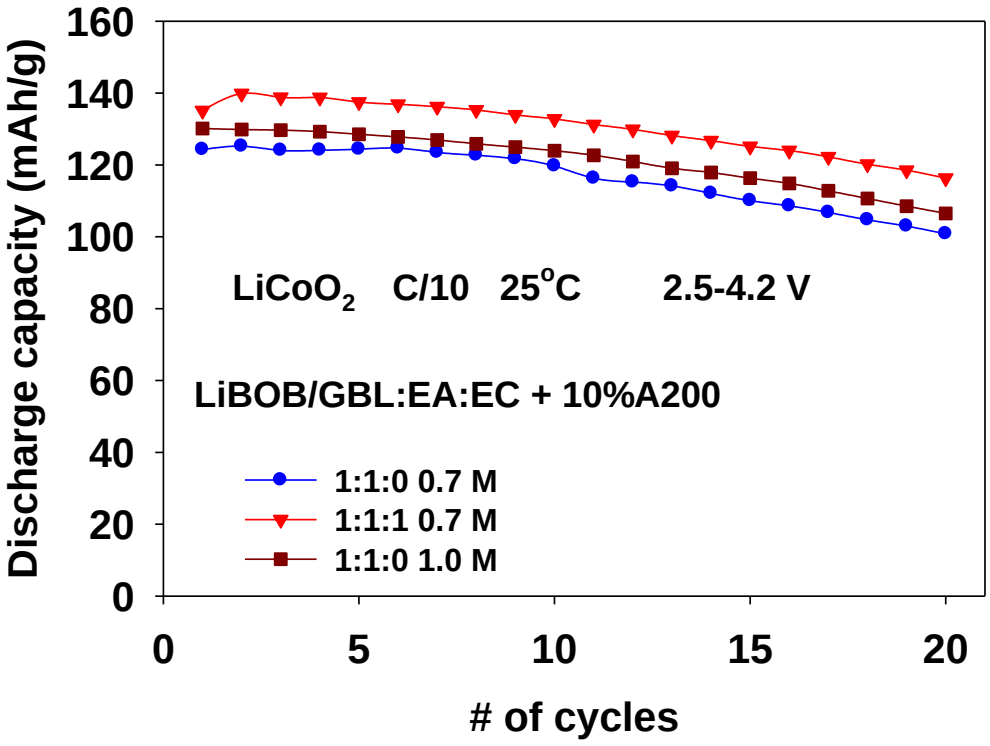

Figure 7.11. Discharge capacity of Li/$LiCoO_2$ half cells using LiBOB/GBL:EA:EC +10% A200.

7.5. References

1. J. M. Tarascon and M. Armand, Nature (London), 414, 395 (2001).

2. S. E. Sloop, J. K. Pugh, S. Wang, J. B. Kerr and K. Kinoshita, Electrochem Solid-State Lett 4, A42 (2001).

3. E. Zinigrad, L. Larush-Asraf, J. S.Gnanaraj, M. Sprecher and D. Aurbach, Thermochim Acta 438, 184 (2005).

4. A. M. Andersson and K. Edstrom, J Electrochem Soc., 148, A1100 (2001).

5. D. Aurbach, K. Gamolsky, B. Markovsky, G. Salitra and Y. Gofer, J Electrochem Soc., 147, 1322 (2000).

6. A. D. Pasquier, A. Blyr, P. Courjal, G. Armatucci, B. Gerand and J. M. Tarascon, J Electrochem Soc, 146, 428 (1999).

7. K. Amine, J. Liu, S. Kang, I. Belharouak, Y. Hyung, D. Vissers, and G. Henriksen, J. Power Sources, 129, 14 (2004).

8. R. Jasinski, and S. Carroll, J. Electrochem. Soc. 117, (1970), 218.

9. K. M. Abraham, J. L. Goldman, and D. L. Natwig, J. Electrochem. Soc. 129, (1982), 2404.

10. C. Nanjundiah, J. L. Goldman, L. A. Dominey, and V. R. Koch, J. Electrochem. Soc. 135, (1988), 2914.

11. V. R. Koch, J. Electrochem. Soc. 126, (1979), 181.

12. A. Webber, J. Electrochem. Soc. 138, (1991), 2586.

13. S. S. Zhang, K. Xu, and T. R. Jow, J. Electrochem. Soc. 149, (2002), A586.

14. N. Takami, T. Ohsaki, H. Hasebe, and M. Yamamoto, J. Electrochem. Soc. 149, (2002), A9.

15. S. S. Zhang, K. Xu, and T. R. Jow, Electrochem. Commun. 4, (2002), 928.

16. S. S. Zhang, K. Xu, and T. R. Jow, J. Solid State Electrochem. 7, (2003), 147.

17. F. Croce, A. D'Aprano, C. Nanjundiah, V. R. Koch, C. Walker, and M. Salomon, J. Electrochem. Soc. 143,(1996), 154.
18. M. Ue, J. Electrochem. Soc 141, (1994), 3336.

19. L. J. Krause, W. Lamanna, J. Summerfield, M. Engle, G. Korba, R. Loch, and R. Atanasoski, J. Power Sources 68, 1997, 320.

20. U. Lischka, U. Wietelmann, and M. Wegner, German Pat. DE 19829030 C1 (1999) doi:10.1149/1.1701584.

21. W. Xu and C. A. Angell, Electrochem. Solid-State Lett., 4, E1 (2001).

22. Zhang SS, J Power Sources 162: 1379 (2006).

23. Xu K, Zhang SS, Lee U, Allen JL and Jow TR, J Power Sources 146: 79 (2005).

24. Xu W and Angell CA, Solid State Ionics 147: 295 (2002).

25. Yu BT, Qiu WH, Li FS and Xu GX, Electrochem Solid-State Lett 9: A1 (2006).

26. K. Xu, S. Zhang, B. A. Poese, and T. R. Jow, Electrochem. Solid-State Lett., 5, A259 (2002).

27. J. S. Gnanaraj, M. D. Levi, Y. Gofer, D. Aurbach and M. Schmidt, J Electrochem Soc 150, (2003), A445.

28. K. Xu Chem. Rev., 104 (10), (2004), 4303.

29. K. Xu, J. Electrochem Soc, 155, (2008), A733.

30. M. Salomon, and E. Plichta, J. Electrochim. Acta 30,(1985), 113.

31. F. Azeez and P.S. Fedkiw, submitted to Journal of Power Sources (2009)

32. Kosinski and Caruthers, 1985; Khan and Zoeller, 1993

33. J. Y. Song, Y. Y. Wang, and C. C. Wan, J. Power Sources, 77, 183 (1999)

34. K. Kezuka, T. Hatazawa, and K. Nakajima, J. Power Sources, 97, 755 (2001).

35. J. Fan, S. R. Raghavan, X.-Y. Yu, S. A. Khan, P. S. Fedkiw, J. Hou, and G. L.Baker, Solid State Ionics, 111, 117 (1998).

36. H. J. Walls, M. W. Riley, R. R. Gupta, R. J. Spontak, P. S. Fedkiw, and S. A. Khan, Adv. Funct. Mater., 13, 710 (2003).
37. H. J. Walls, J. Zhou, J. A. Yerian, P. S. Fedkiw, S. A. Khan, M. K. Stowe, and G. L. Baker, J. Power Sources, 89, 156 (2000).

38. S. R. Raghavan, J. Hou, G. L. Barker, and S. A. Kahn, Langmuir, 16, 1066 (2000).

39. J. M. Tarascon, A. S. Gozdz, C. Schmutz, F. Shokoohi, and P. C. Warren, Solid State Ionics, 86, 49 (1996).

40. F. Croce, G. B. Appetecchi, L. Persi, and B. Scrosati, Nature (London), 394, 456 (1998).

41. G. Eichinger and M. Fabian, J. Power Sources, 68, 381 (1997).

42. G. Eichinger and M. Fabian, J. Power Sources, 68, 387 (1997).

43. H. J. Walls, J. Zhou, J. A. Yerian, P. S. Fedkiw, S. A. Khan, M. K. Stowe, and G. L. Baker, J. Power Sources, 89, 156 (2000).

44. S. R. Raghavan, M. W. Riley, P. S. Fedkiw, and S. A. Khan, Chem. Mater., 10, 244 (1998).

45. C. W. Macosko, Rheology: Principles, Measurements, and Applications, VCH publishers, Inc., New York (1994).

46. M. Riley, P. S. Fedkiw, and S. A. Khan, J. Electrochem. Soc. 149, (2002), A667.

47. J. Zhou, PhD" Fumed Oxide-Based Nanocomposite Polymer

48. F. Azeez, S.A. Khan, and P.S. Fedkiw, in preparation for submission to Langmuir

49. Y. Choquette, G. Brisard, M. Parent, D. Brouillette, G. Perron, J. E. Desnoyers, M. Armand, D. Gravel, and N. Slougui, J. Electrochem. Soc. 145, (1998), 3500.

50. J. Barthel, R. Buestrich, E. Carl, and H. J. Gores, J. Electrochem. Soc. 143, (1996), 3565.

51. J. Barthel, H. J. Gores, and G. Schmeer, and B. Bunsenges. Phys. Chem. 83, (1979), 911.

52. B. E. Conway, Electrochemical Super capacitors-Scientific Fundamentals and Technological Applications, chap. 13, Kluwer Academic/Plenum Publishers, New York (1999).

53. I. Geoffroy, P. Willmann, K. Mesfae, B. Carré, and D. Lemordant, Electrochimica Acta 45,(2000), 2019.
54. F. Azeez, Master Thesis, " Transport properties of lithium bis(oxalate)borate-based electrolyte for lithium-ion cells" , North Carolina State University

55. Y. Shin and A. Manthiram, Electrochem. Solid-State Lett., 6, A34 (2003).

56. L. F. Wang, C. C. Ou, K. Striebel, and J. S. Chen, J. Electrochem. Soc., 150, A905 (2003).

57. Y. X. Li, S. A. Khan, and P. S. Fedkiw, Electrochim. Acta, 47, 3853 (2002).

58. X. W. Zhang, Y. X. Li, P. S. Fedkiw, and S. A. Khan, J. Electrochem. Soc., 151, A1257 (2004).

59. J. Zhou, P. S. Fedkiw, and S. A. Khan, J. Electrochem. Soc., 149, A1121 (2002).

CHAPTER 8: LiBOB-BASED GEL ELECTROLYTE AS A SEPARATOR FOR Li-ION BATTERIES

Fadhel Azeez and Peter S. Fedkiw*

Department of Chemical & Biomolecular Engineering, North Carolina State University, Raleigh, NC 27695-7905, USA

For submission as a short communication to

Electrochemical and Solid State Letters

* Corresponding author. Tel.: +1-919-515-3572; Fax: +1-919-515-3456
E-mail address: fedkiw@eos.ncsu.edu

Abstract

This work reports cycling performance of cathode half-cells using a LiBOB-based gel electrolyte composed of lithium bis(oxalato)borate (LiBOB) salt dissolved in solvent mixtures of γ-butyrolactone (GBL), ethyl acetate (EA), and ethylene carbonate (EC) + nanoparticulate fumed silica (R805) as a gelling agent, with and without a Celgard separator. Conductivity and rheological properties of the LiBOB-based gel electrolyte are presented. A three-dimensional network structure is formed upon adding fumed silica to the base-liquid electrolyte, and the conductivity of gel electrolytes is slightly lowered. Based on scaling models, the effective conductivity of liquid electrolytes in Celgard is ~ 0.05 of the bulk solution conductivity, but in contrast the gel electrolyte conductivity is ~ 0.6 of the bulk solution conductivity. The discharge capacity of $LiFePO_4$ and $LiCoO_2$ half-cells using the gel electrolyte without a Celgard separator is greater than those of cells using a Celgard separator. The cycling performance of $LiMn_2O_4$ half-cells using the gel electrolyte without a Celgard shows that the discharge capacity is stable over 50 cycles, which indicates that mechanical properties of the gel electrolyte is capable of preventing contact between anode and cathode. Discharge capacities of cells using the gel electrolyte without Celgard and the base-liquid electrolyte with Celgard are comparable (differ less than 5 %). However, in the case of $LiCoO_2$ half-cells, the discharge capacities of cells using the gel electrolyte, with and without Celgard, seem to fade more quickly than cells using the base-liquid electrolyte with Celgard.

8.1. Introduction

A separator is used in cells to prevent short-circuit contact of positive and negative electrodes while maintaining the liquid electrolyte between the two. The typical separator used in lithium-ion batteries is a microporous polyolefin membrane, such as polypropylene and/or polyethylene (e.g. Celgard® or Tonen®) with a typical thickness of 25 μm .

There are disadvantages, however, in using a separator, for example an increase in cell resistance by a factor of 6–7 [1] and a decrease in energy density of the battery, the extent which depends on cell size. Polyolefin separators have poor wettabilty with polar solvents [2-3], which is due to their low polarity [4], small pore sizes (0.1 by 0.05 μm), and low porosity (~ 34-45%)[5]. These disadvantages affect a decreased conductivity and a fade in capacity and power capability of a cell because of electrolyte decomposition products clogging the pores with particulate matter, particularly at temperatures ≥60 °C.[6-7] In addition, separators comprise 25–30% [8,9] of the overall manufacturing cost of Li-ion batteries for HEV and EV application. A reduction of manufacturing cost has been identified as a key element for commercialization for HEVs and EVs[6]. Therefore, research has been undertaken recently to search for alternative separators [10- 25].

In this communication, we present the discharge capacities of cathode half-cells using a LiBOB-based gel electrolyte as a separator and compare with the discharge capacity of cells using same the electrolyte with Celgard separator. We also report rheological properties and conductivity of the gel electrolyte.

8.2. Experimental

8.2.1. Conductivity measurements

Conductivity is measured using EG&G Princeton Applied Research PowerSine software to control an EG&G Model 273 potentiostat and EG&G Model 5210 lock-in amplifier in the frequency range 100 kHz to 100 mHz. The cell constants are found using a KCl standard solution (Fisher Scientific) prior to and after each measurement. Details of the solution and gel preparation and the conductivity measurements are provided elsewhere [26]

8.2.2. Rheological measurements

Rheological measurements are conducted using a AR2000 stress rheometer (TA Instrument) at room temperature. Dynamic measurements are used to probe the gel microstructure with minimal disturbance of samples. The relative magnitude and trends of elastic (G') and viscous (G") moduli data as a function of rotation frequency indicate the type and extent of the microstructure of samples. Details of the rheological measurements are provided elsewhere [27]

8.2.3. Cathode half-cell preparation and cell cycling

Three types of cathode materials are studied: $LiCoO_2$, $LiMn_2O_4$, and $LiFePO_4$. The $LiCoO_2$ is obtained from OMG and LICO Technology Corp (Japan); the $LiMn_2O_4$ is obtained from Merck (Germany) and LICO Technology Corp (Japan); the $LiFePO_4$ is obtained from Hydro Quebec (Canada), poly (vinylidene fluoride) (PVDF, KYNAR^{TM}) is

obtained from Elf Atochem; synthetic flake graphite (SFG 6) is obtained from Timcal America; carbon black (Ketjenblack (KJB) EC-600JD) is obtained from Akzo Nobel Inc; and the solvent 1-methyl-2-pyrrolidinone (NMP) is obtained from Aldrich. Two types of carbon additives are used: KJB graphite, which consists of round particles and the SFG type, which is in the form of flat flakes. These materials are used as received.

The typical composition for a $LiCoO_2$ cathode is 90-5-3-2 (wt % active material-PVDF-KS6-KJB EC-600JD). For $LiFePO_4$ and $LiMnO_4$ cathode, the typical electrode composition is 80-10-5-5 (active material-PVDF-KS6-KJB EC-600JD). Aluminum foil (0.024-mm thick, Fisher Scientific) is used as the cathode current collector. Details of the electrode formulation are provided elsewhere [26]

Coin cells, in which an electrolyte/separator is sandwiched between lithium metal and a metal-oxide composite cathode, are used in the cycling measurements. For cells without a Celgard separator, a gel electrolyte is sandwiched between anode and cathode. A stainless steel spacer and spring are used to maintain good contact of electrolyte, electrode, and current collector.

An Arbin battery cycler (Model BT2042 and BT2043) controlled by Arbin ABTS software is employed to carry out constant-current cell cycling in $LiMO_x$/electrolyte/Li cells, where $LiMO_x$ is $LiCoO_2$, $LiMn_2O_4$, or $LiFePO_4$. A C-rate of C/10 was used in all measurements. Cell cycling is terminated upon reaching a cycle number ranging from 20 to 50. The cutoff voltages for each cathode are 2.5-4.2 V for $LiFePO_4$ and $LiCoO_2$ and 3-4.2 V for $LiMn_2O_4$.

8.3. Results and Discussion

The conductivity of 0.7 M LiBOB in GBL:EA:EC (1:1:1) base-liquid electrolyte and 20% R805 as a function of temperature is presented in Figure 8.1. The conductivity of the base-liquid electrolyte decreases with temperature by ~ 68% over the temperature range studied (-3 to 60^{o}C) due to the increase of viscosity and its effect on ionic mobility. The conductivity of gel electrolyte behaves similarly to the conductivity of base-liquid electrolyte and it is lower by 33-50 % than the conductivity of the base-liquid electrolyte at 60 and -3 ^{o}C, respectively.

Using the gel electrolyte as a separator is expected to improve the cell conductivity since Celgard decreases effective conductivity significantly [1,6] as approximated through scaling models such as:

$$\sigma_{eff} = \varepsilon^{\alpha}\sigma_{o} \tag{1}$$

where ε is the void volume fraction of the separator, σ_o is bulk solution ionic conductivity, and α is the Bruggeman exponent, which is 3.3 for separators used in Li-ion batteries [28]. For a Celgard separator, the effective conductivity is ~.05 of the bulk solution conductivity (using ε=0.4 and $\alpha=3.3$), compared to the gel electrolyte's conductivity of ~ 0.6 of the bulk solution conductivity (at room temperature).

Figure 8.2 shows the elastic (G') and viscous (G") moduli of 1 M LiBOB in GBL:EA:EC (1:1:1) + 20% fumed silica as a function of rotation frequency in a dynamic rheology measurment. The elastic modulus (G' ~10^6 Pa) is independent of frequency and is

significantly higher than the viscous modulus (G" ~$5x10^4$), which indicates formation of a solid-like structure (gel) [29.]

Figures 8.3-8.5 report the cycling performance of cathode half-cells using LiBOB-based liquid and gel electrolyte at C/10 and room temperature, with and without Celgard separator. Figure 8.3 shows the cycling performance of $LiCoO_2$ half-cells; cells using the gel electrolyte without Celgard show a better performance than cells using a gel electrolyte and Celgard. One reason for the difference in performance might be a wettability issue with Celgard, which results in electrolyte-deficient portions of the electrode. Figure 8.4 reports the cycling performance of $LiMn_2O_4$ half-cells using the gel electrolyte, with and without Celgard. It's clear that the cycling performance is excellent and there are no short circuits during the test (50 cycles). The mechanical stability of the gel electrolyte is excellent and it prevents contact between anode and cathode without the need for a polymeric separator. Figure 8.5 shows the cycling performance for $LiFePO_4$ half-cells using the gel electrolyte, with and without Celgard. Again the performance of cells using the gel electrolyte without Celgard is better than those with the gel electrolyte and Celgard. Figures 8.3-8.5 also show that the discharge capacities of cathode half-cells using LiBOB-based gel electrolyte without Celgard and cells using the base-liquid electrolyte with Celgard are comparable (differ less than 5%). However in the case of $LiCoO_2$ half-cells, the discharge capacities of cells using the gel electrolyte (with and without Celgard) fade more quickly than cells using the base-liquid electrolyte with Celgard. Since the test is terminated at a low number of cycles, we are not sure if the capacity fade will increase as the number of cycles increases. This is a topic of our ongoing investigation of these polymer separator-free cells.

8.4. Conclusion

Using the fumed-silica based gel electrolyte, cathode half-cells are cycled without use of a Celgard separator. In addition, the LiBOB-based electrolyte allows use of lower-cost cathodes such as $LiMn_2O_4$ and $LiFePO_4$ that face challenges to be used with current state-of-art electrolyte. The fumed silica addition does not affect conductivity significantly compared to the liquid electrolyte (still in the order of ~ 10^{-3} S/cm). In addition, the discharge capacities of $LiFePO_4$ and $LiMn_2O_4$ half-cells using the gel electrolyte without Celgard and the base-liquid electrolytes are comparable (differ less than 5%). Since the gel electrolyte potentially lowers the cost and improves the rate capability of Li-ion batteries, it may be a good candidate for electric vehicles (EV) and hybrid electric vehicles (HEV).

Acknowledgments

The authors gratefully acknowledge funding from the BATT program, Lawrence Berkeley Laboratory, U.S. Department of Energy, and the DOE Office of FreedomCar and Vehicle Technologies, and Basic Energy Sciences. The authors express their gratitude toward Dr. Karim Zaghib at Hydro-Quebec for supply of $LiFePO_4$, Timcal America for supplying SFG 6, LICO Technology Corp for supplying $LiMn_2O_4$, and professor Saad Khan (NCSU) for use of his rheometer.

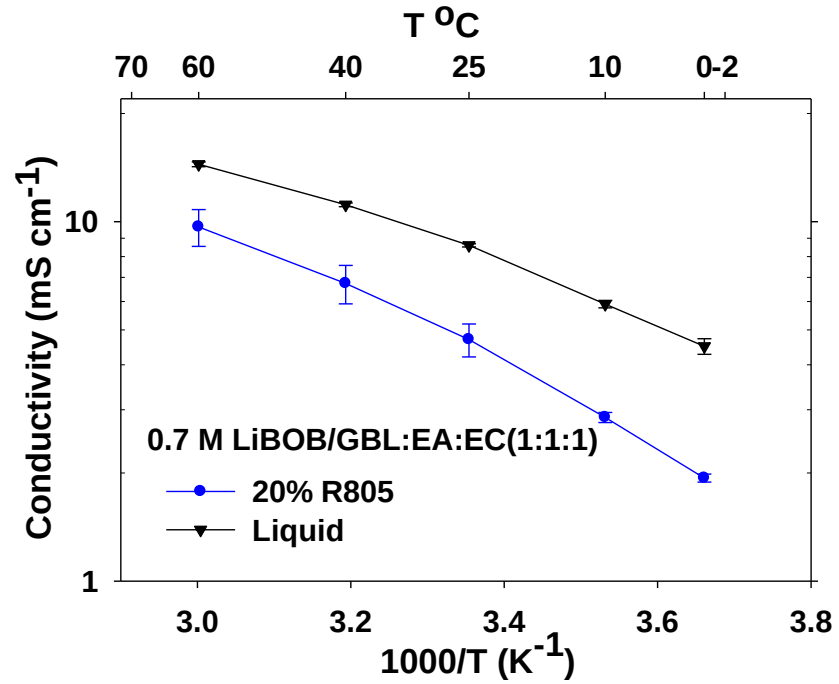

Figure 8.1. Conductivity of 0.7 M LiBOB in mixture of GBL:EA:EC of 1:1:1 composition (wt) with and without 20% fumed silica (R805).

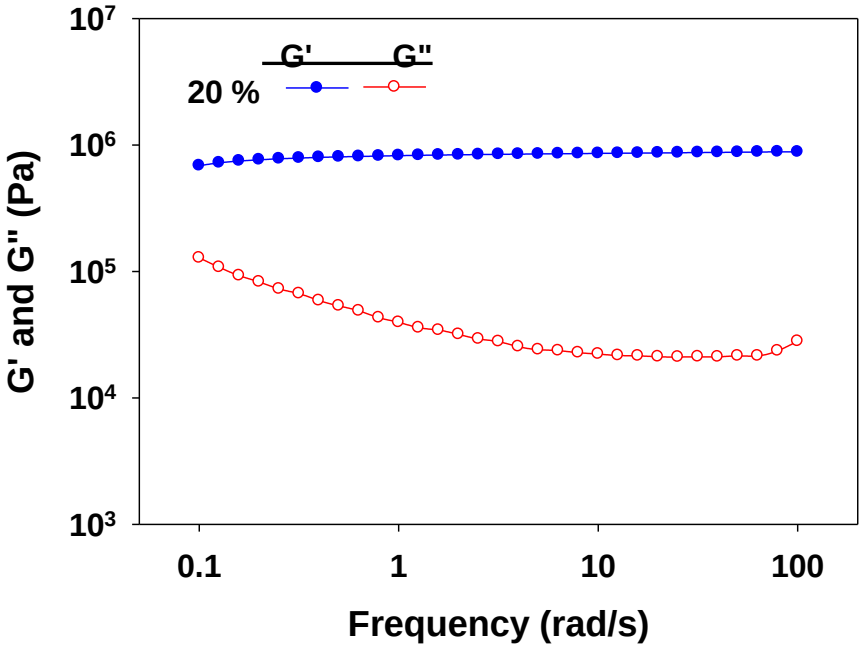

Figure 8.2. Elastic (G') and viscous (G") moduli of 1.0 M LiBOB in GBL:EA:EC (1:1:1) + 20% R805.

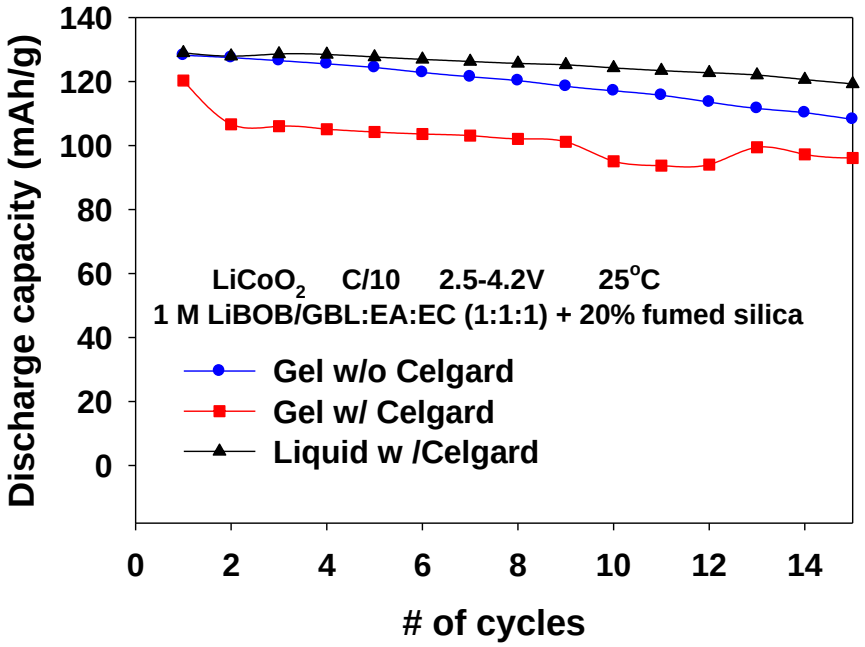

Figure 8.3. Discharge capacity of $LiCoO_2$ half-cells using 1 M LiBOB in mixture of GBL:EA:EC of 1:1:1 composition (wt) with and without 20% fumed silica (R805). Performance with base-liquid electrolyte using Celgard separator is also shown.

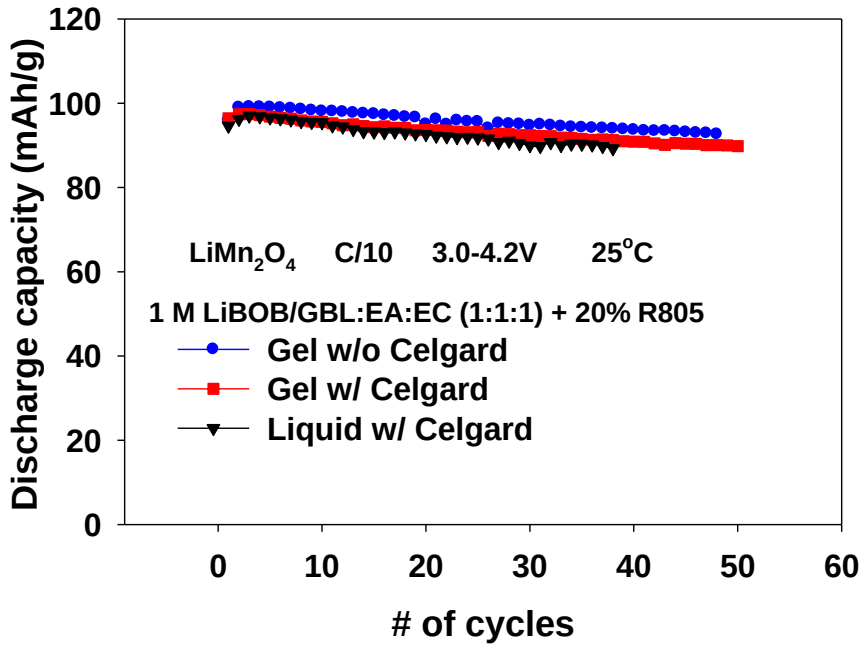

Figure 8.4. Discharge capacity of $LiMn_2O_4$ half-cells using 1 M LiBOB in mixture of GBL:EA:EC of 1:1:1 composition (wt) with and without 20% fumed silica (R805). Performance with base-liquid electrolyte using Celgard separator is also shown.

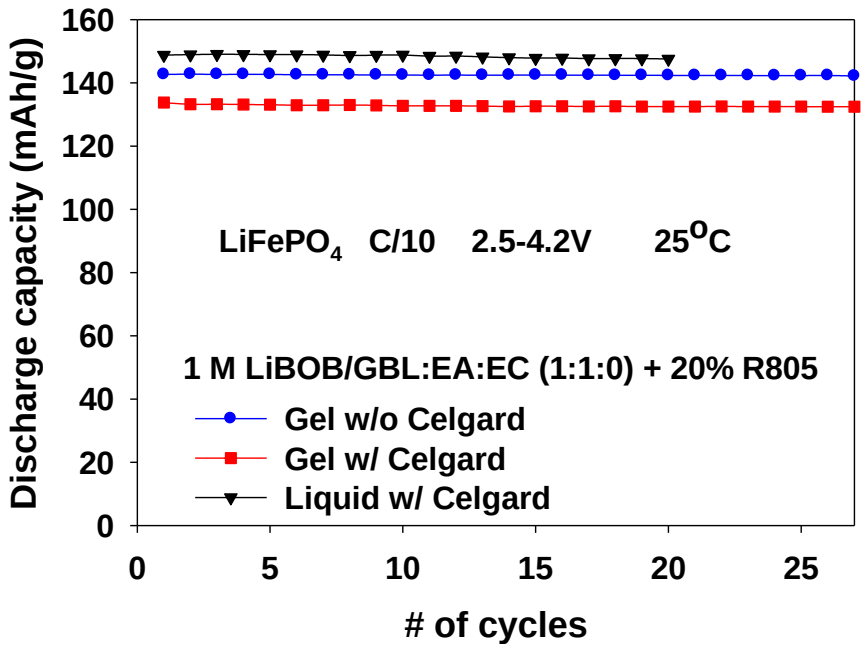

Figure 8.5. Discharge capacity of $LiFePO_4$ half-cells using 1 M LiBOB in mixture of GBL:EA:EC of 1:1:0 composition (wt) with and without 20% fumed silica (R805). Performance with base-liquid electrolyte using Celgard separator is also shown.

8.5. References

1. P. Arora, Z. Zhang, Chem. Rev. 104 (2004) 4419.

2. J. Saunier, F. Alloin, J.Y. Sanchez, G. Caillon, J. Power Sources 119–121 (2003) 454.

3. Y.M. Lee, J.W. Kim, N.S. Choi, J.A. Lee, W.H. Seol, J.K. Park, J. Power Sources 139 (2005) 235.

4. J.Y. Song, Y.Y. Wang, C.C. Wan, J. Electrochem. Soc. 147 (2000) 3219.

5. F.G.B. Ooms, E.M. Kelder, J. Schoonman, N. Gerrits, J. Smedinga, G. Callis, J. Power Sources 97–98 (2001) 598.

6. US Department of Energy, "FY 2006 Progress Report for Energy Storage Research and Development.
"URL:<http://www1.eere.energy.gov/vehiclesandfuels/pdfs/program/2006_energy_storage.pdfl>, accessed July 2009

7. R. Kostecki, L. Norin, X. Song, F. McLarnon, J. Electrochem. Soc. 151(2004) A522

8. D. Bansal, B. Meyer, M. Salomon, Journal of Power Sources 178 (2008) 848–851

9. SS. Zhang , Journal of Power Sources 164 (2007) 351–364

10. F. Boudin, X. Andrieu, C. Jehoulet, I.I. Olsen, J. Power Sources 81–82 (1999) 804.

11. A.D. Pasquier, P.C. Warren, D. Culver, A.S. Gozdz, G.G. Amatucci, J.M. Tarascon, Solid State Ionics 135 (2000) 249.

12. H.P. Wang, H. Huang, S.L. Wunder, J. Electrochem. Soc. 147 (2000)2853.

13. T. Michot, A. Nishimoto, M. Watanabe, Electrochim. Acta 45 (2000) 1347.

14. Y. Saito, H. Kataoka, T. Sakai, S. Deki, Electrochim. Acta 46 (2001) 1747.

15. H. Huang, S.L. Wunder, J. Electrochem. Soc. 148 (2001) A279.

16. A. Magistris, P. Mustarelli, F. Parazzoli, E. Quartarone, P. Piaggio, A. Bottino, J. Power Sources 97–98 (2001) 657.

17. A. Magistris, P. Mustarelli, E. Quartarone, P. Piaggio, A. Bottino, Electrochim. Acta 46 (2001) 1635.

18. D.W. Kim, Y.K. Sun, J. Power Sources 102 (2001) 41.

19. J.Y. Song, C.L. Cheng, Y.Y. Wang, C.C. Wan, J. Electrochem. Soc. 149 (2002) A1230.

20. A.M. Stephan, Y. Saito, Solid State Ionics 148 (2002) 475.

21. D.W. Kim, K.A. Noh, H.S. Min, D.W. Kang, Y.K. Sun, Electrochem. Solid State Lett. 5 (2002) A63.

22. A. Magistris, E. Quartarone, P. Mustarelli, Y. Saito, H. Kataoka, Solid State Ionics 152–153 (2002) 347.

23. A.M. Stephan, D. Teeters, Electrochim. Acta 48 (2003) 2143.

24. Y. Saito, A.M. Stephan, H. Kataoka, Solid State Ionics 160 (2003) 149.

25. S.S. Zhang, K. Xu, D.L. Foster, M.H. Ervin, T.R. Jow, J. Power Sources 125 (2004) 114.

26. F. Azeez and P.S. Fedkiw, submitted to J. Electrochem. Soc (2009)

27. F. Azeez, S. A. Khan, and P.S. Fedkiw, submitted Langmuir (2009).

28. P. Arora, M. Doyle, A.S. Gozdz, R.E. White, and J. J. Newman, Power Sources 88, (2000) , 219.

29. C. W. Macosko, Rheology: Principles, Measurements, and Applications, VCH publishers, Inc., New York (1994).

CHAPTER 9: CONCLUSIONS AND RECOMENDATIONS

9.1. Conclusions

In this work we formulate and characterize LiBOB-based liquid and gel electrolytes for use in lithium-ion batteries. This work demonstrates that LiBOB salt dissolved in a solvent mixture of GBL+EA+EC provides a good conductivity over a wide temperature range. Solvent composition and salt concentration effect conductivity and rheology, and in the temperature range used in the study, the results support the notion that viscosity plays a greater role than dielectric constant in controlling conductivity.

The trends observed in conductivity of LiBOB in GBL:EA:EC solvent mixtures with changing salt concentration, solvent composition, and temperature can be interpreted in terms of the variation in dielectric constant and viscosity with these same variables. Since these factors and their effect on ion conductivity are not unique to the LiBOB/GBL+EA+EC system, these trends provide general guidance on how ion conductivities of other electrolyte systems with similar solvent compositions would change with these same variables, and they should constitute a useful database for the understanding of more complex systems, such as quaternary mixtures.

Rheology and conductivity: Adding fumed silica to LiBOB-based electrolytes yields a mixture with an elastic modulus independent of rotation frequency and larger than the viscous modulus in a dynamic rheology experiment, which indicates a formation of 3-D network structure (gel electrolyte) that is anticipated to enhance safety of Li-ion batteries by eliminating leakage problems associate with liquid electrolyte. Although the elastic modulus

of gel electrolytes is improved by orders of magnitudes with addition of fumed silica, the decrease in conductivity is small (σ is ~ 10% lower in the case of 10% F.S). Fumed silica surface chemistry affects the rheological properties of LiBOB-based gel electrolyte but has negligible effect on conductivity. As a result, one can compose an electrolyte with good conductivity and good mechanical properties by changing surface chemistry of fumed silica. In general, a hydrophobic surface group on fumed silica produces higher modulus than a hydrophilic group due to solubility mismatch between nonpolar surface groups and the GBL:EA:EC solvent mixture.

Rheological properties of A200-containg electrolyte are affected greatly by solvent composition and salt concentration. On other hand, there is no effect of salt concentration or solvent composition on rheological properties of R805-containg electrolyte. For example, changing salt concentration from 0.2 to 1 M LiBOB in GBL:EA:EC (1:1:0) +10% A200 increases G' by one order of magnitude. but only 15%, typically, for 10% R805-containing electrolyte. If the solvent composition is varied from 1:1:0 to 1:1:1 in 0.2 M LiBOB in GBL:EA:EC the gel structure is lost withA200 but not so with R805. FTIR shows that BOB^- anion interacts with silanol groups on A200 and helps in form the gel structure, which is how salt concentration affects the elastic modulus of A200-containg electrolyte.

Cycling performance: Results of cell cycling show that $LiMn_2O_4$ half-cells using LiBOB-based liquid and gel electrolyte perform better than cells that using state-of-art electrolyte. The capacity fade for cells with LiBOB-based electrolyte is 0.025 mAh/g cycles compared to 0.6 mAh/g cycles for cells using state-of-art electrolyte. The HF-free media of a LiBOB electrolyte potentially produces a longer cycle life than $LiPF_6$ electrolyte, which is an

objective for batteries in EV/HEV application. Cathode half-cells using gel electrolyte show a more stable discharge and charge voltage than cells using liquid electrolyte. For example for $LiFePO_4$ half-cells, the average charge and discharge voltages for liquid electrolyte changes from 3.52 to 3.61 V and from 3.31 to 3.21 V, respectively. On the other hand, these voltages are stable for gel electrolyte (3.52 for charge and 3.30 V for discharge). The stability of charge and discharge voltages indicates that gel electrolytes have higher energy efficiency with anticipated less capacity fade. In addition to LiBOB being low cost compared to $LiPF_6$ (~ 33% cheaper), a LiBOB-based electrolyte allows for use of other cheaper cathode material such as $LiMn_2O_4$, which will lower the cost of lithium ion batteries. Performances of anode half-cells cycled at room temperature using LiBOB-based electrolyte and state-art-electrolyte are comparable.

Cycling results for cathode half-cells using LiBOB-based gel electrolyte without using a Celgard separator show that the performance is stable and better than the performance of cells using the separator. It is clear that our gel electrolytes are capable of preventing contact between the anode and cathode and can function as a separator in Li-ion batteries. By using our gel electrolyte as a separator, it is possible to lower the cost of Li-ion by 25-35%.

Based on work presented in this dissertation, LiBOB-based electrolytes have the potential to improve the performance, enhance the safety, and lower the cost of Li-ion batteries.

9.2. Recommendations

The good transport properties of LiBOB-based electrolytes and good performance of half cells using LiBOB-based electrolyte motivate us to continue studies of this salt. The following recommendations for these studies are divided into two sections: Li-ion and Li metal system.

9.2.1. Li-ion batteries

The work presented in this dissertation has focused on the transport properties of LiBOB-based electrolytes and cycling performance of cathode half-cells, but more work needs to be done to study the performance of anode half-cells and full cells using LiBOB-based electrolytes and compare against state-of-art electrolytes at room and high temperature. For these studies, full cells are made using two types of metal-oxide cathode: lithium manganese oxide and lithium iron phosphate. Lithium manganese oxide is chosen because of its cost advantage and the ability of LiBOB to improve performance by decreasing Mn dissolution as shown in Figures 9.1 and 9.2 [1], which show Mn dissolution after four weeks storage at 55 ^{o}C in $LiPF_6$/EC+DEC (1:1) based electrolyte and 1 M LiBOB/EC+DEC (1:1), respectively. $LiFePO_4$ is chosen because it is cheaper and safer than $LiCoO_2$. In addition, LiBOB has the ability to improve the performance of cells using $LiFePO_4$ by lowering the amount of Fe dissolved in electrolyte as shown in Figure 9.3 [2], which shows the amount of Fe ions dissolved from C-$LiFePO_4$ powder after one week of aging the material at 55 ^{o}C in 1.2 M $LIPF_6$/EC:PC:DMC (1:1:3) and 0.7 M LiBOB/EC:PC:DMC(1:1:3) electrolytes. While

more than 535 ppm of Fe ions are dissolved in $LiPF_6$-based electrolyte after only one week, less than 3.5 ppm is observed in the case of LiBOB-based electrolyte. The dissolved Fe^{2+} ions migrate in a cell to the negative electrode, and are reduced at the electrode surface to cause an impedance increase. It is expected that LiBOB-based electrolyte will improve the performance of Li-ion cells with $LiFePO_4$ and $LiMn_2O_4$ cathodes because it is HF free electrolyte and will not dissolve Fe or Mn significantly.

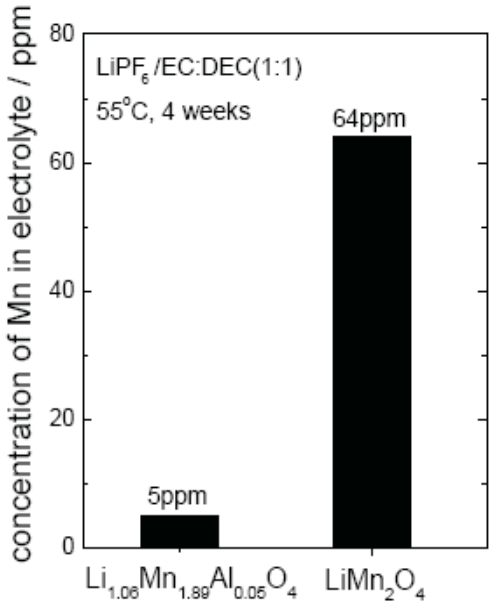

Figure 9.1. Concentration of Mn dissolved from stabilized lithium manganese oxide spinel (SLMOS) and $LiMn_2O_4$ powders stored in $LiPF_6$/EC: DEC (1:1) electrolyte at 55 °C for 4 weeks.[1]

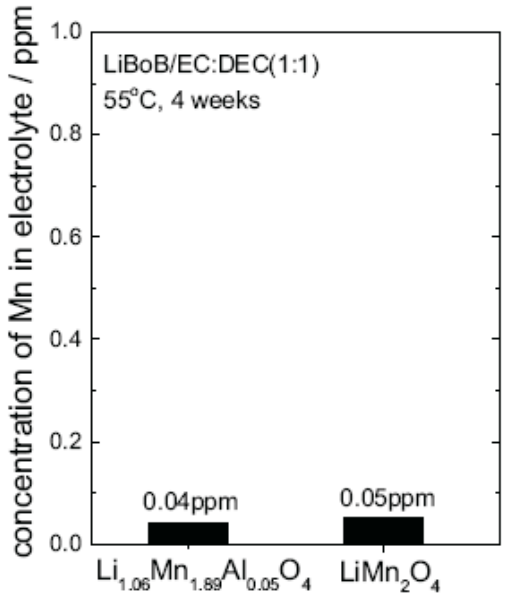

Figure 9.2. Concentration of Mn dissolved from stabilized lithium manganese oxide spinel (SLMOS) and $LiMn_2O_4$ powders stored in 1 M LiBOB/EC:DEC (1:1) electrolyte at 55 °C after 4 weeks.[1]

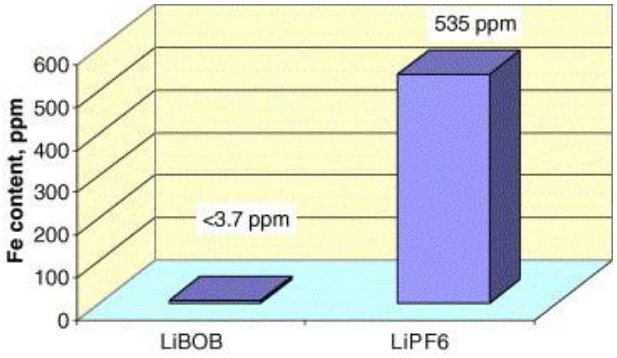

Figure 9.3. Amount of Fe^{2+} ions dissolved from C-$LiFePO_4$ powder that has been aged in 1.2 M $LiPF_6$/EC:PC:DMC (1:1:3) and 0.7 M LiBOB/EC:PC:DMC (1:1:3) for one week at 55 °C. [2]

We have made anode-half cells using MCMB with LiBOB-based and state-of-art electrolytes. The cycling performance of these cells is shown in Figure 9.4. As the figure shows the performance is comparable. In order to study the effect of active material type on the cycling performance of anode half-cells, different types of graphite such as SFG 6, SFG 15, SFG 44, and MCMB with LiBOB-based and state-art-electrolytes are used for anode half-cells.

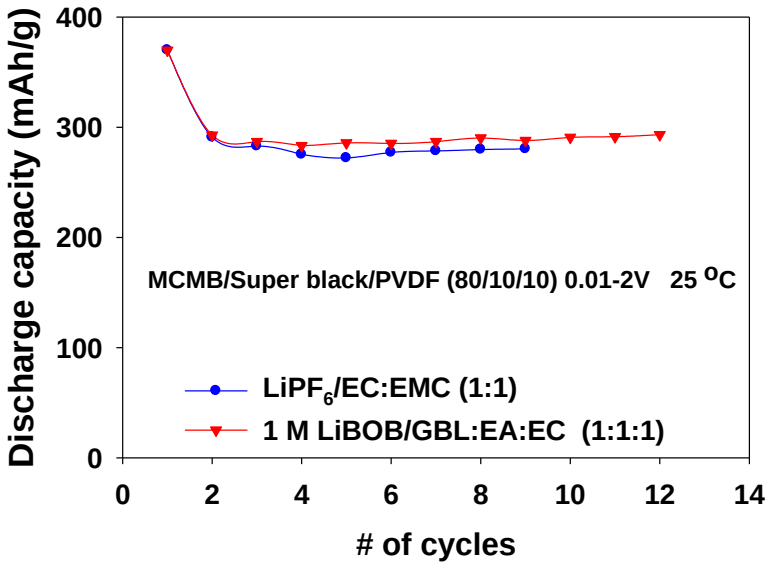

Figure 9.4. Discharge capacity for MCMB/Li cell using 1 M LiBOB-based electrolyte and state-of-art electrolyte.

Safety is a challenge that needs to be addressed in order for Li-ion batteries to be used in broader applications such as hybrid electric vehicle (HEV) and electric vehicle (EV). In order to know if LiBOB-based electrolyte is safe to be used in Li-ion batteries, thermal stability of electrodes with electrolyte needs to be evaluated. Two cathodes ($LiFePO_4$ and

$LiMn_2O_4$) and two anodes (MCMB and SFG 15) are used in this study. Changing salt concentration, solvent composition, anode type, and cathode type will allow us to study their effects on thermal stability. In these studies, hermetically sealed and crimped DSC pans are used [3].

A mixed-salt system is investigated. By using a mixed-salt system we hope to combine the positive effects of both salts so that the shortcoming of one salt will be overcome by the other. For example, we use LiBOB with $LiN(SO_2CF_3)_2$. The problem with $LiN(SO_2CF_3)_2$ is it causes severe corrosion at the Al cathode current collector, as illustrated in the inset of Figure 9.5 [4]. The figure also shows that LiBOB passivates Al. Since LiBOB has the ability to protect Al in lithium-ion batteries, we hypothesize that by mixing LiBOB with $LiN(SO_2CF_3)_2$, LiBOB can form a passivation film on the Al cathode current collector and prevent its corrosion [4, 5].

In order to enhance the safety of Li-ion batteries, we intend to add a fire retardant to our solvent mixture. A fire retardant is used so that continued combustion is not supported when the source of heat is withdrawn, which will not allow for a self-sustaining cell reaction to occur under accidental heating due to external short circuiting or hot-box conditions. Because flames generally require the presence of a chain reaction to be self-sustaining, the majority of workers have sought materials that are known as chain breakers [6]. Trimethyl phosphate (TMP), which used as a fire retardant in plastic production, has been widely studied and recent work at Mitsubishi Chemical has given important results using this material[7]. TMP-based electrolyte might give good performance with no risk of fire. Wang et al [8] introduced the mechanism explain flame retardation. Basically when TMP evaporates, it

breaks to small radical containing phosphorus. These radicals have the ability to scavenge H radical, which are the main active agent of combustion chain branching reactions. The problem of TMP is that it has the tendency to co-intercalate with Li-ion into graphite [9] which impair the cell cycling performance. We hypothesize that using LiBOB, which has been shown to have the ability to prevent co-intercalation of PC in graphite, as a salt would help in solving this problem.

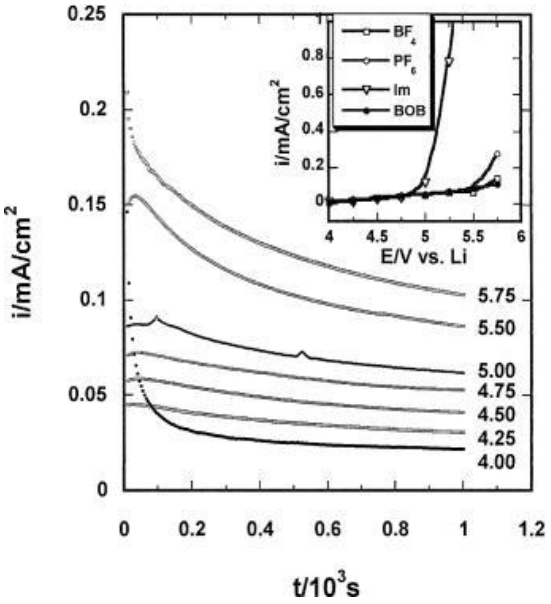

Figure 9.5. Current density obtained on an Al electrode at various potentials vs. Li in electrolyte containing 1.0 M LiBOB in an EC/EMC (1:1) mixture. Inset: Dependence of steady-state current density on applied potential on an Al electrode in electrolytes containing various Li-salts.[4]

9.2.2. Lithium batteries

Impedance analyses show that LiBOB and lithium are compatible due to the formation of a stable passivation layer on the surface of lithium[9]. Thermal studies also demonstrated a superior thermal stability of LiBOB-based electrolyte and surface films formed on lithium in LiBOB-based electrolytes, compared to the thermal stability aspects of the commonly used $LiPF_6$-based electrolyte. For instance, the thermal reaction of an EC–DMC/LiBOB solution with lithium does not start as soon as the lithium melts, but rather at a temperature 5–10 °C higher than that of the Li melting point[10]. This means that the passivation film formed in LiBOB-based electrolytes is so efficient that it can, to some extent, protect even liquid lithium. In addition, it is reported that LiBOB has hindered dendrite formation [11]. We are planning to make electrolytes (using LiBOB) that can be used with lithium batteries. To minimize the dendrite problem of lithium batteries, LiBOB-based gel electrolytes are used. The solvent here will differ from the GBL: EA: EC solvent because of known reactivity of EA with lithium [12]. Currently we have not identified the specific composition of the electrolyte.

9.3. References

1. K. Amine, J. Liu, S. Kang, I. Belharouak, Y. Hyung, D. Vissers, and G. Henriksen Journal of Power Sources 129, (2004), 14.

2. K. Amine , J. Liu and I. Belharouak Electrochemistry Communications, 7, 669, 2005.

3.G. G. Botte, R. E. White, and Z. Zhang, J. Power Sources, 97-98, 570, 2001.

4. K. Xu, S. Zhang, T. R. Jow, W. Xu, and C. A. Angell Electrochemical and Solid-State Lett. 5, (2002), A26.

5. K. Xu, S. Zhang, B. A. Poese, and T. R. Jow Electrochemical and Solid-State Lett. 5, (2002), A259.

6. G. E. Blomgren J. Powersoutces 119-121 (2003) 326

7. X. Wang, E. Yasukawa, and S. Kasuya, J.Electrochem. Soc, 148, A1066 (2001).

8. X.Wang, E. Yasukawa, and S. Kasuya, J.Electrochem. Soc. 148, A1058, 2001.

9. Zhang SS, Xu K, Jow TR, J. Power Sources, 154, 276, 2006

10. L. Larush-Asrafa, M. Bitona, H. Tellera, E. Zinigradaand D. Aurbacha, J. Power Sources, 174, 400, 2007.

11. S.S Zhang, K. Xu, and T.R. Jow, "LiBOB-based gel electrolyte Li-ion battery for high temperature operation ", J. Power Source, in press.

12. W.A. Van Schalkwijk and B. Scrosati. "Advances in Lithium-Ion Batteries" , Kluwer Academic/ Plenum Publishers, New York(2002), p. 171.